Testa, Alvaro Javier

NONDESTRUCTIVE MEASUREMENT OF SURFACE CRACKS USING ULTRASONIC RAYLEIGH WAVES

Iowa State University PH.D. 1982

PLEASE NOTE:

In all cases this material has been filmed in the best possible way from the available copy. Problems encountered with this document have been identified here with a check mark ✓.

1. Glossy photographs or pages _____
2. Colored illustrations, paper or print _____
3. Photographs with dark background ✓
4. Illustrations are poor copy _____
5. Pages with black marks, not original copy _____
6. Print shows through as there is text on both sides of page _____
7. Indistinct, broken or small print on several pages ✓
8. Print exceeds margin requirements _____
9. Tightly bound copy with print lost in spine _____
10. Computer printout pages with indistinct print _____
11. Page(s) _____ lacking when material received, and not available from school or author.
12. Page(s) _____ seem to be missing in numbering only as text follows.
13. Two pages numbered _____. Text follows.
14. Curling and wrinkled pages _____
15. Other _____

Nondestructive measurement of surface cracks using ultrasonic Rayleigh waves

by

Alvaro Javier Testa

A Dissertation Submitted to the

Graduate Faculty in Partial Fulfillment of the

Requirements for the Degree of

DOCTOR OF PHILOSOPHY

Departments: Engineering Science and Mechanics
Civil Engineering
Co-majors: Engineering Mechanics
Structural Engineering

Approved:

Signature was redacted for privacy.

In Charge of Major Work

Signature was redacted for privacy.

For the Major Departments

Signature was redacted for privacy.

For the Graduate College

Iowa State University
Ames, Iowa
1982

TABLE OF CONTENTS

CHAPTER I. INTRODUCTION

With the evolution of the materials used nowadays in industry and the increasingly complex and critical nature of many of the products and structures produced with them, quality control and inspection methods have become a major issue in the daily life of the engineering profession.

The principal goal of a good quality control procedure is to guarantee that a product is highly reliable and relatively free from defects. However, nothing is perfect. The most thoroughly inspected element is still likely to contain some defects, either microscopic or macroscopic. It is, therefore, assumed that all components are defective, hence, have a finite life. It is then important to develop methods by which periodic inspection of any component can be performed.

Today there exists a wide range of inspection methods that cover a large variety of defects, from a tiny inclusion in ceramics to a large open fatigue crack on the surface of metals. Among the most common techniques, we have x-ray diffraction, Eddy current, dye penetrants, thermography and ultrasonics [1]. Of all these, close attention will be given to the ultrasonic methods.

There is a variety of ultrasonic waves that can be used for non-destructive evaluation. Among the most common, one can mention the longitudinal waves, generally called P-waves; the distortional or shear waves, generally called S-waves; and the surface waves which for the case of a semi-infinite half space or plane are known as Rayleigh waves. There are some other types of waves which can coexist with the previous ones in most cases such as the Lamb waves, standing waves, Von-Schmidt waves and others. It is the Rayleigh wave, though, and more specifically the information that it can convey upon interaction with surface flaws, that is the primary concern of the writer.

Statement of the Problem

Among the various kinds of defects that can be encountered in real life situations such as voids, inclusions, highly strained regions,

cracks and others, it is the fatigue crack which threatens the life of most engineering structures such as bridges, nuclear reactors, turbines, pipelines and others.

Shallow surface breaking flaws represent the early stage of the majority of fatigue failures. It is, therefore, important, for quantitative life predictions, to know their initial depth and to monitor their growth so that a trend to failure can be established and, hence, remaining life. As of today a reliable ultrasonic inspection procedure for characterizing small defects (<5 mm) is not available, especially if such defects are located in the near field of the transducers. Various amplitude and time of flight methods have been proposed for measuring deep open cracks; they will be described in the following chapter. Although these methods are accurate for artificial flaws, they generally overestimate the depth of shallow cracks in real structures. This problem may be caused by the effect that residual stresses at the crack tip have on the time of travel or amplitudes or by internal changes in material properties and/or composition. There is a need for an ultrasonic measurement of crack depth that is independent of the usual variables such as material isotropy, state of stress, testing conditions and others which affect other methods.

Surface Rayleigh waves are attractive for interrogating surface and near surface defects. Their energy is confined to a layer of about two wavelengths below the surface. Thus, they are not affected by far surface reflections or by changes in material properties below the indicated depth. The nature of the wave is non-dispersive; that is, the velocity is frequency independent as long as it travels on flat surfaces. It has the capability of following gentle or sudden changes in direction although with higher attenuation losses. There is, therefore, much contemporary interest in the scattering of R-waves from shallow defects.

A broadband Rayleigh wave has the characteristic of having a range of frequencies present at various depth below the surface. As will be shown, the higher frequencies of such waves cannot penetrate as far

into the material as the low frequencies. Therefore, if the Rayleigh wave happens to interact with a surface defect shallower than its depth of penetration for the lowest frequency, there will be a filtering effect on all those frequencies present between the surface and the tip of the defect. On the other hand, the energy that diffracts at the crack or defect tip will be devoid of the higher frequencies. Upon interaction the deeper energy diffracts into a signal that reaches the surface bringing with it pertinent information about the depth of the defect. Hence, by following the pattern of the interaction mechanism, one is able to establish a simple means of sizing surface breaking defects by means of ultrasonic Rayleigh waves.

Experimental evidence will be presented concerning the sensitivity of the method to normal operational variables. This issue is considered of great importance if the method is to be developed for everyday use under various field conditions.

To establish a clear trend of developments it is first necessary to look back at past work performed in the area of flaw characterization using non-destructive ultrasonic methods. The following chapter attempts to do this job very briefly.

The writer acknowledges the contribution of the previous researcher, Mr. Anmol Singh, toward the advancement of the research herein discussed. Mr. Singh did most of the photoelastic studies on the interaction of Rayleigh waves and surface defects; and, in addition, he conducted the first preliminary ultrasonic tests on surface defects such as slots.

CHAPTER II. LITERATURE REVIEW

Rayleigh waves owe their name to Lord Rayleigh who first discovered them in 1885 [2]. Since then much has been written about them, and general solutions for this boundary value problem have been presented. Viktorov [3] treats the surface waves and Rayleigh waves, in particular, in a detailed manner. He provides solutions for the behavior of these waves in a half space or plane, concave or convex spaces or planes, at surface irregularities and at liquid interfaces. More general studies of the mechanics of elastic waves can be found in books by Kolsky [4] and Achenbach [5], which also provide reasonably complete developments of the Rayleigh wave equation.

Originally, the importance of the understanding of Rayleigh waves was mostly associated with geophysics problems. In earthquakes, for instance, the energy carried by the tectonic surface waves is the most destructive; hence, an understanding of their behavior and properties is of extreme importance to earth scientists. Recently, ultrasonic surface waves are being investigated to inspect solid materials and structures. They are becoming evermore important in the areas commonly called Non-Destructive Evaluation (NDE), Non-Destructive Testing (NDT) and Non-Destructive Inspection (NDI). In recent years the overall increased concern for product safety, consumer rights and product reliability [6] has placed enormous pressure on the engineering community to improve their ability for safe design and accurate evaluation of structures. As a result, the general importance of NDE has been rapidly recognized. These are strong motivations for the continuous growth and development of non-destructive methods [7]. There are savings in quality control, materials energy, manpower, product liability and improvements in the detection of imminent failure, consequently, in product reliability. Many techniques have been developed and are used singly or in combination. These include liquid penetrants, hardness testing, magnetic particles, Eddy-current, radiographic, ultrasonic, holographic, thermographic and acoustic techniques [8]. Those directly related to ultrasonic methods are discussed further in the following paragraphs.

Ultrasonic energy is used to perform a wide variety of jobs such as cleaning, plastic welding, metal welding, soldering, machining and others [9]. One of the most recent uses is for generating ultrasonic acoustic waves to detect and size flaws in metals and ceramics to name a few. To be more useful ultrasonic testing techniques must become more quantitative; i.e., they must account for the ways in which the energy is scattered and mode converted by defects.

Because the state of the theory, in the prediction of good scattering models for realistic defects, is not very good, some efforts have been directed toward dynamic photoelastic studies of acoustic waves. This is specially true for Rayleigh waves, which are the main concern of this dissertation.

Due to the high energy absorption of the most common birefringent plastics used in photoelastic studies (CR-39, Homalite-100 and others), it is necessary to produce stress waves by exploding charges on the surface of the test specimens. A theoretical model of the waves generated by such transient loads on an elastic half space is provided in reference [10].

Thau and Dally [11] used photoelastic experiments to study the subsurface characteristics of the Rayleigh wave, while Sorge [12] was able to obtain experimentally the predicted displacement fields at various depths. The agreement between theory and these experiments is very good.

In order to understand the behavior of a Rayleigh wave upon interaction with defects such as slots or cracks, it is first necessary to observe its behavior upon interaction with simpler defects. Henzi and Dally [13] performed studies of Rayleigh wave interactions with a quarter plane. Although their objective was to determine the intensity of the various waves generated upon such an interaction, their knowledge, in addition to the studies performed by Burger, et al. [14], have aided in the basic understanding of the interaction of a Rayleigh wave and the side of a slot.

Lewis and Dally [15] studied reflection and transmission coefficients of Rayleigh wave interactions with wedges. They show that these coefficients vary very rapidly with changes in the wedge angle. This study is important in understanding the effect that an inclined slot or crack may have on a Rayleigh wave.

An interesting piece of work is that performed by Dally and Lewis [16] on Rayleigh wave interactions with steps. This work allows one to observe the various waves generated when steps are increased incrementally until they are deeper than the penetration of the Rayleigh wave. At that time it was observed that there was a Rayleigh wave that leads the one that runs along the surface when the step change in elevation is shallower than the penetration of the incident Rayleigh wave. Not only this, the leading wave was described as being broader than the one that follows the surface.

Reinhardt and Dally [17] did some of the first photoelastic studies of Rayleigh wave interaction with surface flaws, in this case machined slots. Although the system used did not have a very good resolution, it was possible to observe the transmitted and reflected signals that were later used by other researchers.

Rayleigh waves are known to be affected by the curvature of the medium in which they propagate [3]. Marino and Dally [18] made photoelastic studies of this problem and were able to conclude, as theory predicts, that convex surfaces allow the wave to propagate faster as the curvature decreases. This means that if the wave travels around a solid shaft, then it would travel at speeds higher than the Rayleigh wave velocity. On the other hand, a concave surface (think of a cylindrical hole in an infinite medium) slows down the wave in addition to increasing its shear diffraction radially outward.

Plona, et al. [19] studied the case of Rayleigh waves propagating in a solid medium but at a liquid boundary. They found that the velocity of the Rayleigh wave is affected very little by the liquid layer as long as the densities of the liquid and that of the host material differ significantly (order of two or more). When the densities approach each other, then the effects can lead to large errors.

The use of photoelasticity in the study of problems associated with the behavior of elastic waves in solids provides a means for understanding otherwise intractable problems. In a general sense, such wave visualization provides a teaching aid to better understand ultrasonic non-destructive methods [20].

The generation of Rayleigh waves in materials other than the plastics used in photoelastic studies is usually achieved by means of electro-mechanical transducers capable of generating, upon excitation, the desired signal. A discussion of such devices is presented by Morgan [21] and most generally by Krautkrämer and Krautkrämer [1]. Harnik [22] describes a novel unit which is being used to extend data acquisition capabilities to regimes much closer to the surface breaking defect than was possible with previous devices.

Developments in the area of non-destructive evaluation, testing and inspection have been many. In the following sections, only the analytical methods that contribute to improved understanding of the interactions between Rayleigh wave and surface defects are reviewed. Experimental procedures for sizing surface flaws are then discussed and related to the method which is the topic of this dissertation.

Rayleigh wave scattering from surface defects was studied by Akhromeeva and Krylov [23]. They presented the scattering matrix for the mode conversion of Rayleigh waves to bulk waves with good agreement between calculated and measured data.

Tittmann, et al. [24,25] presented a model based on optical diffraction theory for sizing very small surface breaking cracks (>100μm). "The scattered radiation patterns of the flaws when irradiated by acoustic surface waves were interpreted to provide estimates of flaw length and depth with accuracies of 10% or better."

Domarkas, et al. [26] made use of the angular scattering of surface waves from surface cracks and the corresponding shift in frequency to determine their length and depth.

Auld, et al. [27-29] approached the problem of scattering of Rayleigh waves from surface breaking cracks in two ways. One of the methods

was Born's approximation to evaluate the perturbed fields; the second is called the Kirchoff approximation. The two methods are tested and compared to each other and, in addition, with results obtained using geometrical diffraction. They also investigate the resonance phenomenon observed in Rayleigh wave interaction with surface cracks using Freund's [30] results on reflection of Rayleigh waves from the edge of an infinite crack. Calculations are made for a rectangular and half-penny shape cracks.

Gubernatis and Domany [31] developed a quasi static method which involves the use of a surface integral formulation combined with static results from fracture mechanics. This method is improved by approaching the problem with a volume integral formulation of the scattering for which several approximations exist. Their purpose was to illustrate apparent characteristic features of elastic wave scattering from surface cracks.

Achenbach and Gautesen [32] suggest a "membrane analogy" to describe the normal displacement component, at the free surface, of a surface wave. The reduced wave equation thus obtained suggests the existence of a family of surface waves. The motivation for this study was the existing interest in the interaction of surface waves with the edge of a semi-infinite long crack of finite depth.

Gautesen and Achenbach [33] addressed the problem of surface waves guided by a slit and concluded that a slit, or for that matter, a crack, of finite length (transverse to surface of propagation) cannot guide surface waves at speeds smaller than the Rayleigh surface wave speed in the elastic medium where they exist.

Mendelsohn, et al. [34] addressed the problem of scattering of surface and body waves upon interaction with a surface-breaking crack. The solution is obtained by decomposing the scattered fields into symmetrical and anti-symmetrical fields, with respect to the plane of the crack, and solving two boundary value problems for a quarter plane. An exact solution is obtained this way for the case of a finite narrow crack normal to the surface.

Achenbach, et al. [35] presented a ray-theory approach to the surface wave scattering problem. "The basic diffraction mechanism in the high frequency range, $\omega d/v_R > 6$ (ω = circular frequency, d = crack depth, v_R = Rayleigh wave velocity), at the mouth and the edge of the crack were investigated on the basis of elastodynamic ray theory. The results were then superimposed to yield a simple expression for the back and forward scattered Rayleigh surface waves."

Research in Great Britain obtained numerical solutions through the use of finite differences. Bond [36] and Ilan, et al. [37-38] were able to establish a procedure to determine, with certain limitations, the scattered field of a compressional impulse. The same technique has also been used to determine the scattered field of surface acoustic waves interacting with surface slots [39-40].

Some early work on numerical solutions for acoustic Rayleigh wave problems in anisotropic layered media can be attributed to Munasinghe [41].

Most of the work presented thus far was analytical in nature. Much of it was verified by experiments designed to fit the specific models assumed in the theories. Experiments dealing with complex geometries and boundary conditions that approach practical problems more realistically have had to proceed with very little theoretical help.

Quick detection and sizing procedures of real flaws should be the main goal of researchers. Kino, et al. [42] suggest that acoustic imaging techniques, if fully developed, will meet both of these requirements for such imaging. The medium may be excited with bulk waves, Rayleigh waves or Lamb waves.

Cracks which develop in a fatigue specimen change the properties and alter the continuity of the material in that area. It is believed that a phenomenon called acoustic harmonic generation occurs when acoustic waves interact with such flaws [43]. The phenomenon is attributed to the increased anelasticity on the surface of fatigued specimens due to the development of microcracks. A possible mechanism for this acoustic generation is the distortion that the fundamental wave experiences as it passes across an unbounded interface. The main purpose of

this technique is to relate the length and density of microcracks initiated during fatigue with the generation of harmonics of a surface wave so as to determine remaining useful life of structures cyclically loaded [44].

Ultrasonic inspection procedures for surface cracks may use either bulk or surface waves. Pulse echo methods are most commonly used for detection of defects. Basically, sizing of such defects is then attempted by comparing the amplitude of the received echoes with a reference signal or by studying the time between the arrival of at least two different waves. Doyle and Scala [45] and Silk [46] discuss some of these methods in more detail.

Hudgell, et al. [47] proposed a method for sizing surface breaking flaws by measuring the time delay between the surface wave that travels all the way around an open crack and the reconverted Rayleigh wave generated from the shear wave that the first wave sheds when turning the tip of the crack [14]. This shear wave travels outward from the tip of the crack toward the opposite side of the specimen. There it is reflected back toward the crack tip where it reconverts into a Rayleigh wave and continues along the crack. The time delay actually measures the distance between the crack tip and the opposite face of the specimen in terms of shear wave speed. If the thickness of the specimen is known, then the depth of the crack normal to the surface is obtained. Tittmann and Buck [48] used this method for fatigue lifetime prediction.

Mills [49] suggested that planar waves, such as those generated by commonly available unfocused transducers, may be used to search for buried or surface breaking defects. There is no need to know about their orientation or location. The technique is based on the time domain analysis of the refracted signal using geometrical diffraction.

Hall [50] uses the time of travel between two transducers to estimate the crack depth. He first takes a reference time of travel of the surface waves by placing the transducers at a fixed distance and with no crack in the path. Then a time scan is obtained with the same set up on the cracked specimen. The measurement yields the overall length of the crack but not the depth perpendicular to the surface.

Silk [51,52,55] and Silk and Lidington [53,54] have used a diffraction technique which makes use of the scattered energy from the tip of the crack and the back wall of the specimen to determine the length and inclination of the flaw. By using the forward and backward scattered waves, a system of equations based on the geometrical diffraction from surface breaking defects is obtained. The method yields very good results as long as the crack is not too shallow (≤ 6 mm). Length, depth and inclination of the cracks can be estimated. Sigmond and Lien [56] and Grigorév, et al. [57] have done similar work using the geometrical diffraction technique.

Khuri-Yakub, et al. [58] performed experiments in ceramics which allow the detection of flaws as small as 60μm. The specimen is scanned on one surface, and the signal from the back surface becomes the reference depth indicator. Any defects encountered by the elastic wave on its way to the back surface will produce an early scattering record from which the length of the defect can be established.

The techniques so far presented have difficulties in defining the depth of surface breaking cracks in the range of tenths of a milimeter up to a few milimeters in length. Interference of the signals is observed when the testing is performed too close to the near field of the transducer and also when the time delay between signals is too small. Therefore, the diffraction technique becomes difficult to use with shallow defects [59]. Yielding zones at crack tips change the elastic properties of the material sufficiently to induce changes in the propagation velocity and amplitude of waves [60]. Correction values and improved techniques have been proposed to remedy some of the problems [61-63]. Corrections for transducer influence on sound velocity for the pulse echo method and optimization procedures for the geometric diffraction technique are suggested.

In an attempt to overcome some of the difficulties encountered in the diffraction and pulse echo methods, newer techniques, that utilize additional signal processing mainly in the frequency domain, have been developed. Frequency studies of signals can be achieved by performing

Fast Fourier Transformations (FFT) on the time domain scans [64-66]. Gericke [67] presents a very thorough discussion of the possible uses of ultrasonic spectroscopy in non-destructive methods. Some difficulties may arise in the application of frequency analysis. Not every part of the time-domain is useful for transformation. Also, if the use of broadband transducers is favored, there is a reduced sensitivity in the system. Crostack [68] discusses these difficulties. Rose and Meyer [69] published a preliminary study on signal processing in which they discuss the selection of transducers to obtain the most productive data from testing. Procedures for improving the time scanned data to be used for transformation were suggested by Hundt and Frautenberg [70]. They also discuss the use of a deconvolution procedure for filtering out unwanted noise and resonances in the system. These procedures improve image quality.

Spectroscopic methods are increasingly being applied to ultrasonic waves. Haines [71] discussed some of the future uses and existing problems of the method in general, while Morgan [72] reported specifically on its use with surface waves. Initially, a reference Rayleigh wave signal is scanned. Because this reference wave has not interacted with any defects, it only contains information about the Rayleigh wave and the equipment influence on the signal. Subsequently, a frequency spectrum is obtained by means of analogue instrumentation which means that the phase information is lost. The same process is repeated with the scattered signals from a surface defect. The second spectrum is then divided by the first (reference) spectrum which then leaves only the information about the defect. An additional step is then taken; the modulations which are in the frequency domain are subjected to an analogue frequency study, therefore bringing the frequency information back into the time domain. This final result has been termed by the authors of the paper the cepstrum of the original signal. The peaks in the cepstrum are then associated with specific features of the defect. The problem with this method is that there is no simple way of associating a particular feature with any portion of the cepstrum.

Bifulco and Sachse [73] used the time of arrival and power spectral density of the time signal to determine the dimensions of solid cylindrical inclusions in aluminum. Although they did not do any work on surface breaking flaws, their procedure is of general interest.

Vopilkin, et al. [74] used ultrasonic spectroscopy for determining the nature of defects in the range of 1-10 MHz, or equivalent wavelength. They claim that the spectral characteristics of artificial defects of various shapes are different. Based on this, by comparing spectrums of known defects with spectrums obtained in the field upon testing actual specimens, they have been able to categorize several kinds of defects quite reliably (80% of the time). One major problem with this technique is that it is almost dependent on qualitative judgment instead of quantitative evaluation.

Recent studies at Iowa State University applied some aspects of spectroscopy to surface breaking defects in the order of one to one and one half wavelengths in depth (wavelengths as computed from the limits in the frequency band of the transducers). Simple spectroscopic procedures were applied to photoelastic data obtained from the interaction between Rayleigh waves and surface slots [13,75-78]. By studying the Rayleigh wave displacement field after interaction with surface slots, it was observed that in the frequency domain there was an upper frequency limit which was inversely proportional to the depth of the defect. It was determined that this frequency depth correlation existed for the various depths tested and an initial postulate of the process was established.

The next step was to obtain information on the effectiveness of the method in measuring the depth of open and closed cracks. In many aspects, cracks behave in the same way as slots. Birchak and Gordner [79] found that the main difference between the two cases, machined slot and crack, is in the signal level upon interaction. They were mainly concerned with effect on pulse-echo amplitude measurements though.

This dissertation presents the results of experimental studies directed toward further development in the use of Rayleigh waves for measuring the depth of fatigue cracks [80-82].

CHAPTER III. THEORETICAL BACKGROUND

The Rayleigh Wave Equation

The understanding of some of the basic characteristics of the Rayleigh surface waves led to the development of the method presented in this dissertation.

Rayleigh waves are surface disturbances which propagate along the free boundary of a solid. Consider the isotropic, elastic half space of solid material in Fig. 3.1.

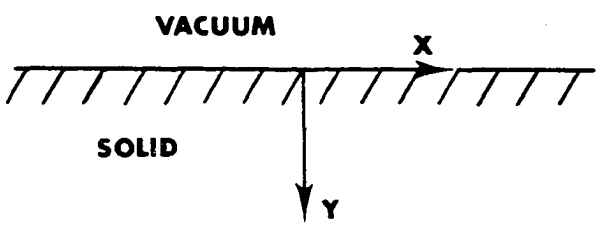

Figure 3.1. Reference axes on an elastic half space

A generalized displacement field for the elastic half space can be represented as

$$\vec{d} = \vec{\nabla}\phi + \vec{\nabla}x\vec{\psi} \tag{3.1}$$

where $\vec{d}$: generalized particle displacement vector

ϕ: scalar potential

$\vec{\psi}$: vector potential

$\vec{\nabla}$: Laplacian operator.

If the motion of the wave is independent of the coordinate z, then the vector component along the z-axis will have a magnitude of ψ and zero in the x- and y- directions. The potentials satisfy for harmonic processes Eq. (3.2).

$$\frac{\partial^2\phi}{\partial x^2} + \frac{\partial^2\phi}{\partial y^2} + k_\ell^2\phi = 0 \tag{3.2a}$$

$$\frac{\partial^2\psi}{\partial x^2} + \frac{\partial^2\psi}{\partial y^2} + k_s^2\psi = 0 \qquad (3.2b)$$

where $k_\ell = \frac{\omega}{v_\ell}$ and $k_s = \frac{\omega}{v_s}$

k_ℓ, k_s: longitudinal and shear wave number, respectively

ω: circular frequency

v_ℓ, v_s: longitudinal and shear wave velocities.

If the potentials are chosen to be represented by the function (3.3)

$$\phi = f(y)\, e^{i(kx - \omega t)} \qquad (3.3a)$$

$$\psi = g(y)\, e^{i(kx - \omega t)} \qquad (3.3b)$$

where k: wave number

t: time,

one can then substitute Eq. (3.3) into Eq. (3.2) and arrive at the following set of ordinary differential equations, Eq. (3.4), for the functions f(y) and g(y):

$$\frac{d^2f(y)}{dy^2} - (k^2 - k_\ell^2)\, f(y) = 0 \qquad (3.4a)$$

$$\frac{d^2g(y)}{dy^2} - (k^2 - k_s^2)\, g(y) = 0. \qquad (3.4b)$$

Equation (3.4) yields two exponential solutions on "y" for the functions f(y) and g(y) of the form $\exp[\pm y\sqrt{k^2 - k_\ell^2}]$ and $\exp[\pm y\sqrt{k^2 - k_s^2}]$. The solution with the positive exponent indicates an exponential increase of the displacements with increasing depth which does not suit the criterion for Rayleigh waves. The negative exponent yields exponentially decaying displacements as "y" increases. Therefore, one can rewrite the potential functions as

$$\phi = A \exp[-y\sqrt{k^2 - k_\ell^2}] \exp[i(kx - \omega t)] \tag{3.5a}$$

$$\psi = B \exp[-y\sqrt{k^2 - k_S^2}] \exp[i(kx - \omega t)]. \tag{3.5b}$$

The problem now reduces to finding the wave number, k, and the relationship between the constants A and B. This is achieved by applying the boundary conditions $\sigma_{yy} = \sigma_{xy} = 0$ at y = 0, which stand for the normal stresses and shear stresses, respectively, being zero at the surface. These are two necessary conditions, and their use in the solution of the problem is presented in Appendix A. One can then write the potential functions as

$$\phi = -A \exp[i(kx - \omega t) - y\sqrt{k^2 - k_\ell^2}] \tag{3.6a}$$

$$\psi = i\, A\, \frac{2k\sqrt{k^2 - k_\ell^2}}{2k^2 - k_S^2} \exp[i(kx - \omega t) - y\sqrt{k^2 - k_S^2}] \tag{3.6b}$$

and the Rayleigh wave velocity comes out to be

$$v_R = \frac{0.862 + 1.14\nu}{1 + \nu}\, v_S. \tag{3.7}$$

Finally, one can represent the Rayleigh wave displacement Eq. (A.1), in Appendix A, in the following form

$$U_R = A\, k_R \left\{ \exp(-y\sqrt{k_R^2 - k_\ell^2}) - \frac{2\sqrt{k_R^2 - k_\ell^2}\sqrt{k_R^2 - k_S^2}}{2k_R^2 - k_S^2} \left[\exp(-y\sqrt{k_R^2 - k_S^2}) \right] \right\} \sin(k_R x - \omega t) \tag{3.8a}$$

where: k_R: Rayleigh wave number

U,V: displacement in the x- and y-directions, respectively.

Also,

$$V_R = A\sqrt{k_R^2 - k_\ell^2}\left\{\exp(-y\sqrt{k_R^2 - k_\ell^2}) - \frac{2k_R^2}{2k_R^2 - k_S^2}\left[\exp(-y\sqrt{k_R^2 - k_S^2})\right]\right\}\cos(k_R x - \omega t). \qquad (3.8b)$$

If one now reviews the obtained results, it will be observed from Eq. (3.7) that the velocity of the Rayleigh wave is independent of frequency; therefore, it is non-dispersive in nature. It is also observable that the main parameter in the solution of the Rayleigh wave problem is Poisson's ratio (ν), which indicates that the wave speed is controlled by a material property only. Equation (3.8) predicts that the displacements, consequently the energy content of the Rayleigh wave, decay exponentially with the increase in depth "y" from the surface.

Figure 3.2 is a graphical representation of the displacement field from Eq. (3.8). Experimental work to confirm the theoretical displacement fields has been done, and there is close agreement between the two [12]. The experimental results in the cited reference indicate that although the displacements do attenuate at a very fast rate as the depth increases, they are up to four times as large as theory predicts at a depth of about one and one-half wavelengths. This may be indicative that in reality Rayleigh waves may have considerably more energy at its deeper layers than is estimated from theory.

Although the stress field has not been mentioned, except in Appendix A, it is important to realize that just by substituting the potential functions into Eq. (A.2) it can be obtained. According to the work done by Thau and Dally [11], the maximum magnitude of the principal stresses occurs right at the surface where only the compressional component of the stress (σ_{xx}) exists. Then from the boundary the principal stresses decay exponentially with increasing depth. One can also note in Fig. 3.2 that the displacements along the direction of propagation (U) suffer a reversal of direction at a depth of about 0.2λ, depending on Poisson's ratio (ν) value. In other words, the Rayleigh wave surface

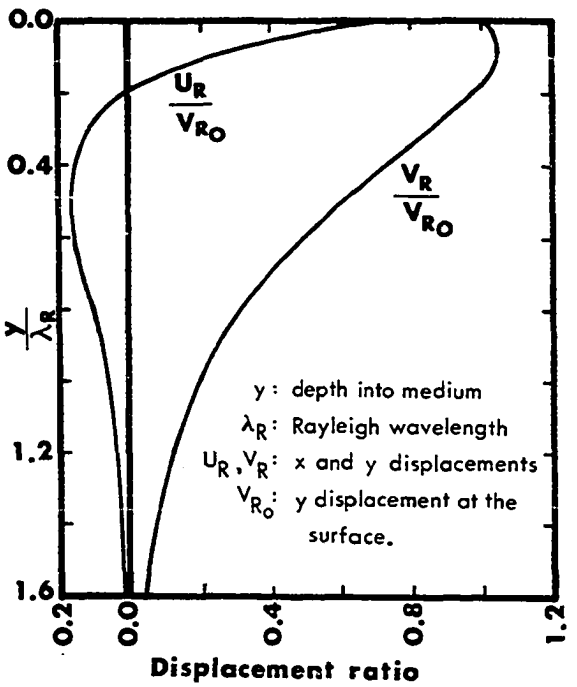

Figure 3.2. Displacement field of a Rayleigh wave

rotation (given by a vector k perpendicular to the page) changes direction [3,5]. Experimental evidence of the change in rotation of the particles with depth has been obtained by Sorge [12].

Mathematically, the reversal point can be obtained by imposing the conditions (u,y) = (0,y) to Eq. (3.8a) which then can be rewritten as

$$y = \ell n \left[\frac{2\sqrt{k_R^2 - k_\ell^2}\sqrt{k_R^2 - k_S^2}}{2k_R^2 - k_S^2} \right] \Bigg/ \left[\sqrt{k_R^2 - k_S^2} - \sqrt{k_R^2 - k_L^2} \right], \quad (3.9)$$

but knowing that $k_{(i)} = \omega/v_{(i)} = 2\pi f/v_{(i)}$, where f is the frequency (Hz), and that the inverse of the velocities can be written as the slowness of the wave ($S_{(i)}$), then Eq. (3.9) can be rewritten as

$$f \cdot y = \ell n \left[\frac{2\sqrt{s_R^2 - s_\ell^2}\sqrt{s_R^2 - s_S^2}}{2s_R^2 - s_S^2} \right] \Big/ 2 \left[\sqrt{s_R^2 - s_S^2} - \sqrt{s_R^2 - s_\ell^2} \right]. \quad (3.10)$$

The righthand side of Eq. (3.10) is a constant in terms of the slowness of the P-, S- and R-waves. The lefthand side can be thought of as being a linear combination of frequency and depth of penetration. By taking standard values for the velocities of the waves in, say, steel 1018 (v_ℓ = 5.85 mm/μs, v_S = 3.23 mm/μs and v_R = 2.96 mm/μs), with a Poisson's ratio of ν = 0.28 one can obtain

$$f \cdot y = \frac{v_R \, y}{\lambda_R} = 0.578 \quad (3.11)$$

which can be rewritten as

$$\frac{y}{\lambda_R} = 0.179. \quad (3.12)$$

One can see from Eq. (3.12) that the reversal point varies linearly with wavelength, or inversely linear with frequency. If this behavior can be expected from a broadband Rayleigh wave, and there is no reason to believe otherwise, it means that at every depth one should expect a linear variation with frequency although not necessarily equal to 0.179 but to some other constant (Fig. 3.2, vertical axis).

Also, by following the behavior of the reversal point, one can conclude that the higher the frequency, i.e., the shorter the wavelength, the shallower the reversal point will be. Consequently, the total depth of penetration is less for higher frequencies. For longer wavelengths the opposite is true.

The discussion presented above gives rise to the experimental method developed in this paper. The main proposition is that if a Rayleigh wave is generated with a broadband transducer, a different range of frequencies will be present at various depths. The deeper the layer,

the more the higher frequencies disappear. Only the lower frequencies will remain until one runs out of the field of penetration of the lowest of all the frequencies. Further discussion of this point will be presented later in the text.

Although the method proposed in this dissertation is based on a very simple concept, the rigorous mathematical solutions to the problem or models do not exist. There have been recent advances in numerical methods [39-40] which tend to agree, but most of the information is purely experimental.

CHAPTER IV. EXPERIMENTAL BACKGROUND

Basic Understanding of Mode Conversion of Rayleigh Waves from Dynamic Photoelasticity Studies

Due to the lack of theoretical mode conversion schemes for Rayleigh waves under real conditions, it was considered necessary to approach the problem from an experimental view point. Dynamic photoelasticity is an attractive method because it provides full field visualization of the stress field in birefringent materials. The birefringent materials, although different in composition and properties from metals, are able to show the general behavior of waves as they travel through the medium and interact with defects. The following paragraphs discuss a few aspects of the actual experimental evidence on the behavior of Rayleigh waves.

The interaction of a Rayleigh wave with a surface breaking slot can be thought to occur in three different stages. First, the wave impinges on the slot; second, it travels the path around the slot; and third, the deeper portions of the wave that do not interact directly with the side of the slot interact with the tip of the slot as if it was a step change in elevation of the surface of the specimen.

In the following experiments, surface waves were generated by detonating a small explosive charge on the surface of a photoelastic specimen some distance away from the geometric detail under study. The explosion generates a Rayleigh wave, R, as well as bulk waves P, S and PS (longitudinal, shear and Von-Schmidt waves, respectively). Figure 4.1 depicts the interaction of a Rayleigh wave and a shear wave with a quarter plane [13,14,77]. The Rayleigh wave approached the corner from the left. At this time the leading P-wave, which travels about twice as fast as the shear wave, has been reflected and is out of the picture. The only waves present in the picture are those resulting from the interaction of the incident Rayleigh and shear waves with the corner.

The R^{1r} wave represents the Rayleigh wave reflected at corner 1. The R^{1t} is the transmitted Rayleigh wave also from corner 1. The higher number of fringes in the R^{1t} as compared to the R^{1r} implies that more

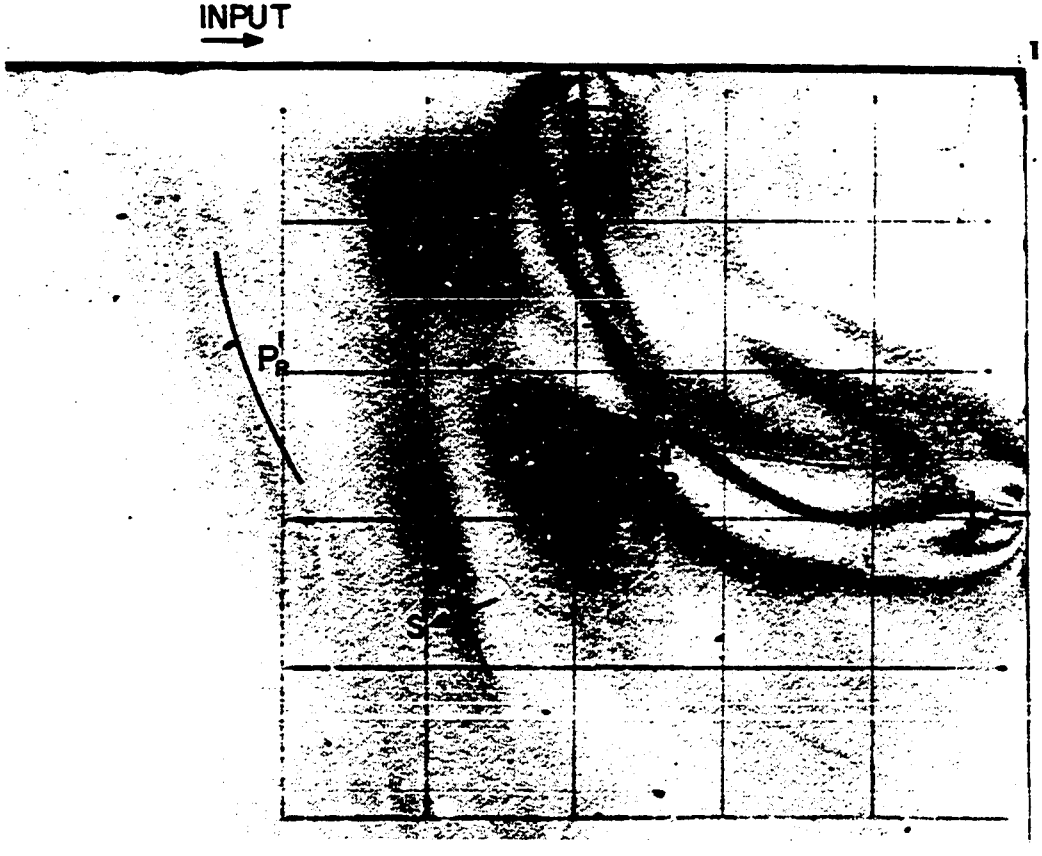

Figure 4.1. Interaction of a Rayleigh wave with a corner [77]

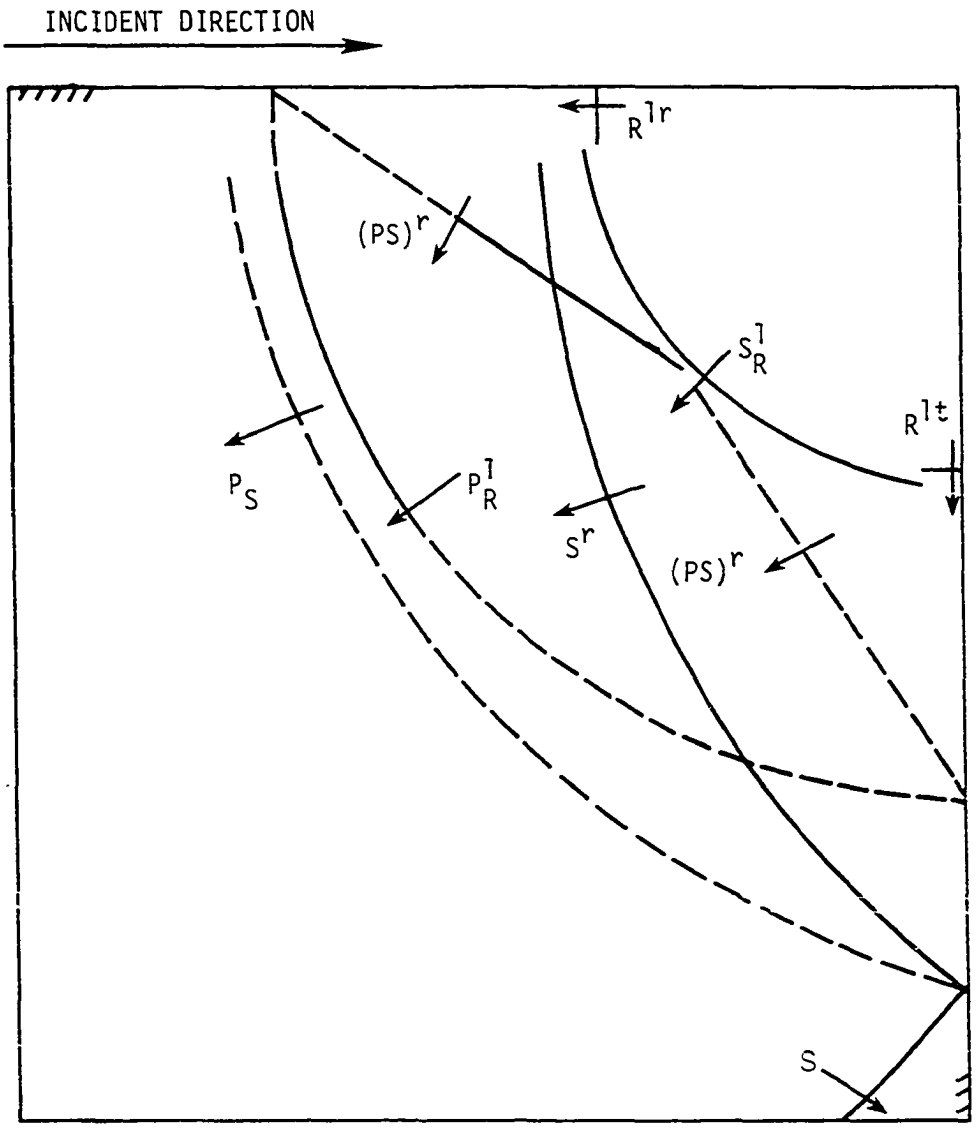

Figure 4.2. Waves expected when S- and R-waves interact with a corner:
(—) waves present in dynamic photoelasticity results
(--) waves absent in dynamic photoelasticity results [77]

energy goes into the transmitted wave than into the reflected wave. Two additional waves can be identified. The P_R^1 is a weak indication of the longitudinal wave generated at corner 1 upon interaction of the incident Rayleigh wave with the corner. The S_R^1 is the shear wave generated by the same mechanism. The reflection of the original shear wave from the right hand edge is shown as S^r. It should be, and is, just ahead of the waves R^{1r} and S_R^1.

Based on knowledge of mode conversions of longitudinal and shear waves [4,5], a scheme for expected mode conversions upon interaction of such waves and Rayleigh waves with a quarter plane can be postulated. The basic idea is that when a wave interacts with a boundary, inclusion or defect of one kind or another, it is capable not only of reflecting but also of generating other types of waves. Figure 4.2 depicts an idealized mode conversion scheme for the interaction of the incident Rayleigh and shear waves with a 90° corner (quarter plane). It is expected that from the reflection of the incident shear wave, S, a longitudinal wave, P_S, and a reflected shear wave, S^r, will be observed. Instead, only the simple reflection of the S-wave can be identified on Fig. 4.1. From the interaction of the incident Rayleigh wave, R, and the corner, it is expected to observe the reflected R^{1r} and the transmitted R^{1t}. Rayleigh waves as well as a longitudinal P_R^1 and a shear S_R^1 wave accompanied by their respective Von Schmidt $(PS)^r$. Instead, only portions of the P_R^1 and S_R^1 can be observed and possibly part of the $(PS)^r$. The reasons why some of the waves in Fig. 4.2 are absent in the photograph of Fig. 4.1 are either that some of the expected waves just do not exist or that the resolution of the optical system is too low to measure them. In either case they contain little or no energy at all.

Similar photoelastic studies [14,77] dealt with the resulting waves that arise when a Rayleigh wave running down the side of a slot reaches the tip of the slot. Figure 4.3 is a photograph of the wave field after such an interaction. The incident Rayleigh wave approached the slot tip (2) from the right along the lower edge of the slot. Upon reaching the tip, some of the energy reflects as the R^{2r} wave. A large amount of energy mode converts to a shear wave, S_R^2, which propagates into the

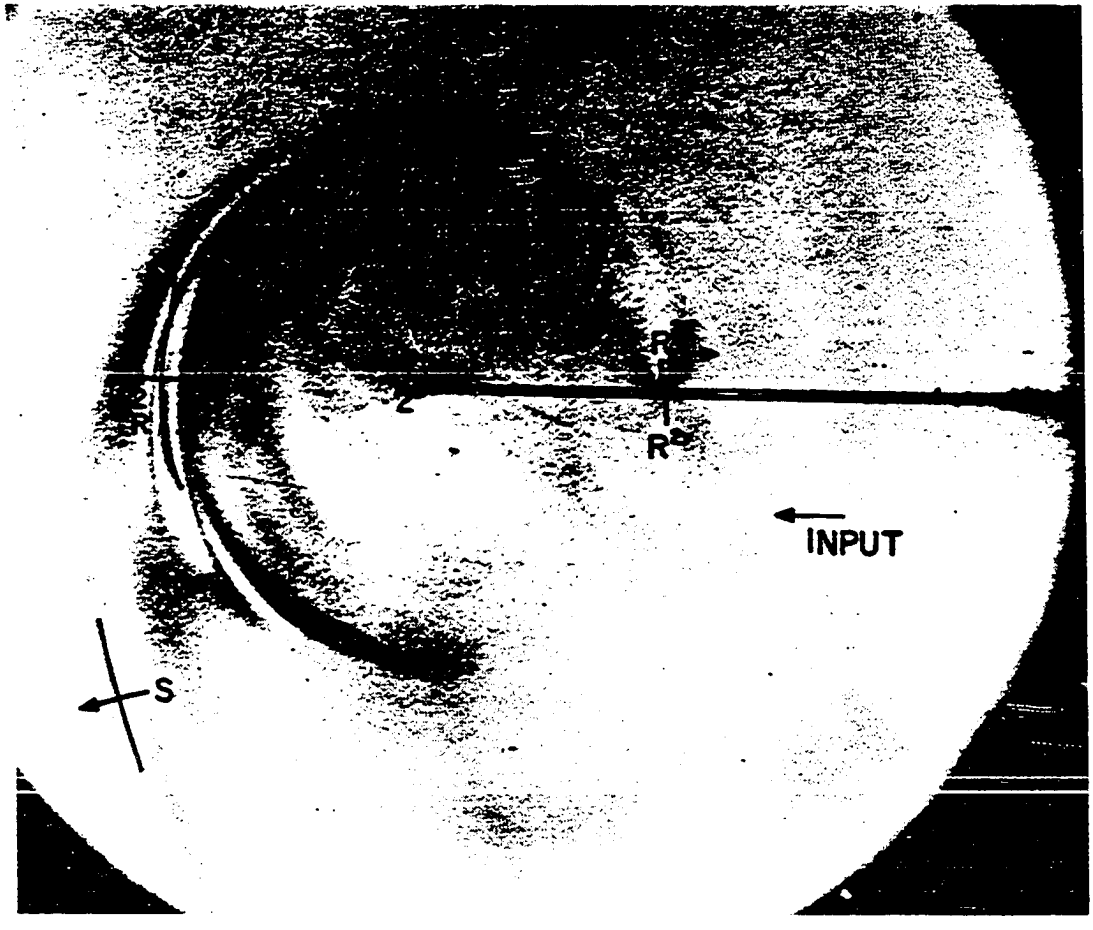

Figure 4.3. Interaction of a Rayleigh wave with the tip of a slot [77]

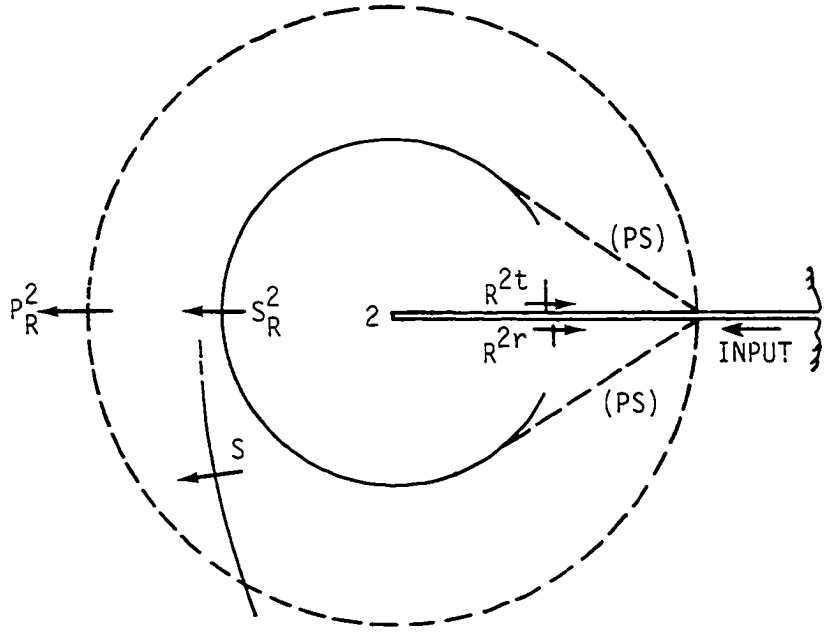

Figure 4.4. Waves expected when an incident Rayleigh wave runs off the end of a slot [77]

material along a cylindrical wave front. The rest of the energy of the incident R-wave proceeds around the tip of the slot which is narrower than the shortest wavelength of the Rayleigh wave so that it behaves as a point source. The R^{2t} then propagates along the other side of the slot. This behavior is predicted from theory [3]. It can be observed that the magnitude of the fringe order, which is proportional to the shear stress in the plane of the model, is high in the S_R^2 and small in the R^{2r}. The transmitted R-wave, R^{2t}, is stronger than the reflected. one R^{2r}. The method by which the incident wave was generated, a small explosion, also creates an incident S-wave. This S-wave can be observed, in Fig. 4.3, leading the S_R^2 shear wave.

Intuitively, the manner in which a Rayleigh wave should respond to the interaction with a tip can be represented as in Fig. 4.4. After reaching the tip of the slot, the energy in the incident Rayleigh wave could generate a longitudinal wave, P_R^2, as well as a shear wave, S_R^2. Of those only the shear wave is evident in the photograph of Fig. 4.3. The absence of the Von Schmidt waves (PS) is indicative of the non-existence of the P-wave as well. Only the wavefronts represented by the solid lines in Fig. 4.4 can be identified on the photograph of the stress field.

Rayleigh wave interactions with step changes in the elevation of a free surface were studied by Dally and Lewis [16]. Some of their photoelastic pictures are presented in Fig. 4.5. Even though this information was acquired long ago, it is not until now that a Rayleigh wave interaction mechanism is being developed and tested which accounts for most of the transmitted and reflected Rayleigh waves. This mechanism is discussed in the following two sections of this dissertation and is the motive of all the research presented. Figure 4.5a shows a typical incident Rayleigh wave, R, with maximum fringe order N = 4, which shows as a teardrop pattern located just below the surface and half way between the surface fringe orders marked as N = 4 and N = 3. This wave is preceded by a longitudinal (P), a shear (S) and a, not separable yet, Von Schmidt wave (PS). It can be observed that the Rayleigh wave stresses penetrate to about 1-1/2 inches from the surface. The grid spacing in

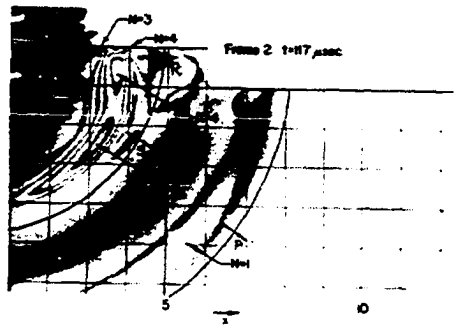

a. Incident waves

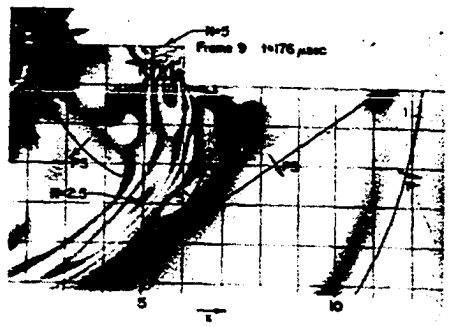

b. Interaction

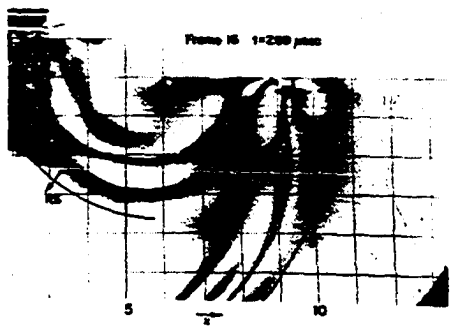

c. Reflection and Transmission

Figure 4.5. Interaction of a Rayleigh wave with a step [16]

these photographs is 1 inch (25.4 mm). The step is one inch high; therefore, the deeper portions of the Rayleigh wave interact at the lower surface. Figure 4.5b shows the reflected and transmitted Rayleigh waves from the quarter plane interaction at the top corner (90°) of the step. In addition, there is another Rayleigh wave already identifiable along the lower surface. This comes from the deeper portions of the incident wave. The complete group of transmitted waves is depicted in Fig. 4.5c. Dally and Lewis [16] observed that the first or leading R-wave propagating along the lower level of the step (Fig. 4.5c) is broader spatially than the one immediately following it. At that time this did not appear to have any significance. It is, in fact, the basis of the research reported here.

Some work has also been done to study the effect of wedge-like corners (<90°) on Rayleigh waves [15]. This work may have some significance in the NDE of inclined slots. Singh [77] did some experimental work with such slots, but much remains to be done.

A reasonably large amount of research has been conducted by means of photoelastic studies on Rayleigh wave interaction with slots normal to the surface [17,75-77]. Figure 4.6 is a sequence of images of the interaction of a surface wave with a slot 10 mm deep. On Fig. 4.6a, all the components of the incident wave can be identified. They are, in order, the P-, PS-, S- and R-waves. Zachary, et al. [75], Singh, et al. [76] and Singh [77] collaborated in interpreting the fringe photographs of the complete interaction of the incident waves with the slot. They determined what was believed to be the correct progression of the various R-waves generated upon the interaction with the slot. These are the reflected and transmitted Rayleigh waves, R^{1r} and R^{1}, respectively, as shown in Fig. 4.6b on the right side of the slot. In addition, another perturbation which comes from the deeper portions of the incident Rayleigh wave is shown to be making its way on the opposite side of the slot. This is believed to be a cut-off or low frequency Rayleigh wave. Figure 4.6c depicts all the waves transmitted and reflected after the interaction. The waves shown in the figure as "R^{2t} cut-off" should

a

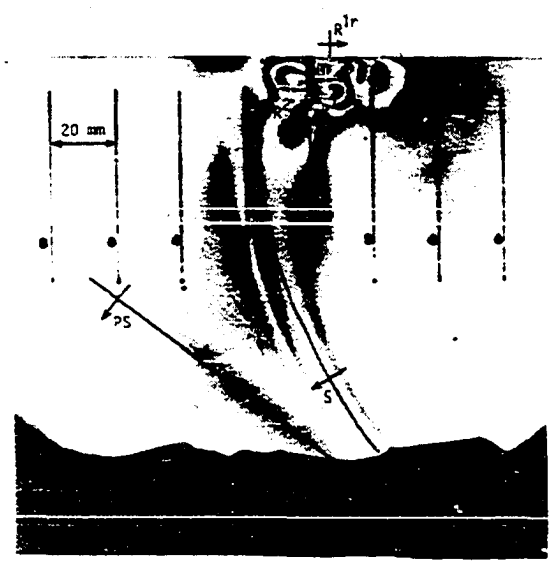

b

Figure 4.6. Interaction of a Rayleigh wave with a slot [14]
a. Incident waves
b. Interaction

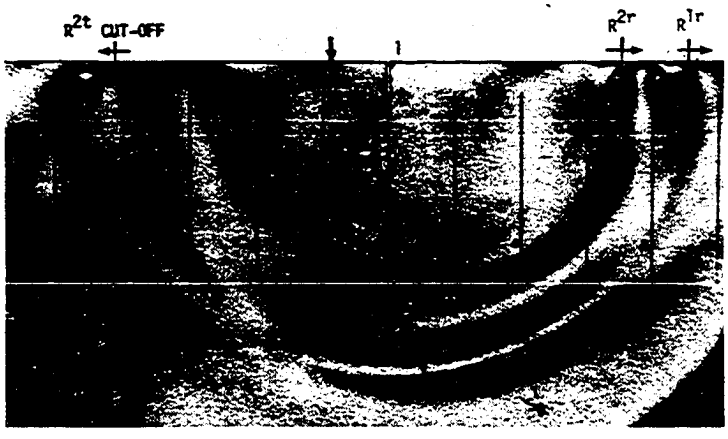

c

Figure 4.6. (cont.)
c. Reflected and transmitted waves

actually be a combination of the cut-off, R^2, and transmitted, R^1, Rayleigh waves which, because of the poor resolution of the optical system, cannot be separated.

All the results from the aforementioned photoelastic studies of Rayleigh wave interaction with various features helped in the development of the novel technique herein presented. The following sections discuss a postulate for the interaction of Rayleigh waves with slots which then evolves into a testing technique for sizing open surface cracks.

Proposed Interaction Mechanism for a Rayleigh Wave and a Slot

Careful observation of photoelastic data, similar to those presented in the preceding section of this chapter, led to the proposed interaction mechanism for Rayleigh waves to be discussed. Appendices

E and F of this dissertation include a thorough discussion of the basic mechanism.

After understanding the basic interaction mechanism explained in Appendixes E and F, it remains to be shown how the leading Rayleigh wave, that shows in a typical time scan, is generated (refer to Figs. E.7, F.4-F.9). Figure 4.7 depicts the interaction scheme of the incident Rayleigh wave. For simplicity, one could think of the slot length "d" to be deeper than the penetration of the incident wave so as to overlook momentarily the interaction of the deeper portions of the Rayleigh wave with the slot tip.

One can follow the AFR^{i} (All Frequency Rayleigh--incident) propagating along the surface until it reaches corner "1" in Fig. 4.7. At this instant it undergoes mode conversion as presented in Fig. 4.1. In Fig. 4.7 the reflected Rayleigh wave and all the bulk waves have been left out and only the Rayleigh wave that propagates along the face of the slot is depicted. Upon reaching the tip of the slot, point 2 in Fig. 4.7, the incident Rayleigh wave turns the tip and in the process sheds a strong shear wave (refer to Fig. 4.3). It then proceeds along the opposite face of the slot until it reaches corner "3" where it interacts in the same fashion as discussed for corner "1". This run-around-the-slot Rayleigh wave can be used as a Reference wave. The shear that was shed by the Rayleigh wave at the tip of the slot travels to the opposite side of the specimen (distance h-d) and back to the slot tip where it reconverts on both sides of the slot to Rayleigh waves grazing the surface. These Rayleigh waves have been named by the author RSR which stands for Reconverted Shear Rayleigh wave.

The idea of using the time delay between these two waves, the run-around Rayleigh and the RSR wave, is not new [47]. Although the aim of this dissertation is the use of the frequency information in the transmitted signals, it is necessary to check the accuracy of the statements by some known technique. For this reason the time delay technique just discussed, as a part of the interaction mechanism between a Rayleigh wave and a slot, will be used.

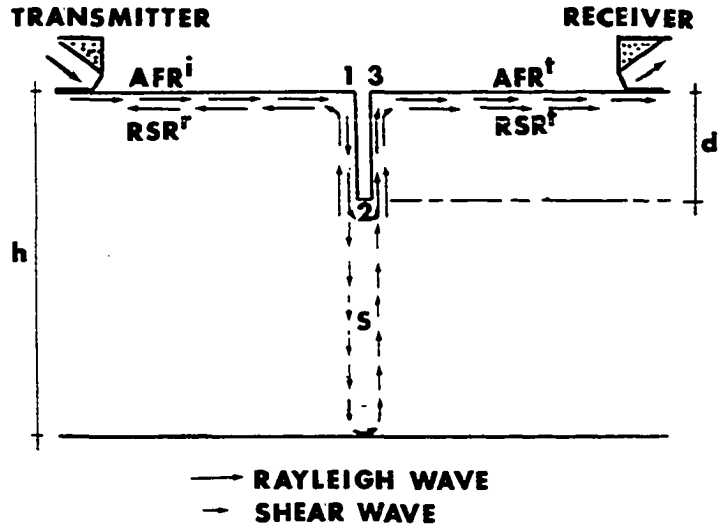

Figure 4.7. Schematic representation of the generation of the RSR wave

Nature of Transmitted Signals in a Typical Time Scan

The interaction patterns and proposed transmitted waves discussed in the preceding sections were obtained from photoelastic information and from research performed in other places and previously referenced. It is necessary, though, to check the nature of the observed waves in a typical ultrasonic scan and see if they, indeed, behave or generate in the order that has been assumed.

To achieve this goal, a sequence of experiments were planned on a piece of structural steel 1018 as shown in Fig. 4.8. First, the depth of the slot will be obtained by the time of travel method discussed above. Second, a frequency study of the waves will be conducted to observe any deviations from the proposed interaction mechanism. Third, the nature of the LFR, leading Rayleigh waves, must also be fixed. One must remember that thus far every wave has been assigned a name based on what the author believes they should be and not on any factual data.

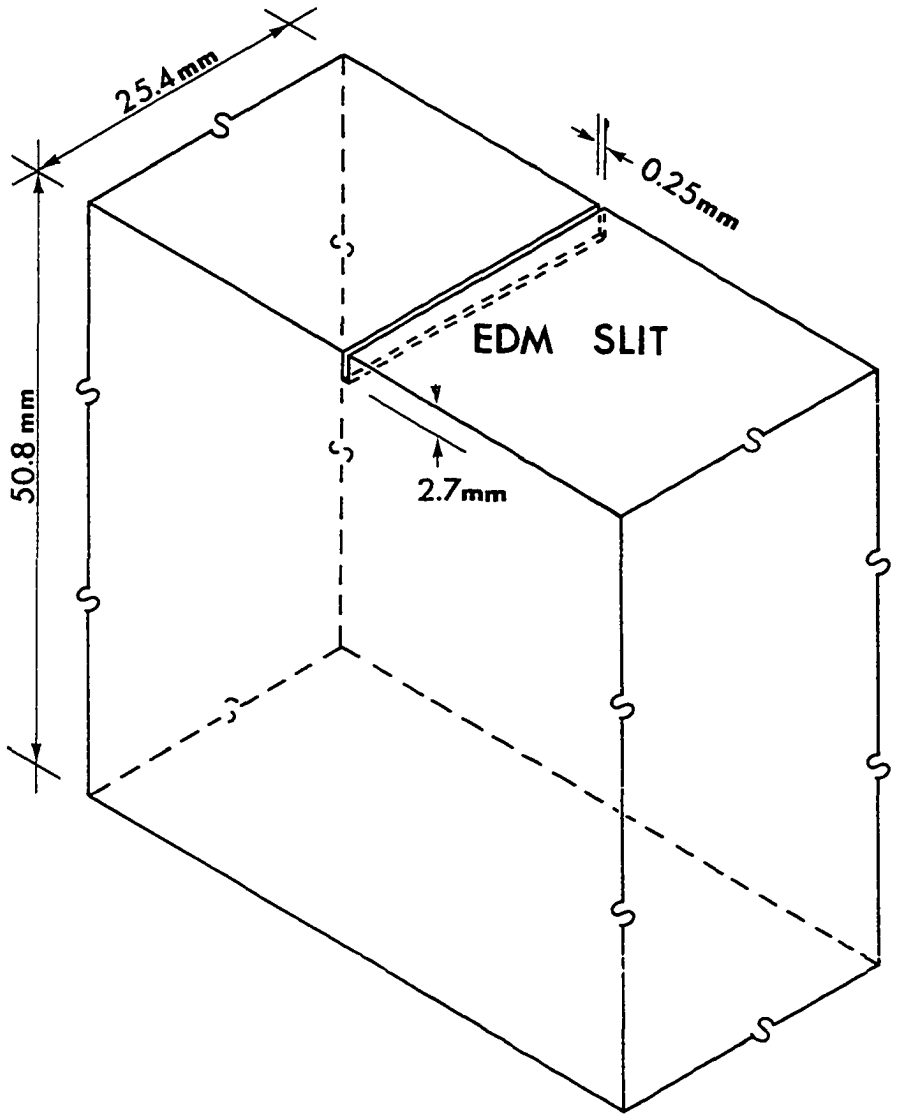

Figure 4.8. Typical steel specimen dimensions for ultrasonic tests

The experiments were conducted with two 5.0 MHz broadband P-wave transducers mounted on 90° lucite wedges. The angle of the wedge (90°) indicates the angle of propagation, from the normal to the surface, of the inhomogeneous waves that give rise to the Rayleigh wave. The mechanism for the generation of the Rayleigh wave is discussed further in Chapter 5.

By means of the utility program USPO (Chapter 5, Appendix C), one can then sample and process the signals displayed by a sampling scope (Chapter 5). Typical scanned signals look as depicted in Fig. 4.9. Figure 4.9a depicts all the signals received from time zero (main burst) up to 100μs. Within this span one can observe what the author identifies as the AFR and the LFR wave group, the RSR wave, and a far end reflection of the specimen tested. The time difference between the AFR and the RSR should be twice the time needed for a shear wave to travel from the slit tip to the opposite side of the specimen. This time is found to be about 29.4μs. Knowing the shear wave velocity in this material to be 3.26 mm/μs, as given in Table 4.1, one can readily find that the path between the slit tip and the opposite face of the specimen is 1/2(29.4μs x 3.26 mm/μs) = 47.9 mm. Knowing also that the depth of the specimen is 50.8 mm, one can then conclude that the slit should be 50.8 - 47.9 = 2.9 mm long which agrees somewhat with the actual length of 2.7 mm. Therefore, one can conclude that it is very likely that this portion of the mode conversion mechanism occurs as predicted. The small prediction error found for the depth of the slit is the major reason why time of travel methods are not used for shallow cracks when reliable measurements are needed. Figures 4.9b and 4.9c represent an expanded view in time of the LFR + AFR and the RSR waves, respectively.

By making frequency spectrum comparisons of the various waves shown in Fig. 4.9, it is possible to determine which is the most likely source of the energy that generates them. To achieve this it is necessary to obtain a reference spectrum, which is selected to be that of a Rayleigh wave traveling along a flat surface with no scatterer between the transmitter and receiver transducer. Figure 4.10 represents a typical time scan of such a wave and its frequency spectrum. It can be observed that

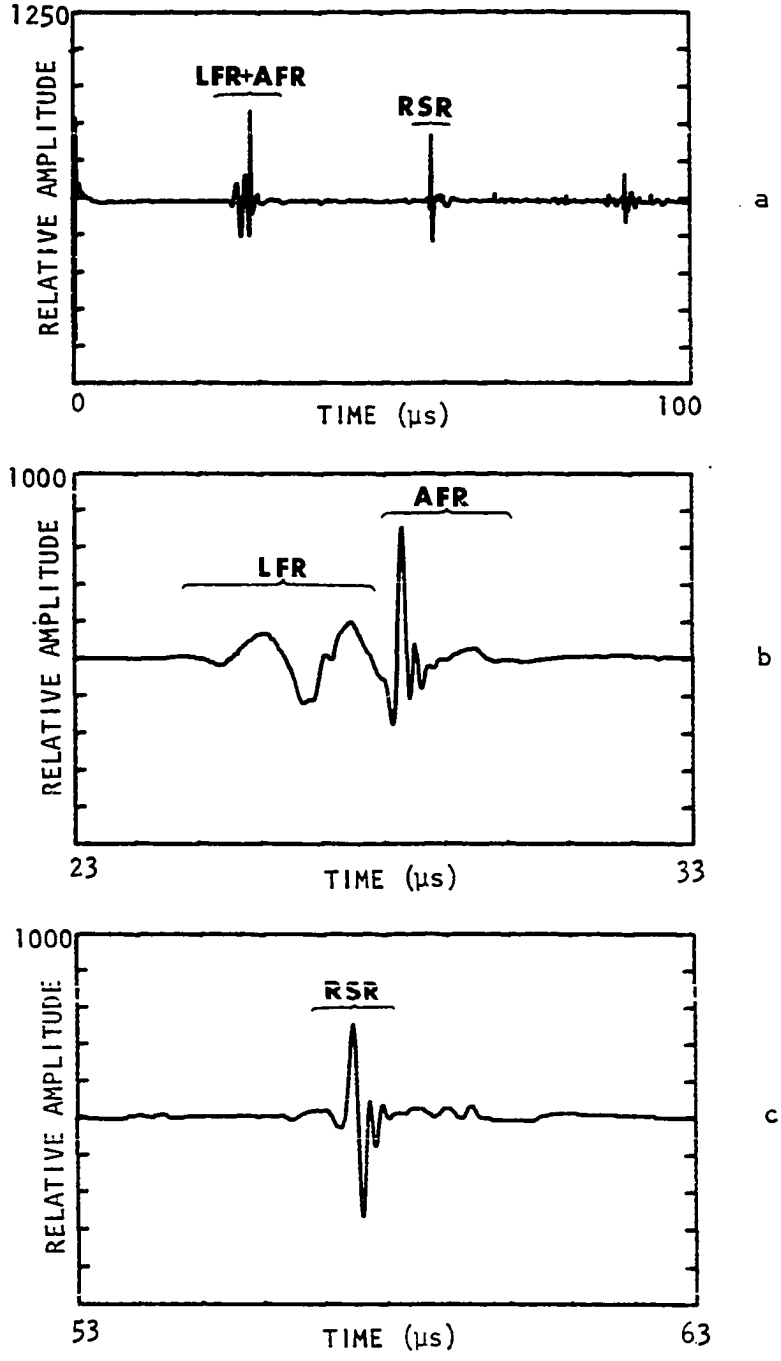

Figure 4.9. Time scans from a 2.7 mm deep slot in a steel specimen
a. Scan of all waves received
b. Expansion of the LFR and AFR portion of scan in "a"
c. Expansion of RSR portion of scan in "a"

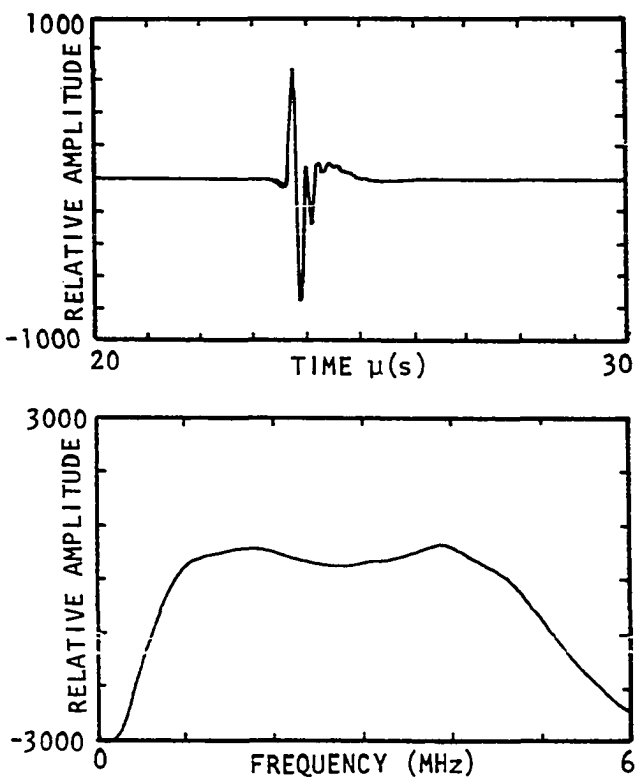

Figure 4.10. Reference Rayleigh wave
a. Time scan
b. Frequency spectrum

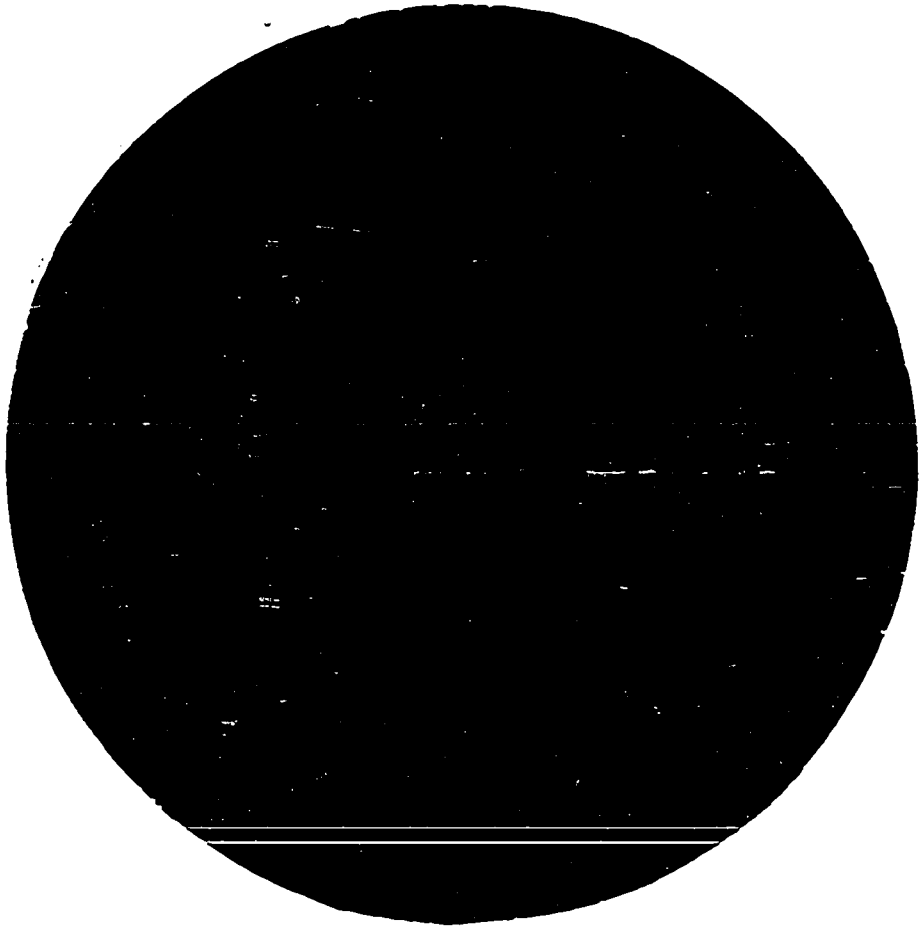

Figure 4.11. Frequency spectrums of the waves received upon interaction of a Rayleigh wave and a 2.7 mm slot
a. Spectrum of the AFR + LFR combined
b. Spectrum of the LFR portion of the time scan only
c. Spectrum of the AFR portion of the time scan only
d. Spectrum of the RSR portion of the time scan only

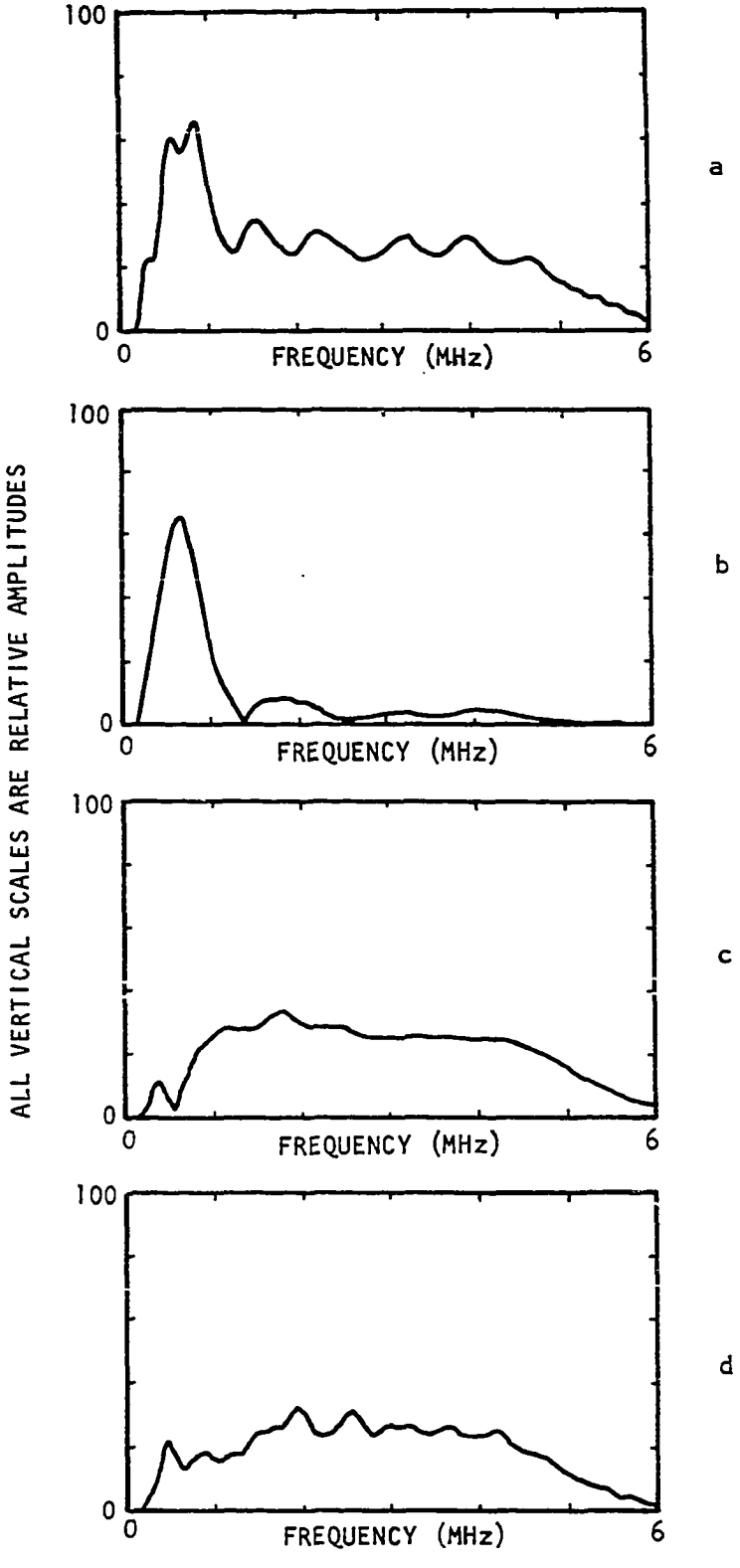
100
0
0
FREQUENCY (MHz)
6
a
100
0
0
FREQUENCY (MHz)
6
b
100
0
0
FREQUENCY (MHz)
6
c
100
0
0
FREQUENCY (MHz)
6
d
ALL VERTICAL SCALES ARE RELATIVE AMPLITUDES

the spectrum covers all frequencies from about 0.5 MHz to about 5.5-6.0 MHz. This allows a penetration of 0.5-6.0 mm into the material.

It is possible now to compare, qualitatively, the spectrum of the reference Rayleigh wave (Fig. 4.10b) with those of the other waves in Fig. 4.9. Figure 4.11a represents the frequency spectrum of all the waves in Fig. 4.9b. Knowing that this package of waves is part of the transmitted signals, after interaction of the reference Rayleigh wave with the slot, one can search for differences between Fig. 4.10b and 4.11b. There is in Fig. 4.11b a biased shift to the low frequency side of the spectrum. The modulations in the spectrum are created by the superposition of the FFT of two or more waves out of phase. Figure 4.11b represents the frequency spectrum of the LFR wave only (see Fig. 4.9b). It is evident that the LFR is composed mainly of low frequency components, which agree with the idea that it is generated by the deeper (low frequency) portions of the incident Rayleigh wave. Figure 4.11c is the frequency spectrum of the AFR, or run-around-the-slot Rayleigh wave. It can be observed that it contains a spectrum similar to that of Fig. 4.10b; and thus leads one to think that it, indeed, comes from the run-around-the-slot Rayleigh wave. Finally, one can also study the spectrum of the RSR wave, Fig. 4.9c, as depicted in Fig. 4.11d. Although very modulated, probably due to scattering of the shear wave as it travels to the opposite side of the specimen, it does show a rather broad spectrum. This is indicative that the wave may, indeed, have been generated by the turning of the run-around-the-slot Rayleigh wave at the tip of the slot.

The fact that the waves studied in Fig. 4.9 seem to match the general interaction pattern presented in this dissertation does not guarantee that they are Rayleigh waves. A simple experiment confirms that the waves observed are Rayleigh waves.

By using a similar specimen to that shown in Fig. 4.8, in this case with the slot being 2 mm deep by 0.8 mm wide, one can set up the transmitting and receiving transducers at fixed intervals, say 20 mm before and after the slot, respectively, and then at a further distance

apart, say 50 mm for the receiving transducer, to pick up any time changes between waves. Figure E.7 depicts the time scans of such an experiment. Figure E.7a presents the case with the transducers placed 20 mm on each side of the slot. The time to wave A from time zero is given as 37.5μs. In Fig. E.7b, with the receiver transducer placed 50 mm from the slot, the time to wave A is given as 48.5μs. The time difference between such waves should be that required by a Rayleigh wave to travel the additional 30 mm path which, by using the measured wave velocities as given in Table 4.1, should be 30/2.96 = 10.1μs. The time measured yields 11μs. Although there is some error in the measurement of the time difference, the implication of assuming a faster wave other than a Rayleigh is to increase the error even more. Therefore, one can conclude that wave A is, indeed, a Rayleigh wave. Also, because there is no time drift between waves A and B, wave B must also be a Rayleigh wave. Similarly, one could imply the same about wave A1. Instead, an additional experiment which was performed on an open crack in a steel specimen is presented because it provides a clear understanding of the behavior of the wave (A1).

Figure 4.12 represents various time scans obtained from the interaction of a Rayleigh wave with open cracks. The specimen tested was made out of A387 steel and contained a fatigue crack 5.05 mm deep grown by loading the specimen cyclically on an MTS machine. The sequence of samples (a-n) was obtained by gradually machining thin layers from the top of the specimen. This yielded a series of cracks of identical shape and roughness but various depths. LFR and AFR waves are clearly identified in Fig. 4.12a, which is the sampling of the transmitted signals from the deepest crack. As the crack becomes shallower, Fig. 4.12b-g, it is possible to observe how the LFR starts to overlap with the AFR. Not only that, the LFR picks up amplitude while the AFR loses it. This behavior is in accordance with the predicted origin of the LFR. As stated earlier, the LFR is generated by the deeper interaction of the incident Rayleigh wave. If this interaction occurs closer to the surface, it must contain higher frequencies, and, consequently, more energy and amplitude. The opposite holds true for the Rayleigh wave (AFR) that

Figure 4.12. Time scans of waves received upon interaction of a Rayleigh wave and various depths open fatigue cracks
a. 5.05 mm deep
b. 3.02 mm deep
c. 2.52 mm deep
d. 2.01 mm deep
e. 1.5 mm deep
f. 1.27 mm deep
g. 1.14 mm deep
h. 1.02 mm deep
i. 0.89 mm deep
j. 0.76 mm deep
k. 0.64 mm deep
l. 0.57 mm deep
m. 0.13 mm deep
n. No crack (reference)

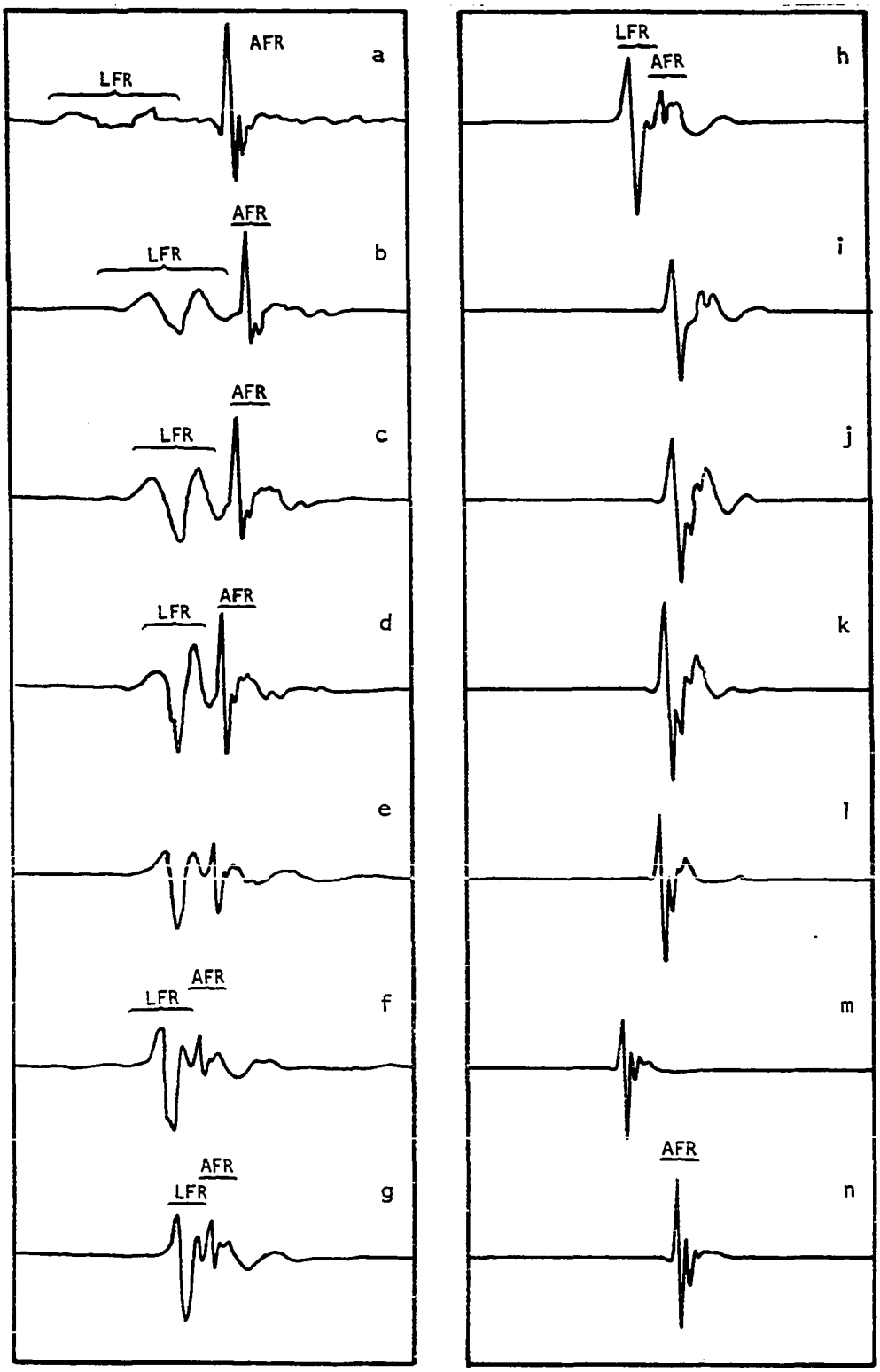
LFR
AFR
a
LFR
AFR
b
LFR
AFR
c
LFR
AFR
d
e
LFR
AFR
f
LFR
AFR
g
LFR
AFR
h
i
j
k
l
m
AFR
n

travels around the crack. As the interaction point moves closer to the surface, less energy there is available. Finally, in Fig. 4.12n, one can observe that what used to be the LFR becomes the AFR when there is no scatterer in its path.

One can conclude then that, by simple inspection of the waves generated in the interaction of a Rayleigh wave with a surface breaking defect, all the transmitted waves are Rayleigh waves and that the LFR wave is, indeed, the result of a diffraction mechanism at the tip of the crack.

Velocity of Acoustic Waves in Steel

Wave velocity is a parameter involved in almost every acoustic problem. In this research, the velocity of a Rayleigh wave in steel has been used to transform all frequency data into wavelength data. This transformation is achieved by using a relationship such as given by Eq. (4.1).

$$\lambda = v/f \tag{4.1}$$

where

λ = wavelength (mm)

v = wave velocity (mm/μs)

f = wave frequency (MHz).

Acoustic wave velocities can be obtained for any material by using analytically derived expressions such as given by Eq. (4.2) [1].

$$v_\ell = \left[\frac{E}{\rho} \cdot \frac{1-\nu}{(1+\nu)(1-2\nu)}\right]^{1/2}$$

$$v_s = \left[\frac{E}{\rho} \cdot \frac{1}{2(1+\nu)}\right]^{1/2} \tag{4.2}$$

$$v_R \approx \frac{0.87 + 1.12\,\nu}{1+\nu} v_s$$

where

v_ℓ, v_s, v_R = longitudinal shear and Rayleigh wave velocities (m/sec)

ν = Poisson's ratio

E = Young's modulus (GPa)

ρ = Mass density (kg/m^3).

It was decided, though, to use in this research the actual measured velocities from typical test specimens. Simple echo tests were run on 1018 steel and A387-74A-Gr.22-Cl.2 steel. Also, by using measured values for the properties of these steels such as $\nu = 0.285$, E = 207 GPa, and $\rho = 7{,}878\ kg/m^3$, it was possible to compute the theoretically predicted values. Table 4.1 shows the obtained values.

Table 4.1. Acoustic Velocities in Steel

Steel	Experimentally Measured Velocities (mm/μs)		
	v_ℓ	v_s	v_R
1018	5.85	3.23	2.96
A387	5.90	3.24	2.96
Theoretical	5.83	3.20	2.96

There is remarkable agreement between the experimentally measured velocities and the theoretical velocities. The Rayleigh wave velocity (v_R) which is used mostly throughout this dissertation will be taken as 2.96 mm/μs for all calculations.

Experimental Design

This chapter has been devoted to the presentation of some photoelastic and ultrasonic studies of the interaction of Rayleigh waves with a slot. Also, a generalized interaction scheme has been put forth which will be used to determine the potential in the spectroscopic method suggested (refer to Appendixes E and F).

Tests will be run on various kinds of defects such as steps, square-corners-slots, rounded thin slits, and fatigue cracks. The purpose is to determine if the method can be applied equally well to slots and cracks. If successful, it should yield a very powerful tool for the characterization of flaws. Another desirable characteristic for the suggested technique is that it be insensitive to most operational variables such as that encountered in typical field situations. Tests will be performed to observe the effects caused by variable coupling layers during test, amount of damping in system, weld splatters between transducers, transducer frequency, slot inclination and others.

Before presenting the results from the tests performed, the equipment and signal handling capabilities will be discussed.

CHAPTER V. EQUIPMENT AND SIGNAL PROCESSING

Equipment

The ultrasonic data studied in this dissertation were obtained by means of a simple microprocessing system put together at Iowa State University by Professors Schmerr and Burger as part of a National Science Foundation Grant ENG 76-06970. Figure 5.1 depicts the layout of the system.

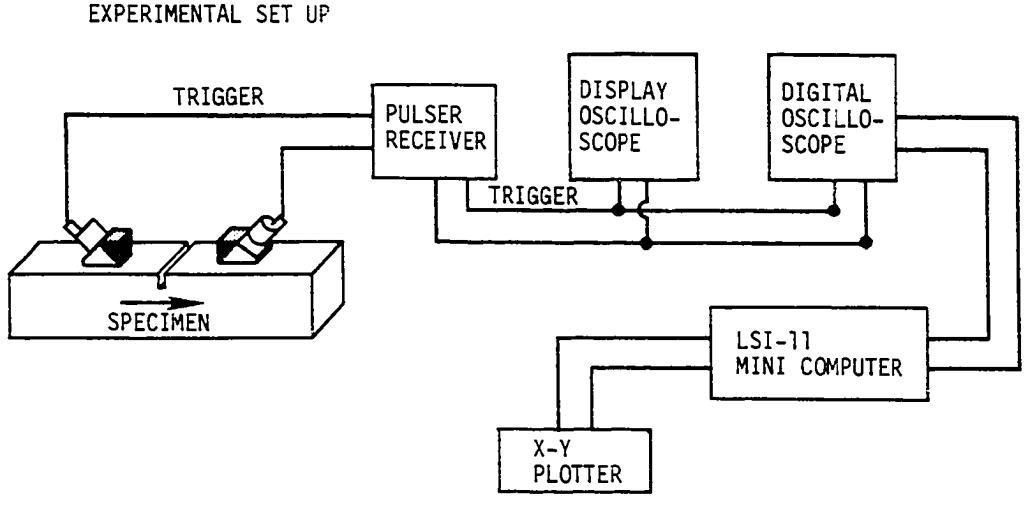

Figure 5.1. Experimental set up for ultrasonic tests

The pulser-receiver unit was used to generate repetitive pulses of energy about 0.5μs in duration. The pulses, about 100 volts in amplitude, were set at a repetition rate of eight on the generator which yielded a burst of energy every 880μsec. Figure 5.2 depicts the pulser-receiver (Model 5052 PR) and the gated peak detector (Model 5052 GPD-2), both from Panametrics. The gated peak detector was used to select portions of the signals to be studied and to zero electronically the rest of the samples.

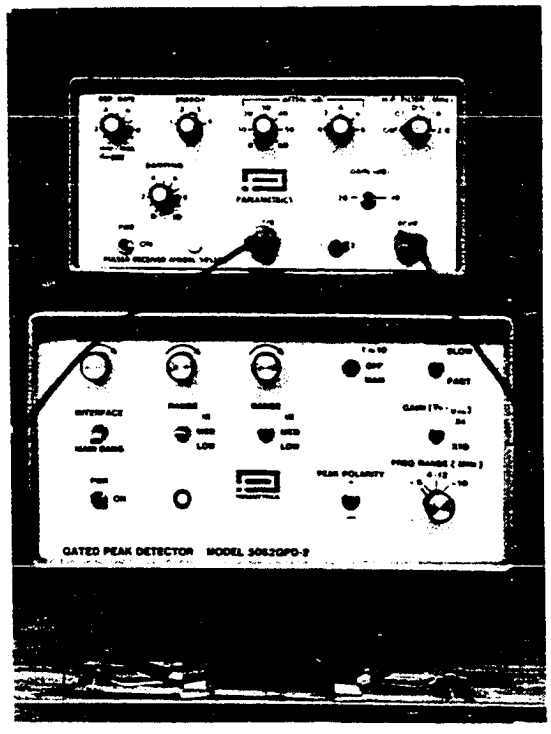

Figure 5.2. Pulser receiver and gated peak detector

The pulses generated were used to excite any of four different P-wave transducers (0.5, 2.25, 3.5 and 5.0 MHz central frequency) which consisted of a 1/2-inch lead-metaniobate piezoelectric crystal backed with pressed tungsten to increase the damping and yield a broadbanded signal. Any of these transducers could be mounted on a 90° lucite (acrylic) wedge to launch the mechanical pulse into the specimen. The 90° denomination in the wedge indicates that the wedge is used for generating surface waves which propagate at 90° from the normal to the surface. Figure 5.3 depicts the general mechanism through which this generation is accomplished and the transducer arrangement. All the transducers were acquired from a commercial house (KB-Aerotech); and they are sold to meet specific needs, in this case the generation of surface Rayleigh waves.

By following Snell's law, it is possible to verify how the Rayleigh wave is generated [5]. Knowing that the longitudinal wave velocity in the wedge material is 2.75 mm/μs (measured experimentally), that the shear wave velocity in steel is about 3.2 mm/μs, and that the minimum diffraction angle for the shear should be 90°, one can compute the incidence angle of the longitudinal wave (P) using relationship 5.1,

$$\frac{v_L}{\sin\theta_L^i} = \frac{v_S^d}{\sin\theta_{SV}^d} \qquad (5.1)$$

where

v_L, v_S - longitudinal and shear wave velocities

θ - angle of incidence or diffraction

from which one can find that the P-wave should strike the surface at an angle $\theta^i \approx 59.2°$. But the actual value is more like 67°. This means that the critical angles of diffraction of the P- and S-waves have been exceeded. Therefore, the waves reflect internally. However, the surface disturbances generate what are known as inhomogeneous waves which are phase matched at the interface to generate the sought Rayleigh wave. It can be observed in Fig. 5.3 that the apparent velocity of the P-wave on the material's surface comes out to be $v_{surf} = 2.75/\sin 67° = 2.99$ mm/μs which, indeed, approximates the velocity of a Rayleigh wave in steel. It is then the inhomogeneous waves which become the Rayleigh wave.

All tests performed in the transmit-receive mode (toggle switch on generator in position 2). This means that a second transducer, aligned with the transmitting transducer and facing it, picks up the diffracted mechanical impulses by means of a similar mounting as described above. Figure 5.4 depicts a typical testing setup on a fatigue specimen of steel A387. The received signal is sent to the sampling oscilloscope through a receiving channel in the pulser-receiver.

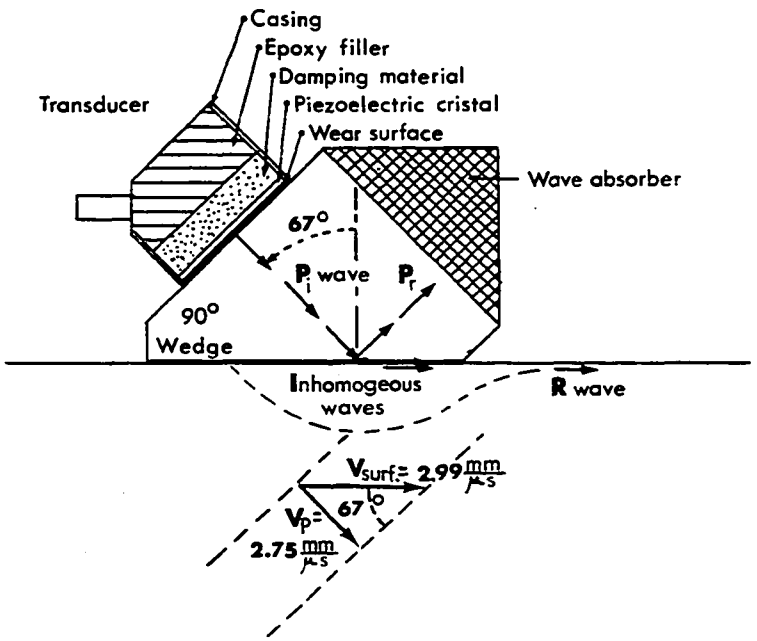

P_i, P_r	Incident and reflected longitudinal waves
V_p, V_{surf}	Longitudinal and surface wave velocities

Figure 5.3. Transducer-wedge arrangement for Rayleigh wave generation

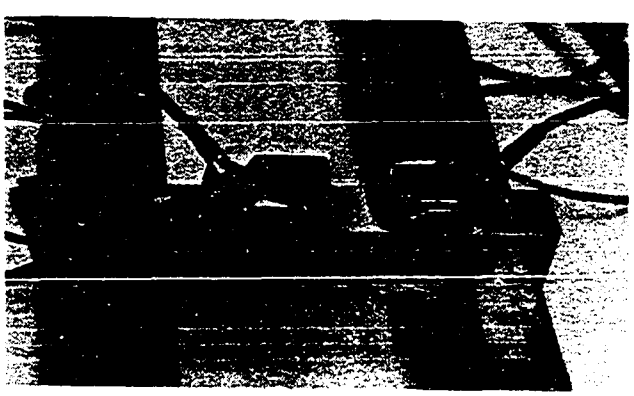

Figure 5.4. Typical transducer set up on a steel specimen

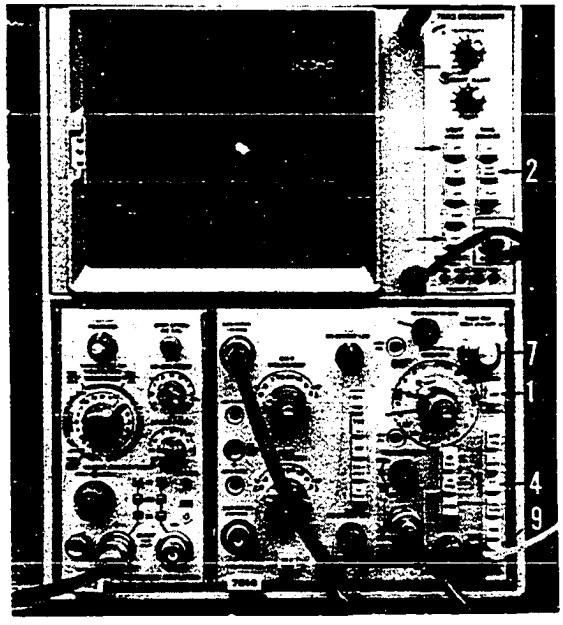

Figure 5.5. The Tektronix 7603 sampling oscilloscope

The use of a display oscilloscope (Fig. 5.1) is optional. Its only purpose is to present a continuous scan of the received signals so as to select the proper time scales to be used on the sampling oscilloscope.

The main oscilloscope used was a Tektronix 7603 with a Dual Trace Delayed Sweep Sampler-7S14 plug-in unit (Fig. 5.5). The oscilloscope was triggered internally by the sampling unit; in addition, it allowed the microprocessor to digitize the sampled data. Sampled signals already in the microprocessor can be displayed back on the oscilloscope through a 7A22 Differential Amplifier plug-in unit from Tektronix. The oscilloscope unit is the means of communication between signal generator-receiver, computer, and person running the test.

The signal handling operation with the oscilloscope occurs in two stages. First, the controls are internal so that the person running the test can fix on the screen the desired signals. Second, the controls are set to external at which time all operations must be performed from the computer terminal. For typical test situations, such as those

presented throughout this dissertation, the following steps were followed. For the initial signal selection (refer to Fig. 5.5), push in delaying button 1, vertical mode button 2, right button 3, repetition button 4, set time base 5 at 10μsec/div, set delay zero button (first dot) 6 all the way counterclockwise, turn delay time multiplier button 7 until the second moving dot on screen sits before the desired signal, select the proper delayed time setting (button 8), depress button 1 for expanded view of signal. At this time one should be able to observe the desired signal to be sampled. To give command to the computer one should now press the external button 9 and the vertical mode left button 10. At this time the signal must be handled by the computer. The basic structure of the microprocessor is shown and discussed in Appendix B, and the signal processing capabilities of the system are discussed briefly in the next section of this chapter.

Most of the information gathered by the microprocessor was plotted on paper through an X-Y plotter (Hewlett-Packard). All the results produced in this dissertation were obtained through this plotter.

Signal Processing

The heart of the signal processing system is the LSI-11 microprocessor. A complete picture of the internal hardware layout is presented in Appendix B, and the basic software needed to process data is presented in Appendix C.

After the preliminary process of selecting the desired signal to be stored in the computer, one must first make use of a general utility program developed at Iowa State University by C. Sieck and D. Heyveld for the purpose of handling ultrasonic data. The name of this program is "USPO," and it is presented in Appendix C. The basic capabilities that this program provides can be depicted as in Fig. 5.6. Upon reading the program USPO into the microprocessor, the only instructions that can be used are those provided by the program. Each instruction is actually a program or set of programs. These programs are activated by the use of macroinstructions.

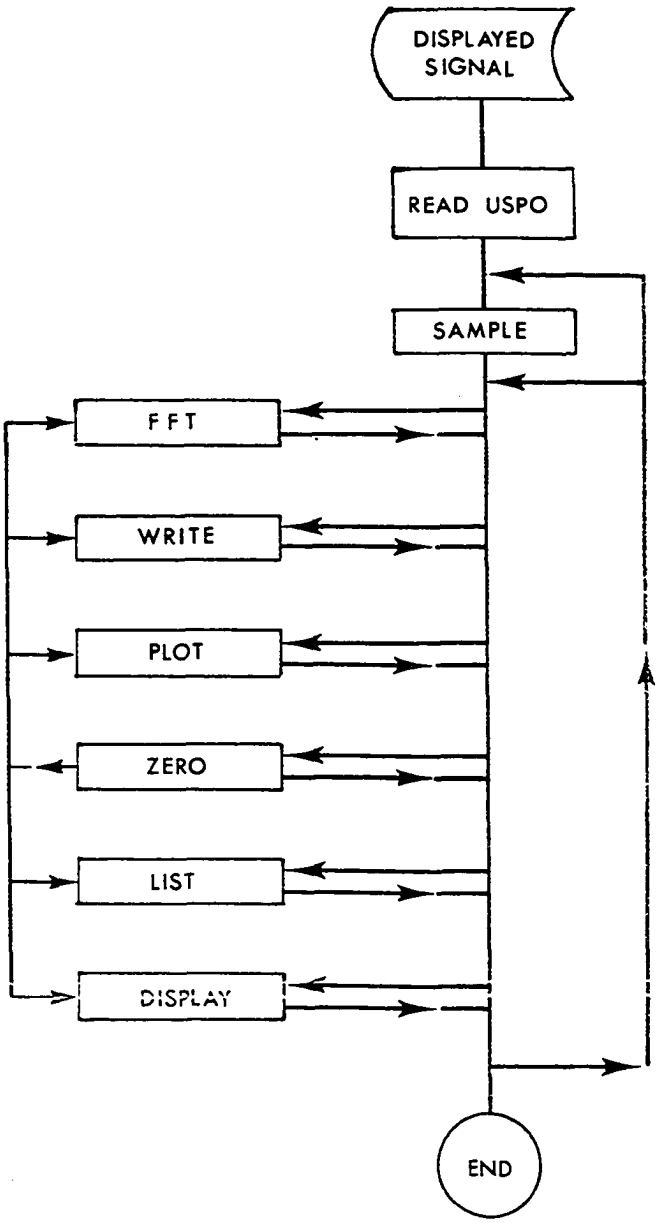

Figure 5.6. Capabilities of the USPO program

Under the USPO program one can then sample the desired signals from the oscilloscope. The data sampled are automatically stored in a memory array (OBUF). In addition, it is copied onto a file, SAMPLE.DAT, and onto the real portion of the CBUF memory array. All these files are used to perform various operations through the monitor (refer to Appendix C). The last sampled file is also protected against equipment failure.

Sampled signals can undergo a variety of operations. A Fast Fourier Transformation (FFT) of a time domain signal is used to extract the frequency information. This process allows one to display all signals in terms of their frequency and phase spectrums. This is the most desirable capability of the program, and it is the basic tool for the research presented here. There has to be a change of scales when frequency data is used instead of time data. Appendix D covers the basic process for finding such scales and Table D.1 provides some typical values such as those encountered throughout this dissertation.

Operations such as WRITE, PLOT, LIST and DISPLAY can be performed at any time to any of the existing files. The ZERO instruction is used to modify the sampled signal. This can only be done to the CBUF file, keeping always the OBUF file as sampled. The ZERO operation is very useful before performing any frequency extraction of the signals (the use of this instruction will be mentioned during the presentation of the results). The file that undergoes a ZERO operation can later be instructed by any of the other operations.

A sampled file in SAMPLE.DAT can be used for renewing a modified CBUF file to its original content or to perform any new operations. Additional capabilities to the system are added by the use of the DATA program. This program is presented in Appendix C. Although its use is more restricted to hand-fed or pre-sampled information, it does provide better plotting capabilities than the USPO program. All data sampled through USPO and to be handled by the DATA program must be written to a personal file (format XXXXXX.XXX).

It is impossible to thoroughly familiarize anyone with the systems used for this research by means of the content in this section, but it is hoped to have developed an idea of the basic system and processes involved.

CHAPTER VI. RESULTS AND DISCUSSIONS

The material presented in this chapter and in Appendixes E and F contain most of the data used to determine the validity of the proposed technique for sizing surface breaking flaws introduced earlier in this dissertation.

Interaction of Rayleigh Waves with Steps

The discussion in Chapter 4 of the photoelastic data obtained from the interaction of Rayleigh waves with steps [16] pointed out the existence of a leading "Low Frequency Rayleigh wave" (LFR). This wave was spatially wider than the "All Frequency Rayleigh wave" (AFR) that traveled along the surface of the step. This observation tends to support the argument for a frequency cut-off which is related to slot depth. So steps also become part of the study reported in this dissertation.

A typical test setup for the ultrasonic experiments on steps is shown in Fig. 6.1. The specimen was made from 1018 steel (hot rolled) one inch wide and with various sizes of steps. Two steps are shown along the top surface, and two shallower steps can be identified along the bottom edge of the plate. The two R-wave transducers were held in place with a light Plexiglass clamp. The transducers were 5.0 MHz broadband longitudinal wave transducers mounted on Lucite wedges, as described in Chapter 5. The centerline of the transducers were placed 20 mm on each side of the steps. The signal originated at the left transducer and was received at the right transducer; i.e., below the step.

The received time scans for different steps are depicted in Fig. 6.2. It is apparent from these scans that there are two well defined signals A and B. Waves A are the so-called AFR (All Frequency Rayleigh) waves which have followed the surface path down the step. Waves B lead the AFR waves; hence, they are presumed to be the LFR (Low Frequency Rayleigh) waves generated by the deeper interaction of the incident Rayleigh waves with the lower corner of the steps.

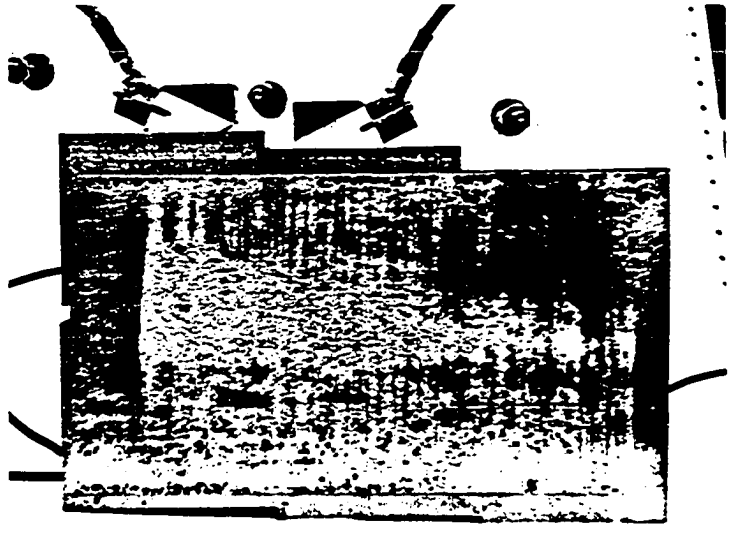

Figure 6.1. Typical setup for the study of steps using ultrasonic Rayleigh waves

It is necessary to study the frequency content of the waves in Fig. 6.2 to observe the expected shifts in frequency that contain the information about the depth of the step. To achieve this the waves must first be separated and studied independently of each other to see what information they carry. One way to separate the signals is by means of a zeroing function available in the "USPO" program discussed in Chapter 5. For example, a signal, such as the one in Fig. 6.2b, can be split into two discrete signals, Fig. 6.3, so that their frequency spectrums can be obtained independently.

The results of this signal screening process may be inaccurate due to the destruction of some of the information available at the splitting point. However, the issue here was to find major characteristics or differences in the frequency spectra of the two waves. Small perturbations in the frequency spectrum may carry additional information, but they were not pursued further at the time.

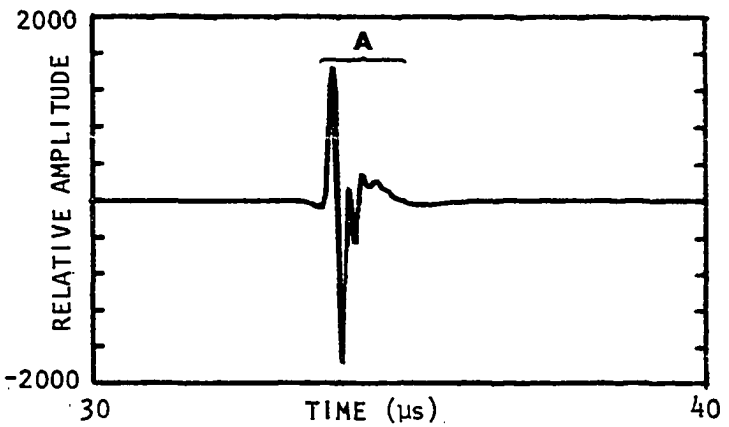

a. Reference wave (no step)

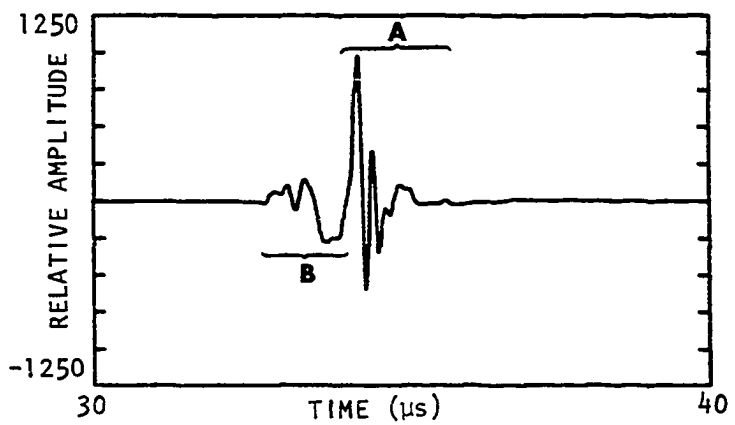

b. Step depth = 1.93 mm

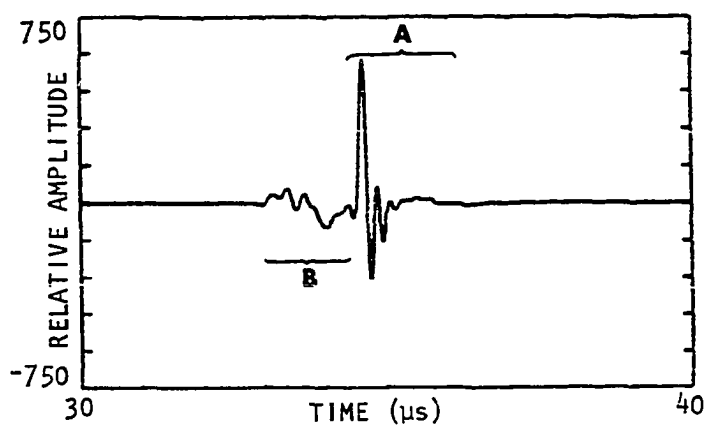

c. Step depth = 2.45 mm

Figure 6.2. Received waves upon the interaction of a Rayleigh wave and a step

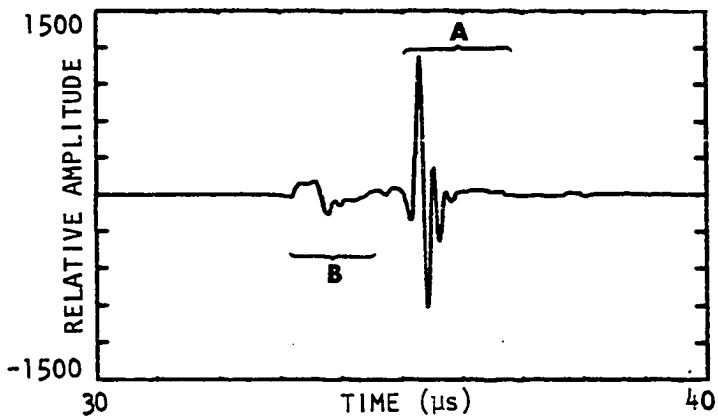

d. Step depth = 3.90 mm

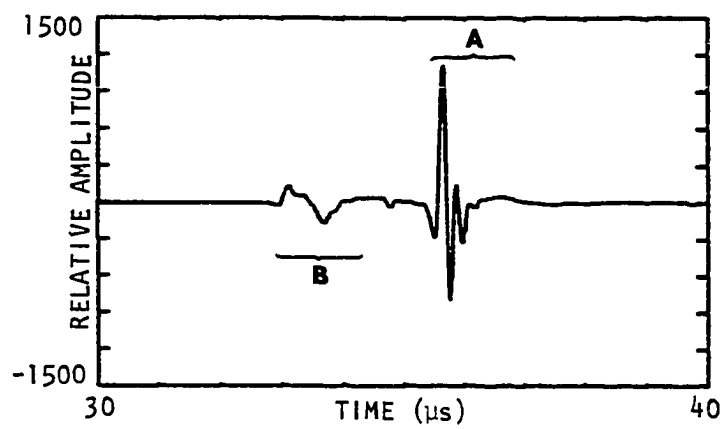

e. Step depth = 5.84 mm

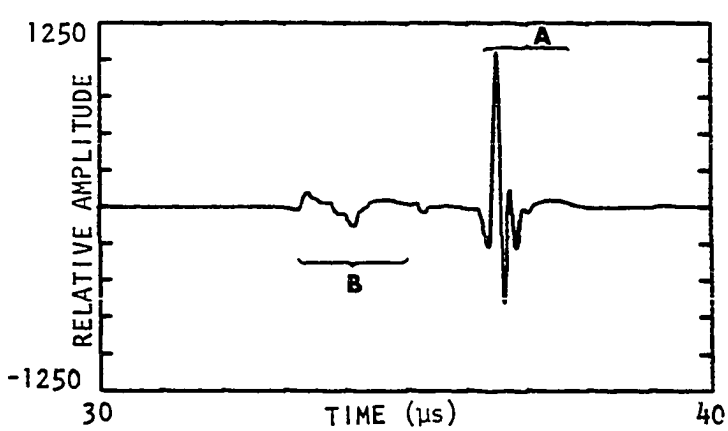

f. Step depth = 7.96 mm

Figure 6.2. (cont.)

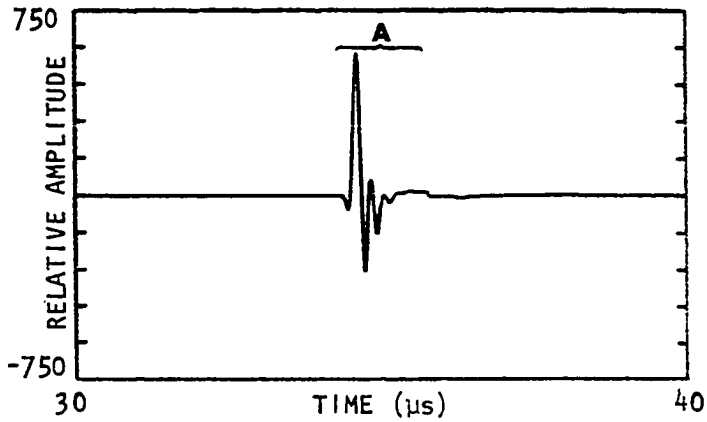

a. Zeroing leading wave "B"

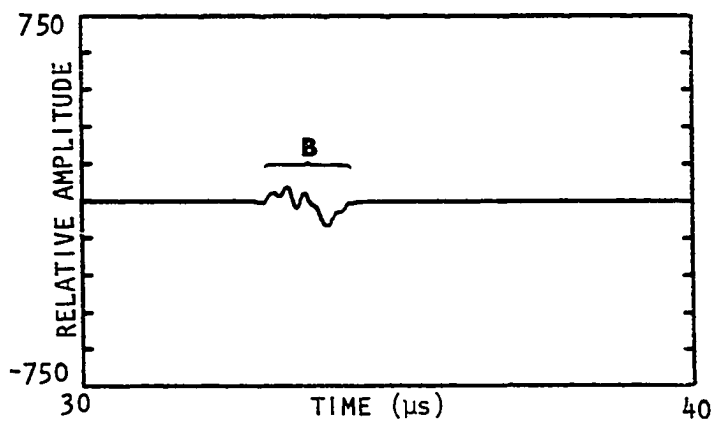

b. Zeroing the run-around-the-step wave "A"

Figure 6.3. Modified time scans upon use of the zeroing function

Figure 6.4 depicts the frequency spectrums of the leading waves, B, of Fig. 6.2. Although there is not any obvious frequency break or feature that could be associated with the depth of the step, it is possible to observe the general tendency of the waves to contain fewer high frequency components as the steps become deeper. Figure 6.4b shows the spectrum of the transmitted B wave for the shallower step (1.93 mm). The vertical scales of these plots is not the same; this must be kept in mind when comparing relative values. By comparing this spectrum with that of a reference Rayleigh wave, Fig. 6.4a, one can observe the loss of the higher frequencies. Figure 6.4c,d,e,f show the spectrums for increasingly deeper steps. By simple qualitative inspection of these spectra, one can conclude that there is a tendency for the B (LFR) waves to show a bias toward the lower frequencies as the steps become deeper.

Discussion

Although the results obtained from the steps do not yield any definite correlation between the step depths and any particular frequencies, they do tend to contain fewer high frequency components as the steps become deeper. This agrees with the idea that a discontinuity in the path of a Rayleigh, such as a step, not only induces mode conversions along the surface path of the wave, but also at the deeper levels. Also, because the higher frequencies do not penetrate as deep as the lower frequencies, the transmitted waves generated at the deeper levels are devoid of the higher frequencies.

Interaction of Rayleigh Waves with Slots

The next step in the course of this research was to determine if the shift of frequencies observed in the results from steps could also be observed in the frequency spectrums from saw-cut slots. An additional parameter that may come into play in this case is the width of the saw-cut slot. It was decided that, to avoid any more diffraction than it is necessary and to resemble better an actual flaw, the slots should be narrower in width than the shortest wavelength that could be

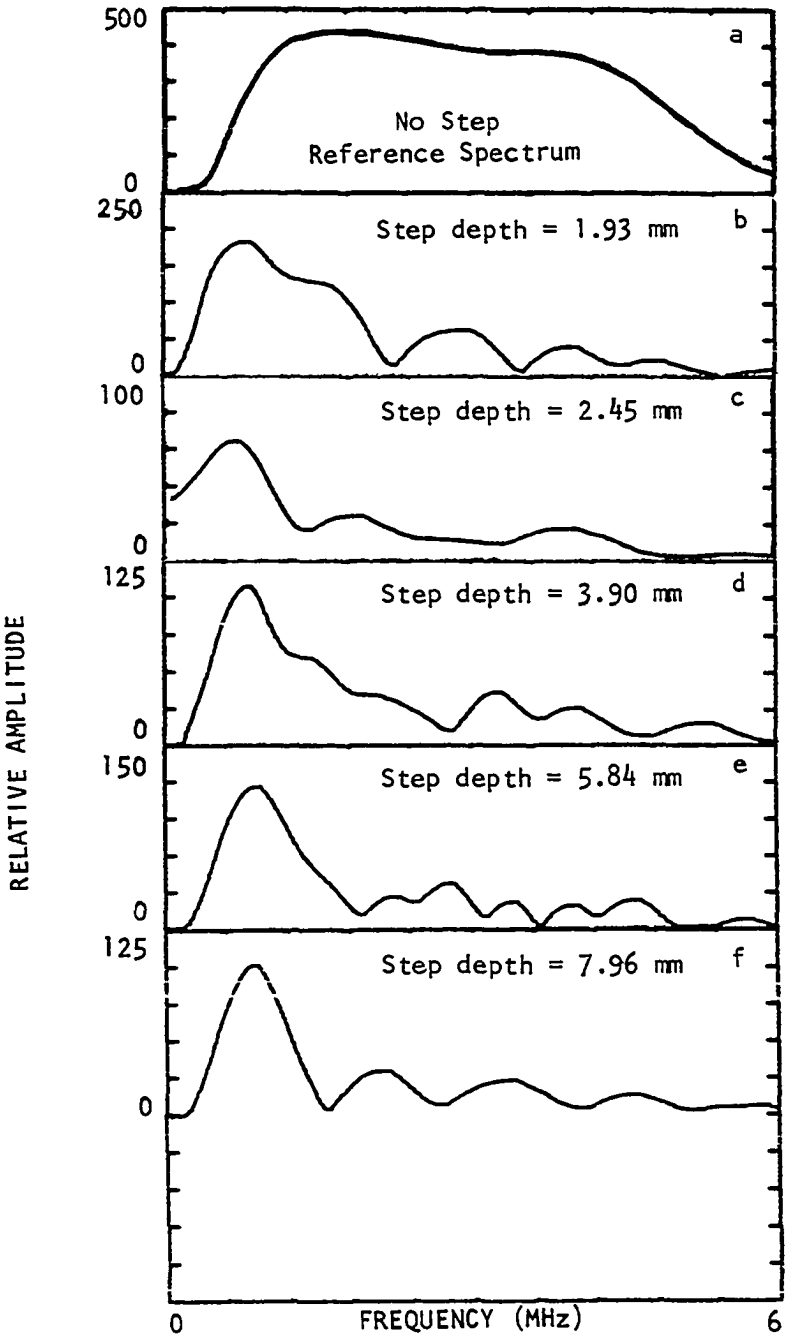

Figure 6.4. Frequency spectrums of the leading waves ("B") scanned and depicted in Figure 6.2.a-f, respectively

generated by the transducers in use. The tests conducted here used either 2.25 or 5.0 MHz transducers. These transducers were broadbanded between 0.5-3.5 and 0.5-5.5 MHz, respectively. Therefore, the highest useful frequency was 5.5 MHz from which one could compute the shortest wavelength (λ) using Eq. (4.1). The wavelength so obtained is λ = 2.96 (mm/sec)/5.5 MHz = 0.54 mm. The saw-cut slots were all made using a 0.5 mm thick rotary cutting saw. Figure 6.5 depicts a typical saw-cut slot. The tip of the slot is formed by two sharp 90° corners, but it should feel like a point tip to the incident wave because the slot is narrower than the shortest wavelength in the incident wave.

Figure 6.5. Typical view of a saw-cut slot normal to the surface

Early results for the frequency spectrum of the transmitted LFR wave, after interaction with slots, are depicted in Figs. E.3b and E.6 (Appendix E). At the time these samples were taken, the sampling procedure was to discretize the time signals into 256 points. It can be noticed from Fig. E.3a that typical sampling windows were 10 microseconds

in width; this indicates that the resolution of the system was marked by a time increment (Δt) of 10 μs/256 points = 39.1 ns/point. The curves depicted in Fig. E.6 seem to correlate reasonably well the cut-off and peak wavelengths with slot depth. Later studies on EDM slits and surface open cracks suggested that a reduction in the time increment would improve the sampling of the time signals; consequently, improvement in the frequency spectrum of the signals was also expected. The original sampling level of 256 points was doubled to 512 points which, in effect, reduced the time increments to 19.5 ns/point. The FFT level was changed to 2048 points. Appendix D provides the necessary equations to change scales upon modification of any of the sampling, Fast Fourier Transformation or displaying levels.

Table 6.1 shows the resampled and re-evaluated data obtained for the interaction of an AFR wave with a slot. Figure 6.6 depicts the plotted data and the new slot depth prediction equation.

Table 6.1. Summary of test results on saw-cut slots normal to the surface at various electronic damping levels

	Damping = 0		Damping = 4		Damping = 8	
Depth (mm)	λ_p	λ_c	λ_p	λ_c	λ_p	λ_c
1.03	2.82	1.00				
1.36	3.70	1.10	3.11	1.35		
1.95	3.48	1.56	3.48	1.60	3.22	1.60
2.40	3.95	2.04	3.95	2.11	3.84	2.04
2.75	4.23	2.19	4.11	2.28	3.95	2.19
3.20	4.55	2.57	4.23	2.57	3.95	2.57
3.93	4.77	2.96	4.93	2.96	4.23	2.96
4.35	5.38	3.29	5.19	3.29	4.93	3.29
4.87	5.92	3.48	4.93	3.48	4.93	3.48
5.97	5.92	4.23	5.92	4.23	5.92	4.23
8.11	9.87	5.38				

External Influences on Test Results

It is important that any technique for characterizing surface flaws not be affected by external variables which are likely to be present

under practical test conditions. Tests were run to check how sensitive the proposed technique was to various changes that may occur during a typical test.

Effect of Electronic Damping One setting on the ultrasonic instrument that has to be chosen by the operator is the extent of the "damping" that is included in the circuit to reduce apparently irrelevant "noise" or resonances in the signals. This variable can be set at different values during the course of a test. The effect on the signal is very noticeable, especially when high frequencies are involved, because increasing damping reduces the noise and the amplitude on the transmitted signals. The data for three differend damping levels (0, low to 8, high) are given in Table 6.1 and is plotted in Fig. 6.6. It is clear that the effect of damping on the cut-off values is small. However, the peak wavelengths, which were thought to be another candidate for predicting slot depth, varied considerably with the amount of damping in the system.

Three best fit equations were found for the cut-off wavelength (λ_c) values vs slot depth (d) yielding Table 6.2. The correlation is excellent for all four equations.

Table 6.2. Slot depth prediction equations

Damping Level	Equation	Correlation (r)
0	$\lambda_c = 0.42 + 0.63\ d$	0.997
4	$\lambda_c = 0.52 + 0.62\ d$	0.997
8	$\lambda_c = 0.46 + 0.63\ d$	0.997
Average Eq. using all points (Solid Line Fig. 6.6)	$\lambda_c = 0.47 + 0.63\ d$	0.997

It is difficult, however, to fit a curve through the peak wavelengths. There are modulations in the curves which cannot be explained at this stage. The band shown in Fig. 6.6 for the peak-wavelength vs

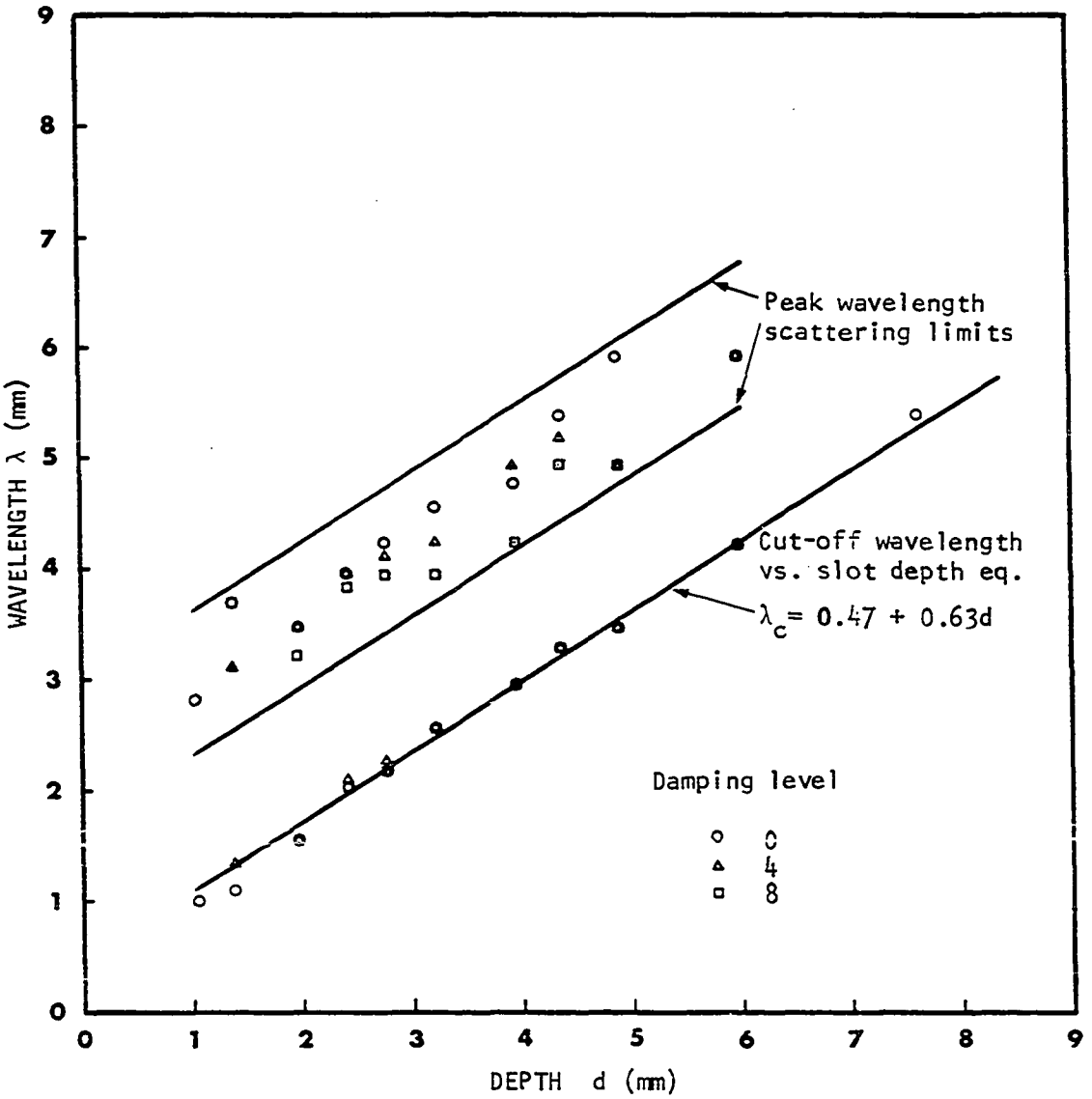

Figure 6.6. Effect of electronic damping on peak and cut-off wavelength vs. slot depth curves

slot depth values encompasses all the obtained points and it is parallel to the cut-off wavelength vs slot depth curve for which the prediction equations have been found. This band offers an upper and lower limit for finding the depth of a defect. In other words, the use of this band can help find a range of values that should encompass the right slot depth.

Effect of Distance Between Sending and Receiving Transducers A very common variable in any ultrasonic testing situation is that of the location of the transducers with respect to each other. A specimen made from 1018 steel with a 1.9 mm deep slot was tested, as previously described for other slots, except that the distance between the transducers was progressively increased for a succession of tests. Figure 6.7a-f show, in order, the frequency spectrums of the LFR waves received at various distances from the 1.9 mm slot. Table 6.3 presents a summary of the results and the error analysis. It is apparent that changes in transducer placement did not have a significant effect on the predicted values for the depth of the slot.

Table 6.3. Effect of distance between transmitting and receiving transducers on the spectrum of the LFR waves

	Distance of Transducers From Slot (mm)		Cut-Off Frequency f_c (MHz)	Cut-Off Wavelength λ_c (mm)	Predicted Depth (mm)	Error %
Fig. 6.7	Transmitter	Receiver				
a	20	10	1.85	1.60	1.79	-6
b	20	20	1.75	1.69	1.94	2
c	20	30	1.80	1.64	1.86	-2
d	20	40	1.75	1.69	1.94	2
e	20	60	1.77	1.67	1.90	0
f	30	40	1.70	1.74	2.02	6

Average Error = 2.3%

Effect of the Inclination of a Slot with Respect to the Surface Normal Often cracks do not grow perpendicular to the surface of the material. It is, therefore, necessary to observe the effect that a slanted slot may have on the prediction curves obtained by testing slots normal to the surface.

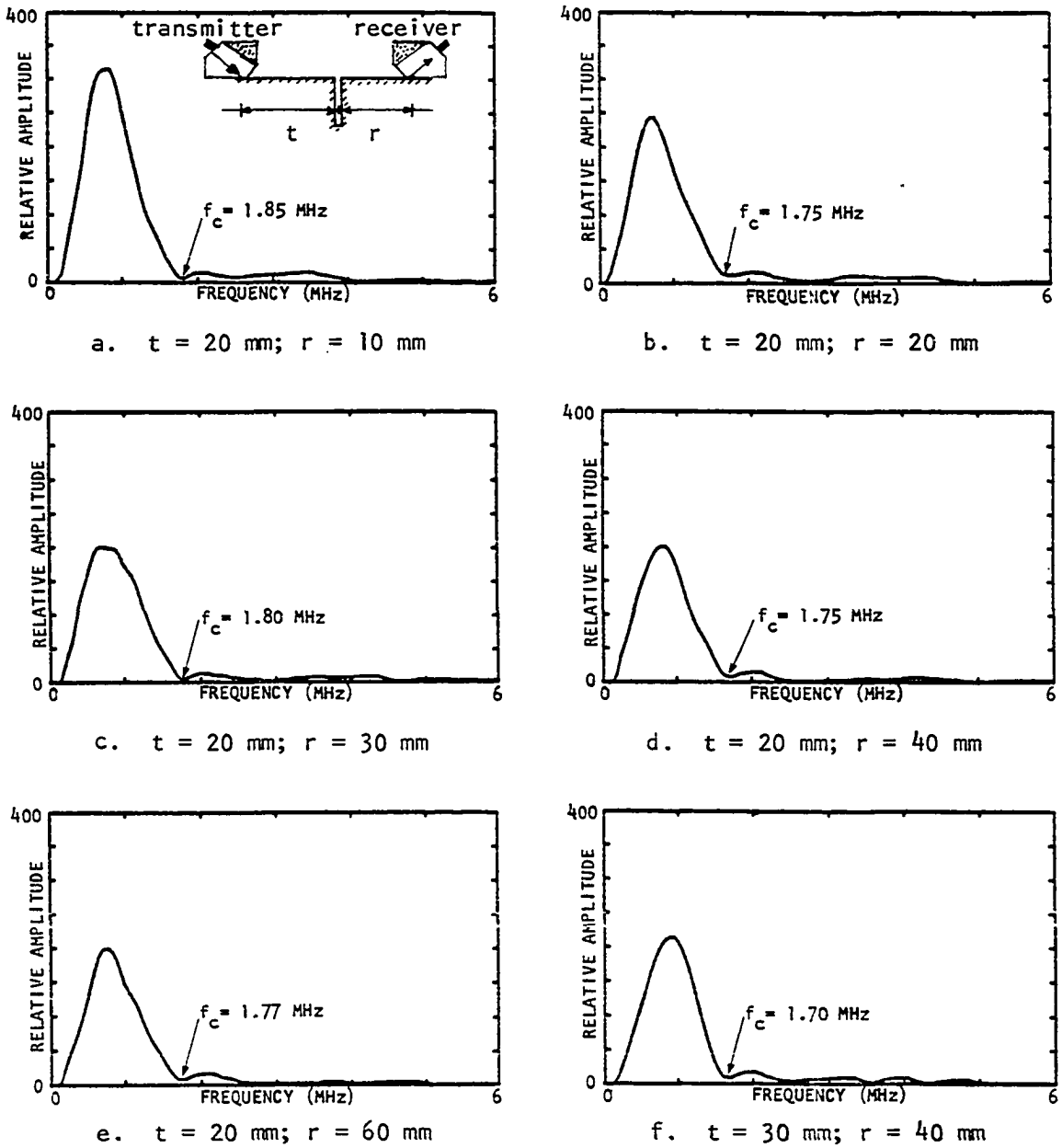

Figure 6.7. Effect of separation between transmitter and receiver transducers on the cut-off frequency of an LFR wave diffracted from a 1.9 mm deep slot

Figure 6.8 shows a typical testing setup on a 1018 steel specimen containing a slot inclined at 15° to the surface normal. Tests were conducted for various depth slots at angles of 15° and 30° from the normal to the surface. The 5.0 MHz wideband transducers were used.

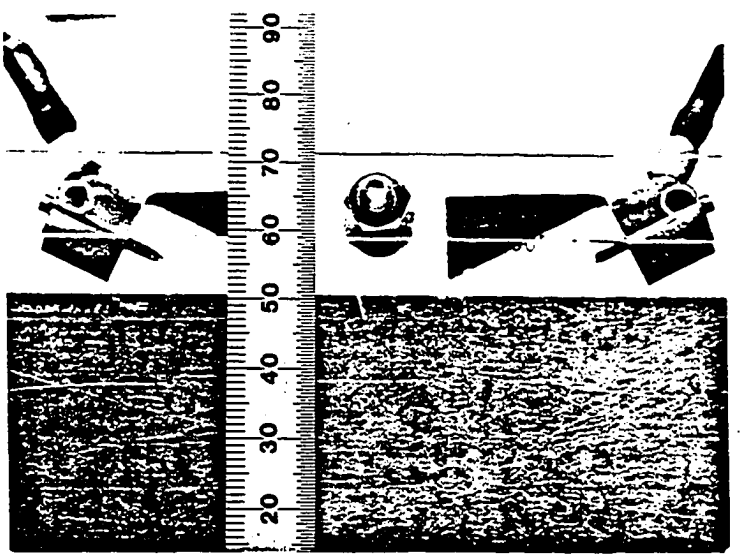

Figure 6.8. Typical view of a saw-cut slot inclined 15° to the surface normal

Figure 6.9 shows the results obtained. It is apparent that the inclination of the slot is very detrimental to the results previously obtained. Although the modulations that are now present in the cut-off data are very large, it can be concluded, nevertheless, that there is a tendency for the slope of the curves (wavelength vs slot depth) to become flatter with increasing angle of inclination. An inclined slot with a flat bottom; i.e., two 90° angles at its base, presents to the incident wave a line of interaction points at different depths which presents a much different case than when the slot is normal to the surface. The presence of a sharp cut-off frequency is then not likely to occur. So the previous arguments seem hard to implement when applied to inclined slots. For surface defects such as cracks with a single

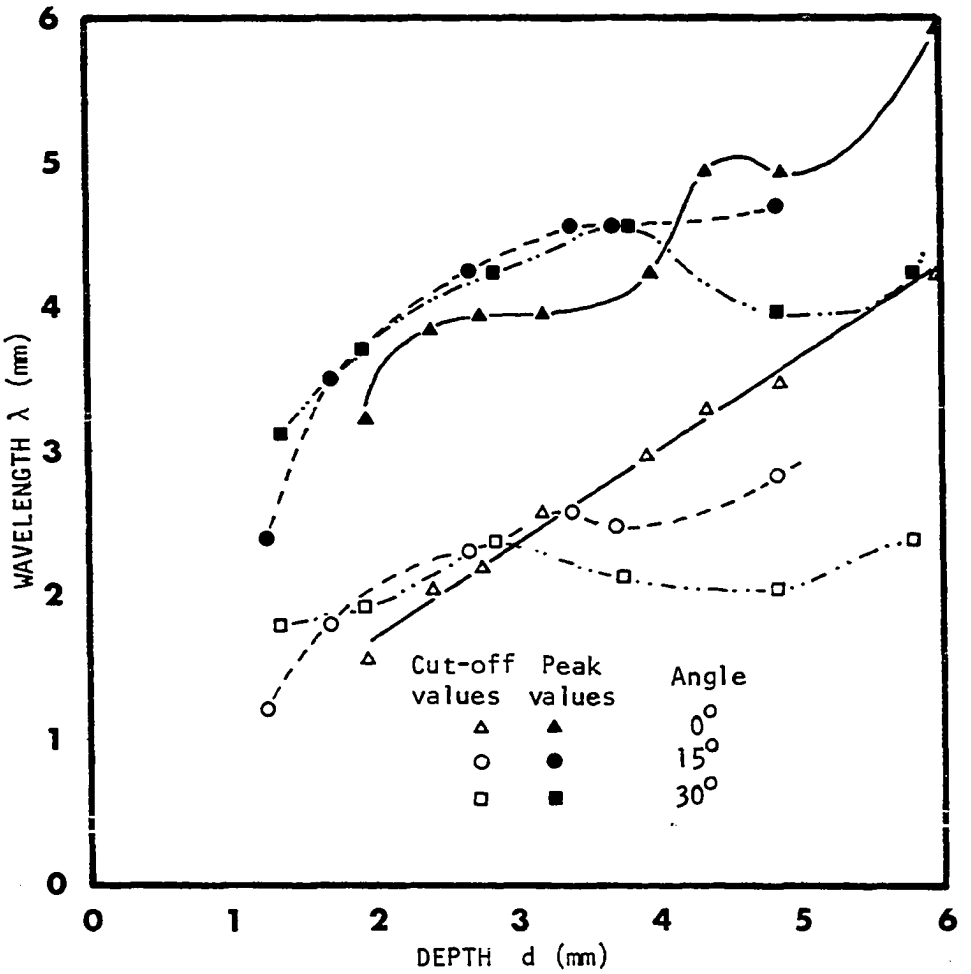

Figure 6.9. Effect of the inclination of slots, with respect to the surface normal on the LFR wave peak and cut-off frequency values

point tip the results may well be better. The results for a slightly inclined open crack, about 5° with the normal, are presented in Fig. 6.14 and discussed later. These results were much easier to interpret than the data for inclined slots in this section.

Effect of Polluting Elements on the Testing Surface and in the Slot

Under normal testing conditions in the field it is very difficult to encounter situations in which the element, or elements, to be tested is impeccably clean. For example, machine components are usually covered with some kind of oily compound on their surface. Rayleigh waves propagating in media with a polluted surface tend to dissipate some of their energy. It is, then, important to observe how sensitive is the LFR wave under study in this research to this surface variable. Figure 6.10 depicts the frequency spectrum of the LFR wave after interaction with a 1.9 mm slot under various surface conditions. The slot was filled with the polluting liquid, and the surface was wet. The cut-off frequencies seem to vary from 1.73 to 1.79 MHz with the value for the clean slot falling somewhere in this interval (about 1.75 MHz).

The clean slot cut-off frequency predicts a slot depth of $d = (1/0.63)(\lambda_c - 0.47)$, where $\lambda_c = v_R/f_c$, 1.94 mm. The prediction equation in Table 6.2 can be used to determine what is the effect of the shifts in the frequency readings of Fig. 6.10 on the measurement of slot depth. Equation (6.1) can easily be obtained and used to find the error in the length measurement. By substituting the above values and the velocity of the Rayleigh wave

$$\Delta d = \frac{v_R}{0.63} \frac{\Delta f}{f_1 - f_2} . \qquad (6.1)$$

For v_R = 2.96 mm/μs and substituting the values for f_1 and f_2 from Fig. 6.10, Δd is equal to 0.09 mm. Most defects being measured are in the range of 1 mm to 8 mm; therefore, the worst this error can get is around 10% of the actual crack length. One can conclude that in most instances the effect of polluted surfaces can be tolerated by the technique proposed.

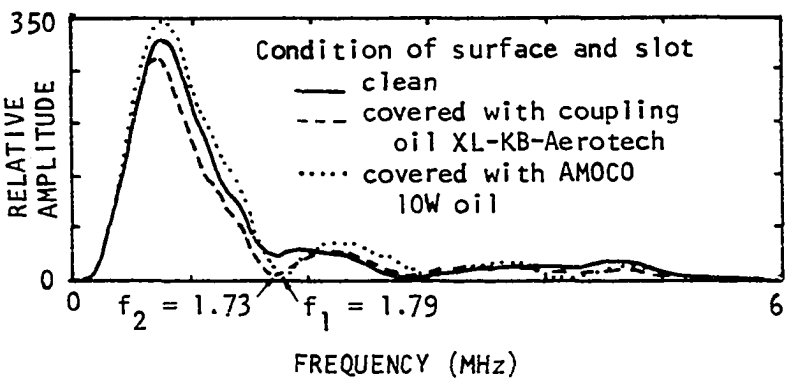

Figure 6.10. Effect of polluting liquids, on the testing surface and in the slot, on the LFR wave cut-off frequency values (slot depth = 1.9 mm)

Effect of Surface Barriers on the Transmission of the LFR Welds and very rough surfaces are potential crack initiation areas. It is, therefore, important to be able to determine how applicable the proposed technique is to testing for crack depth when the surface between the transducers contain rough weld details.

Figure 6.11a shows the frequency spectrum of a LFR wave after interaction with a slot 2.8 mm deep by 0.5 mm wide located at the side of a protruding (unfinished) weld. The incident wave was first sent from the side without a weld and was picked up by the receiver past the weld. Then the test was run in the other direction. Although most of the energy that belongs to the run-around-the-slot Rayleigh wave is diffracted, it is found that there is a significant amount of energy in the LFR wave received in both cases. It is possible to determine, by means of the prediction equation, what is the depth of the defect according to the cut-off frequency information received. This depth prediction comes out to be 3.17 mm which is in error by 13% from the actual size of 2.8 mm.

Figure 6.11b depicts the spectrum of the LFR wave after interaction with weld splatters. The incident wave was first sent from the smooth side, through the slot and into the weld splatters. Then the test was run vice versa. Needless to say, the surface waves that travel around the slot practically vanish after interacting with so many defects. However, the energy from the LFR wave does contain and show relevant information on the cut-off frequency in both cases. It yields a slot depth value of 2.73 mm. This predicted depth is in error by -2.5% with respect to the actual depth of 2.8 mm.

It is possible to conclude then that the method proposed seems to be applicable for sizing defects close to welds and rough surfaces such as that created by weld splatters. Not only that, but the direction from which the test is performed does not affect the results to any observable amount.

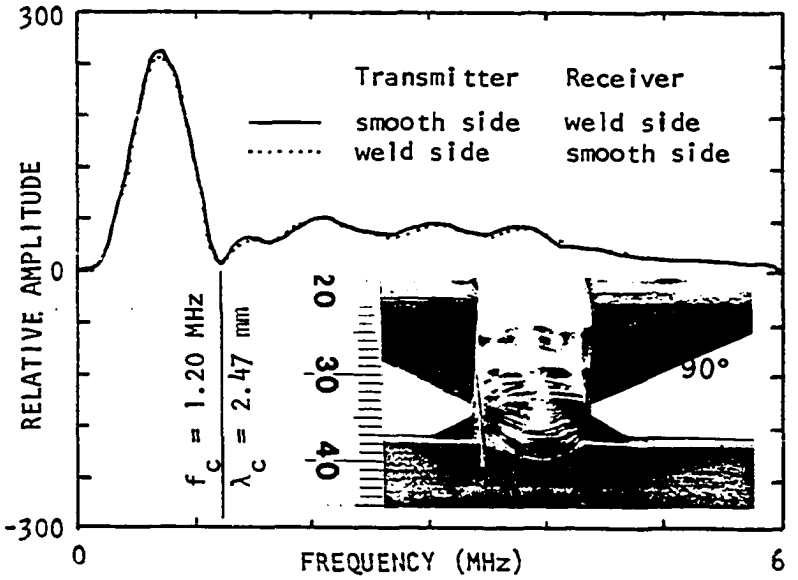

a. Spectrum of the LFR wave from the interaction with a continuous weld

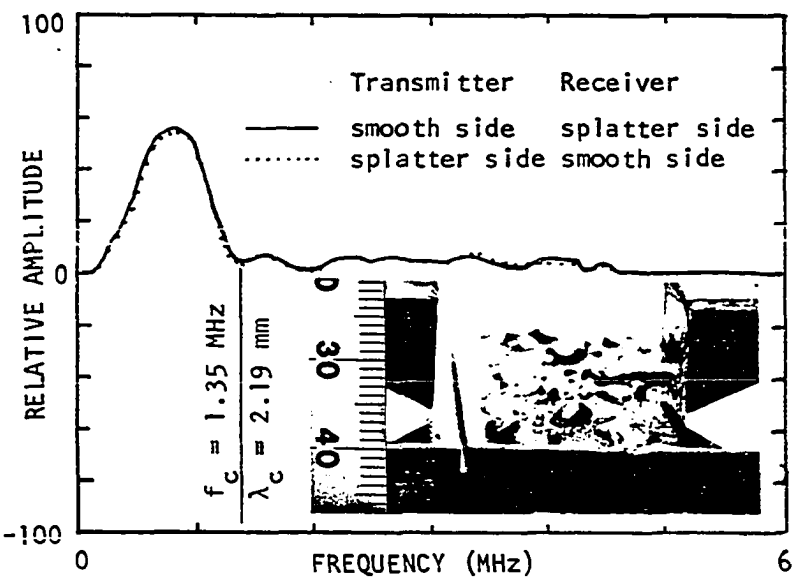

b. Spectrum of the LFR wave from the interaction with weld splatters

Figure 6.11. Effect of surface barriers on the cut-off frequency of the LFR wave upon interaction with a 2.8 mm deep slot

Interaction of Rayleigh Waves with Slits

Results from the foregoing tests suggest that there is a correlation between slot depth and cut-off frequency or cut-off wavelength. However, the data obtained from the slot specimens presume that the flat tip of the slot behaves as a point source or point scatterer. If this statement is true, then there should be no difference in the scattered waves upon interaction with an EDM slit which has a round tip and is very narrow as compared with a slot. Figure 6.12 depicts a 1.95 mm deep Electric Discharge Machined slit. The wire used to produce this slit was 0.1 mm in diameter. The slit width was double the wire diameter because there is material being eroded away as the cutting takes place. The tip was semicircular with a radius of 0.1 mm.

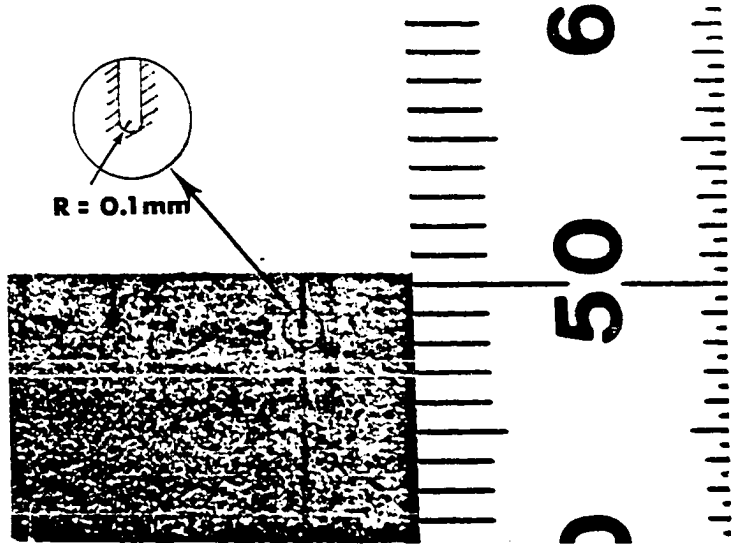

Figure 6.12. Typical view of a narrow EDM slit with a rounded tip (R = 0.1 mm)

Appendix E introduces some preliminary results that were obtained from a slit cut in steel 1018. Figure E.8 shows the reference Rayleigh wave and its frequency spectrum. A new variable was introduced at this point. Instead of using the 5.0 MHz set of transducers previously used, it was selected to use a set of 2.25 MHz transducers. By observing the

spectrum in Fig. E.8a, it is possible to determine that the testing limits of these transducers are between 0.5-3.5 MHz. This indicates that it should only be possible to gage defects around 0.6-8.7 mm deep, as computed from the equation derived from slot data in Table 6.2. Figure E.8 yields the desired cut-off wavelength to be 1.78 mm which, when used with the prediction equation, yeilds a depth of 2.08 mm. This compares well with the actual depth of 2.2 mm.

Figure 6.13 compares the results obtained for various depth slits in steel 1018 specimens with the prediction curve for slots. It is apparent that the use of narrower slits did not significantly alter the results obtained from slot tests.

The major difference between the tests was the width of the cut (slots--0.5 mm; slits--<0.2 mm) and the shape at the tip of the cut (slots--squared with two 90° corners; slits--rounded). It has been shown that neither of these two parameters seems to influence the results significantly. It is possible to say also that if the frequency range of the transducers is within the right limits for a particular defect, it is feasible to size defects, within these limits, independently of the central frequency of the transducers. There is no reason to believe that if higher frequency broadband transducers were used, the same type of results could not be obtained for shallower defects. The opposite would be true for deeper defects.

Effect of Yield Stresses at the Tip of a Slit on the LFR Wave Spectrum Before proceeding with the testing schedule on open fatigue cracks, it was necessary to investigate the possible effects that the yield zone at the tip of a fatigue crack could have on the spectrum of the transmitted LFR wave. The tests were performed on a 2.3 mm deep by 0.5 mm wide EDM slit in a specimen of steel 1018. The transducers used were the 5.0 MHz set. The slit was tested on the tension side, opposite to the center load, in a three point load bending test. The specimen was loaded to various load levels so as to leave every time an increasing amount of permanent deformation in the member. The amount of plastic deformation was not measured directly from the specimen, but rather through an X-Y plotter which indicated the amount of load vs

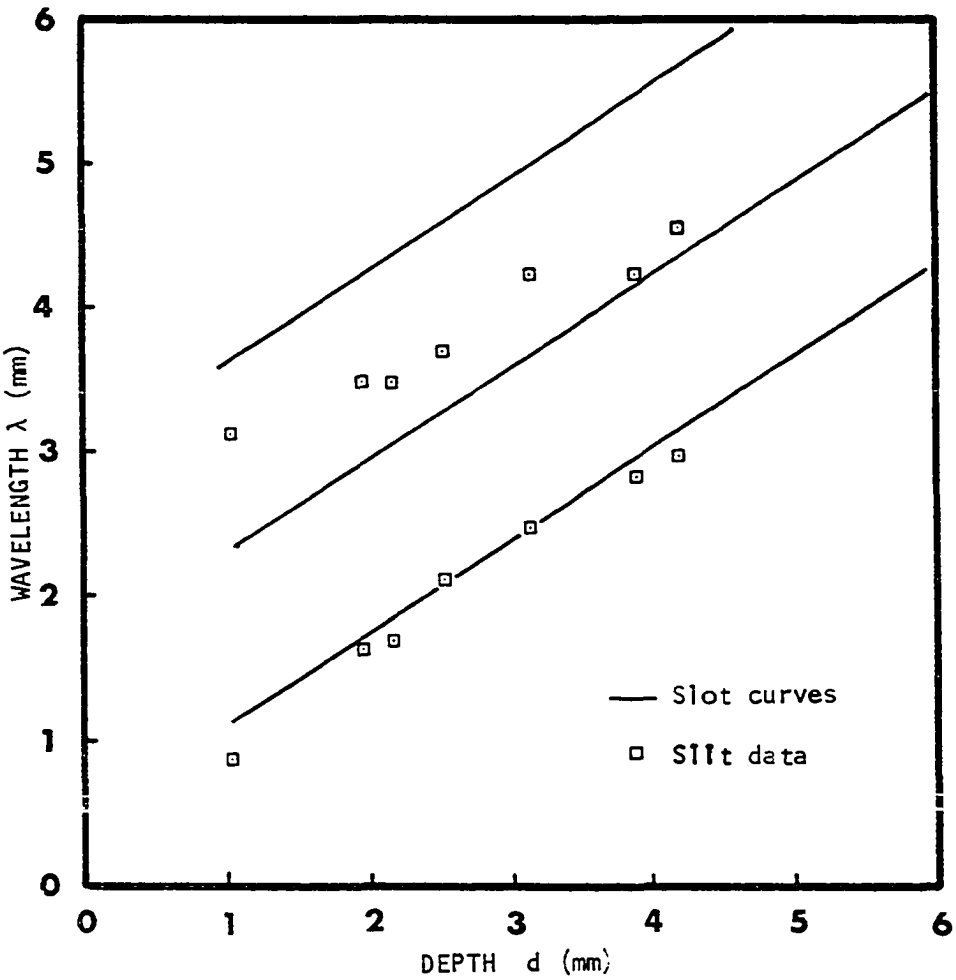

Figure 6.13. Comparison between the results obtained from EDM slits and saw-cut slots

displacement. As soon as the plot became nonlinear, the specimen was unloaded and the ultrasonic experiment was conducted. Each time there was an observable amount of permanent deformation in the member.

The results for this experiment are presented in the paper reproduced as Appendix E (Fig. E.9). It is apparent that there is no significant change in either the cut-off wavelengths or the peak wavelengths. By using the slot prediction equations with the cut-off wavelength obtained from the test, λ_c = 1.85 mm, one can predict a slit depth of 2.19 mm which compares favorably well with the actual depth of 2.3 mm. It is, therefore, possible to conclude that the yield zone around the tip of the crack does not affect the accuracy of the testing method being investigated.

Interaction of Rayleigh Waves and Open Fatigue Cracks

The final aim of this research is to be able to gage the depth of fatigue cracks. Fatigue cracks can be subdivided into two categories: open cracks and closed cracks. The behavior of an open crack is expected to be very similar to that of a narrow slot or slit. On the other hand, a closed crack is capable of transmitting most of the energy in an incident wave across the two contacting surfaces.

Preliminary results on open fatigue crack data are discussed in Appendix E and plotted in Fig. E.10b. The obtained cut-off wavelength of 3.5 mm, if substituted into the prediction equation given in Table 6.2, yields a predicted crack depth of 4.8 mm as compared to the actual externally measured depth of 4.2 mm.

Appendix F presents in detail the testing of partially open-partially closed cracks. It also gives the results for tests on a fully open crack. It is believed at this stage that the improvement on the sampling interval for a typical signal, from 256 discrete points to 512, improved also the frequency information and, consequently, the depth prediction equations. Therefore, the values obtained from testing cracks have been replotted against the newer prediction curves derived from slot data as shown in Fig. 6.14.

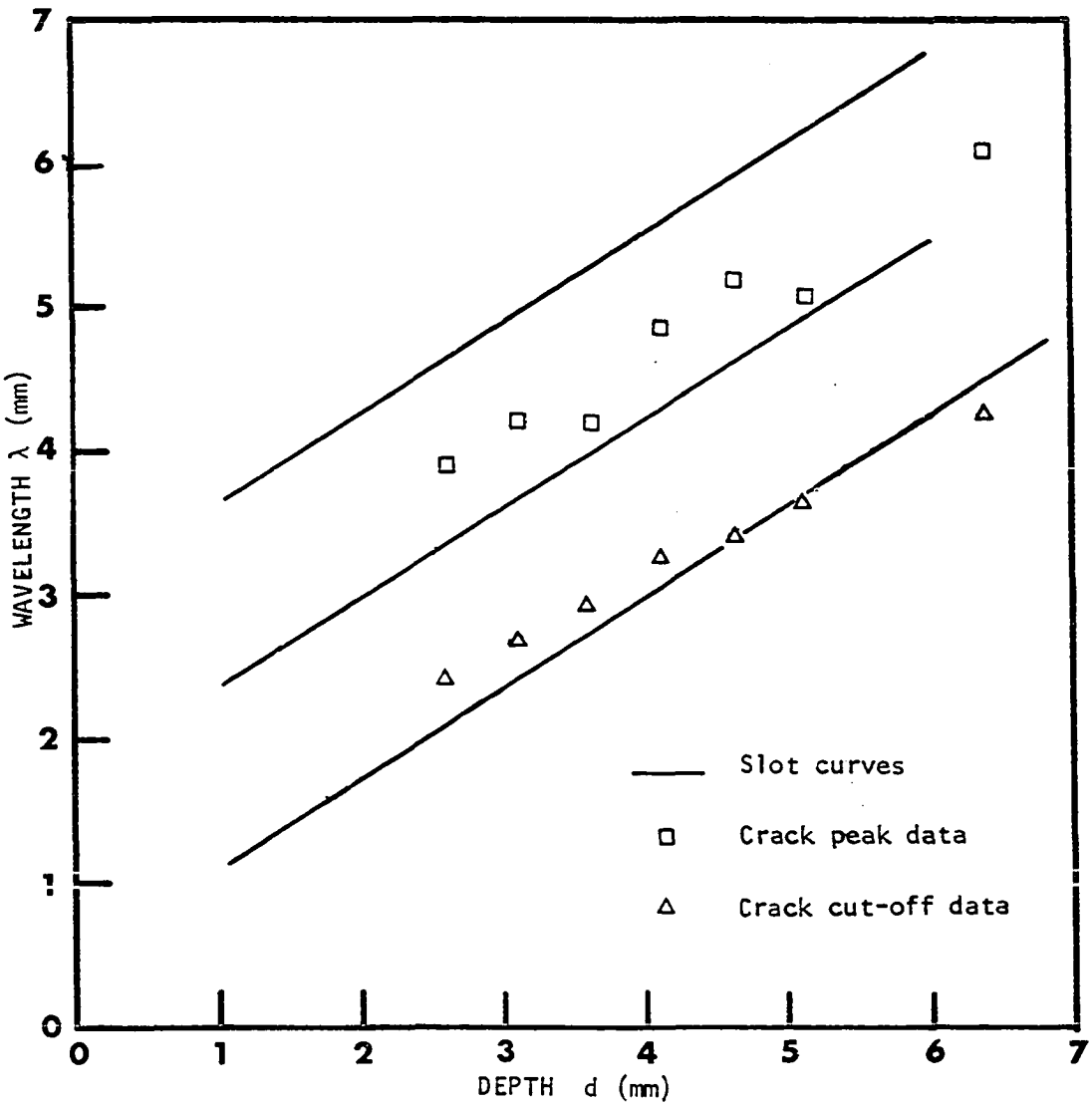

Figure 6.14. Comparison between the results obtained from an open fatigue crack in steel A387 and saw-cut slots

It is apparent from Fig. 6.14 that there is reasonable agreement between the data obtained from open cracks and slots. The peak wavelengths, although not discussed extensively in the context of this dissertation, also fall within the limits established from the tests on slots.

The tendency of the data points for the crack to lie on a line with a shallower slope than for slots and slits can be explained in terms of the inclination of the crack. It was shown earlier that when slots are inclined to the surface, there is a tendency for the data points to describe a curve with a shallower slope that that of the data for slots normal to the surface, Fig. 6.9. For the crack, the inclination was 5° with the surface normal; hence, the inclination of the data points.

Discussion

It is observed that the diffraction patterns from surface breaking cracks (for example, Fig. E.10) and saw-cut slots or EDM slits (for example, Fig. E.3 and Fig. E.8b) are very similar and can be explained in the same terms. However, some difficulty is encountered when the crack is not perfectly normal to the surface. The fatigue crack studied and presented in Fig. 6.14 was slightly inclined with respect to the normal to the surface, about 5°. This inclination with respect to the normal to the surface seems to account for the difference in slope between the two sets of cut-off data in Fig. 6.14.

In addition to the results presented in Appendix F, it can be said that no matter how meticulously the cleaning of a crack is before testing, it is much harder to identify a clear cut-off frequency which can be associated with the depth of the crack. However, it has been shown that the information necessary to gage the crack is present and that is just a matter of electronically separating the important portions of a signal so that information is not destroyed as with the actual method.

CHAPTER VII. CONCLUSIONS AND PROPOSED RESEARCH

Conclusions

After the presentation of all the results, it is possible to conclude that, in general, the proposed interaction mechanism for Rayleigh waves and surface breaking defects is, indeed, accurate. As one progresses through the dissertation, it is possible to see how the photoelastic information obtained for a similar type of interaction is reproduced in the ultrasonic tests with even more clarity.

Man-made defects such as slots or slits seem to be reasonably good models for actual cracks except when the inclination of the slot becomes a parameter. It was established that the effect of the inclination of a crack, with respect to the surface normal, on the cut-off frequency information is much less severe than on saw-cut slots.

The LFR (Low Frequency Rayleigh) wave, which is the wave believed to carry the information on the slot depth, seems to be affected very little by factors such as electronic damping of the testing system, yield zones at defect tips, roughness of surfaces (if limited to less than 0.2 mm), coupling condition of transmitting and receiving transducers, surface impurities and crack impurities. The frequency of the transducers used for the tests only affects the range of crack depths that can be detected. It has also been shown that surface barriers, such as contious welds and weld splatters, do not destroy the ability of the LFR wave to extract pertinent cut-off frequency data for gaging defects.

Further manipulation of the LFR wave is needed to be able to sort out more of the information it conveys. So far only the possibility of gaging a surface breaking defect has been sought. Indirectly, it was found that there are observable effects due to the inclination of the cracks or slots. It is very difficult, though, at the present stage of the technique to separate the various features that characterize additional features.

Time of travel measurements used in combination with the method proposed may prove to be very useful, especially when gaging partially

open-partially closed cracks. The main problem with a closed crack seems to be that when the energy of an incident Rayleigh wave impinges on the crack, most of it is transmitted through the crack and very little is diffracted into the medium. However, when the crack is partially open at the surface, it allows for some diffraction at the crack opening, then some energy is transmitted along the side of the crack toward the open and closed tips. Some of this energy converts to Rayleigh waves that travel around the crack tips allowing for time delay measurements.

It can be said then that the potential for the method proposed is very good and that implementation studies; i.e., computerization and signal recognition procedures, should be undertaken to see if it is possible to sort out the needed information automatically.

Proposed Research

Most of the signal handling and processing presented in this dissertation has been performed by using arbitrarily selected separation points between the LFR and AFR waves. Consistent observations were obtained on the behavior of the waves, but there was still that little touch of qualitative judgment, instead of a purely quantitative technique. It is proposed that research be conducted on possible techniques of separation of the LFR and AFR waves. Pattern recognition procedures could be used to achieve this purpose.

As a first approach to a large problem, it is possible to develop computer programs that will select specific features in the time domain and consistently zero the portion of the scanned waves not relevant to the study. Some of the information will be destroyed, but at least the human factor can be eliminated and a more systematic crack gaging technique implemented.

BIBLIOGRAPHY

1. J. Krautkrämer and H. Krautkrämer. Ultrasonic Testing of Materials. 2nd Edition. New York: Springer-Verlag, 1977.

2. Lord Rayleigh. "On Waves Propagated Along the Plane Surface of an Elastic Solid." Proc. London Math. Soc., 17 (1885), 4-11.

3. I. A. Viktorov. Rayleigh and Lamb Waves. 1st Edition. New York: Plenum Press, 1967.

4. H. Kolsky. Stress Waves in Solids. 1st Edition. London: Clarendon Press, 1953.

5. J. D. Achenbach. Wave Propagation in Elastic Solids. Vol. 16. London: North-Holland Publishing Company, 1973.

6. M. J. Buckley. "The Future Role of NDE." IEEE Trans. on Sonics and Ultrasonics, SU-23, No. 5 (1976), 287-292.

7. E. P. Papadakis. "Future Growth of Non-Destructive Evaluation." IEEE Trans. on Sonics and Ultrasonics, SU-23, No. 5 (1976), 284-287.

8. H. E. Boyer and W. J. Carnes. Metals Handbook. Vol. 11, 8th Edition. Metals Park, OH : American Society for Metals, 1976.

9. A. Shoh. "Industrial Applications of Ultrasound--A Review." IEEE Trans. on Sonics and Ultrasonics, SU-22, No. 2 (1975), 60-71.

10. M. J. Forrestal, L. E. Fugelso, G. L. Meidhardt and R. A. Felder. "Response of a Half Space to Transient Loads." Proc. of Engr. Mech. Div. Speciality Conference, ASCE, 1966.

11. S. A. Thau and J. W. Dally. "Subsurface Characteristics of the Rayleigh Wave." Int'l. J. of Engr. Sci., 7 (1969), 37-52.

12. W. A. Sorge. "Rayleigh Wave Motion in an Elastic Half Space." Geophysics, 30, No. 1 (1965), 97-101.

13. A. N. Henzi and J. W. Daily. "A Photoelastic Study of Stress Wave Propagation in a Quarter Plane. Geophysics, 36, No. 2 (1971), 296-310.

14. C. P. Burger, A. J. Testa and A. Singh. "Dynamic Photoelasticity as an Aid in Developing New Ultrasonic Test Methods." Proc. Spring Meeting of SESA, Brookfield Center, CT: Soc. of Exp. Stress Anal., 1981, 87-98.

15. D. Lewis and J. W. Dally. "Photoelastic Analysis of Rayleigh Wave Propagation in Wedges." J. of Geophysics Res., 75, No. 17 (1970), 3387-3398.

16. J. W. Dally and D. Lewis. "A Photoelastic Analysis of Propagation of Rayleigh Waves Past a Step Change in Elevation." Bulletin of the Seismological Soc. of America, 58, No. 2 (1968), 539-563.

17. H. W. Reinhardt and J. W. Dally. "Some Characteristics of Rayleigh Wave Interaction with Surface Flaws." Materials Evaluation, 28 (1970), 213-220.

18. R. L. Marino and J. W. Dally. "Rayleigh Wave Propagation Along Curved Boundaries." Dev. in Mech., 5 (1969), 819-831.

19. T. J. Plona, M. Behravesh and W. G. Mayer. "Rayleigh and Lamb Waves at Liquid Solid Boundaries." Ultrasonics, 13 (1975), 171-174.

20. G. Hall. "Ultrasonic Wave Visualization as a Teaching Aid in Non-Destructive Testing." Ultrasonics, 15 (1977), 57-69.

21. D. P. Morgan. "Surface Acoustic Wave Devices and Applications." Ultrasonics, 11-12 (1973-74), 121.

22. E. Harnik. "A Broadband Probe for Studies of Acoustic Surface Waves." J. of Physics E, 10 (1977), 121-131.

23. I. D. Akhromeeva and V. V. Krylov. "Rayleigh-to-Bulk Wave Conversion at Local Surface Defects." Sov. Phys. Acoust., 23, No. 4 (1977), 292-295.

24. B. R. Tittmann, M. DeBilly, F. Cohen, A. Jungman and G. Quentin. "Measurements of the Angular and Frequency Dependence of Acoustic Surface Wave Scattering from Surface Cracks." Ultrasonic Symp. Proc. New York: IEEE, 1978, 379-383.

25. B. R. Tittmann, O. Buck, L. Ahlberg, M. DeBilly, F. Cohen, A. Jungman and G. Quentin. "Surface Wave Scattering from Elliptical Cracks for Failure Prediction." J. Appl. Phys., 51, No. 1 (1980), 142-150.

26. V. Domarkas, B. T. Khuri-Yakub and G. S. Kino. "Length and Depth Resonances of Surface Cracks and Their Use for Crack Size Estimation." Appl. Phys. Letters, 33, No. 7 (1978), 557-559.

27. B. A. Auld, S. Ayter and M. Ton. "Theory of Scattering of Rayleigh Waves by Surface Breaking Cracks." Ultrasonics Symp. Proc. New York: IEEE, 1978, 384-390.

28. B. A. Auld and S. Ayter. "Acoustic Wave Scattering from Surface Cracks." Report. Thousand Oak, CA: Rockwell Int'l. Sci. Ctr., 1979.

29. S. Ayter and B. A. Auld. "On the Resonances of Surface Breaking Cracks." Proc. DARPA/AMFL--Review of Progress in Quant. NDE Thousand Oaks, CA: Rockwell Int'l. Sci. Ctr., 1980.

30. L. B. Freund. "The Oblique Reflection of a Rayleigh Wave from a Crack Tip." Int'l. J. of Solids and Structures, 7 (1971), 1199-1210.

31. J. E. Gubernatis and E. Domany. "Rayleigh Scattering of Elastic Waves from Cracks." J. of Appl. Phys., 50, No. 2 (1979), 818-824.

32. J. D. Achenbach and A. K. Gautesen. "Elastic Surface Waves Guided by the Edge of a Slit." J. of Sound and Vibration, 53, No. 3 (1977), 407-416.

33. A. K. Gautesen and J. D. Achenbach. "On the Existence of Surface Waves Guided by a Slit." SIAM J. Appl. Math., 35, No. 2 (1978), 301-306.

34. D. A. Mendelsohn, J. D. Achenbach and L. M. Keer. "Scattering of Elastic Waves by a Surface Breaking Crack." Wave Motion, 2 (1980), 277-292.

35. J. D. Achenbach, A. K. Gautesen and D. A. Mendelsohn. "Ray Analysis of Surface Wave Interaction with an Edge Crack." IEEE Trans. on Sonics and Ultrasonics, SU-27, No. 3 (1980), 124-129.

36. L. J. Bond. "Finite Difference Methods Applied to Ultrasonic Non-Destructive Testing Problems." Proc. of the ARPA/AFML--Review of Progress in Quant. NDE Dayton, OH: A. F. Materials Lab (1979).

37. A. Ilan, L. J. Bond and M. Spirack. "Interaction of a Compressional Impulse with a Slot Normal to the Surface of an Elastic Half Space." Geophysics J. R. Astr. Soc., 57 (1979), 463-477.

38. A. Ilan and L. J. Bond. "Interaction of a Compressional Impulse with a Slot Normal to the Surface of an Elastic Half Space--II." Geophysics J. R. Astr. Soc., 65 (1981), 75-90.

39. L. J. Bond. "A Computer Model of the Interaction of Acoustic Surface Waves with Discontinuities." Ultrasonics, 17 (1979), 71-77.

40. L. J. Bond. "Surface Cracks in Metals and Their Characterization Using Rayleigh Waves." Ph.D. Dissertation, The City University, London, 1978.

41. M. Munasinghe. "Numerical Solutions for Acoustic Rayleigh Wave Problems in Anisotropic and Layered Media." Ultrasonics, 14 (1976), 9-14.

42. G. S. Kino, T. M. Wangh, P. D. Carl, C. S. DeSilets and P. M. Grant. "Acoustic Imaging Techniques for Non-Destructive Testing." Preprint, G. L. Report No. 2815. Department of Electrical Engineering, Stanford University, Palo Alto, California, 1978.

43. W. L. Morris, O. Buck and R. V. Inman. "Acoustic Harmonic Generation Due to Fatigue Damage in High-Strength Aluminum." J. Appl. Phys., 50, No. 11 (1979), 6737-6741.

44. O. Buck, W. C. Morris, M. R. James and R. J. Richards. "Life Predictions for Aℓ in the Microcrack Regime Using SAW NDE." Proc. DARPA/AFML--Review of Progress in Quant. NDE Thousand Oaks, CA: Rockwell Int'l. Sci. Ctr., 1980.

45. P. A. Doyle and C. M. Scala. "Crack Depth Measurement by Ultrasonics: A Review." Ultrasonics, 6, No. 4 (1978), 164-170.

46. M. G. Silk. "Developments in Ultrasonics for Sizing and Flaw Characterization." Dev. in Pressure Vessel Technology, 2 (Inspection and Testing) (1978), 101-139.

47. D. J. Hudgell, L. L. Morgan and R. F. Lumb. "Non-Destructive Measurement of the Depth of Surface Breaking Cracks Using Ultrasonic Rayleigh Waves." British J. of NDT, 16, No. 5 (1974), 144-149.

48. B. R. Tittmann and O. Buck. "Fatigue Lifetime Prediction with the Aid of SAW NDE." Proc. DARPA/AFML--Review of Progress in Quant. NDE Thousand Oaks, CA: Rockwell Int'l. Sci. Ctr., 1980.

49. G. S. Mills. "Time-Domain Analysis of Ultrasonic Pulse Diffraction for Defect Characterization." Mat. Eval., 32, No. 12 (1974), 256-258.

50. K. G. Hall. "Crack Depth Measurement in Rail Steel by Rayleigh Waves Aided by Photoelastic Visualization." Non-Destructive Testing, 9 (1976), 121-126.

51. M. G. Silk. "The Transfer of Ultrasonic Energy in the Diffraction Technique for Crack Sizing." Ultrasonics, 17 (1979), 113-121.

52. M. G. Silk. "The Determination of Crack Penetration Using Ultrasonic Surface Waves." NDT Int'l., 9 (1976), 290-297.

53. M. G. Silk and B. H. Lidington. "The Potential of Scattered or Diffracted Ultrasound in the Determination of Crack Depth." Non-Destructive Testing, 8 (1975), 146-151.

54. M. G. Silk and B. H. Lidington. "An Evaluation of Single Probe Bulk-Wave Time-Delay Techniques in Sizing Cracks in Steel." NDT Int'l., 10 (1977), 129-134.

55. M. G. Silk. "Defect Sizing Using Ultrasonic Diffraction." British J. of Non-Destructive Testing, 21 (1979), 12-15.

56. R. S. Sigmond and E. Lien. "Ultrasonic Diffraction Measurements of Fatigue Crack Growth." British J. of NDT, 22, No. 6 (1980), 281-283.

57. M. V. Grigorév, A. K. Gurvich, V. V. Grebennikov and S. V. Semerkhanov. "Ultrasonic Technique for the Determination of Crack Dimensions." Soviet J. of NDT, 15, No. 6 (1979), 495-500.

58. B. T. Khuri-Yakub, G. S. Kino and A. G. Evans. "Acoustic Surface Wave Measurements of Surface Cracks in Ceramics." J. Am. Ceram. Soc., 63, No. 1-2 (1980), 65-71.

59. B. H. Lidington, D. H. Saunderson and M. G. Silk. "Interference Effects in the Reflection of Ultrasound from Shallow Slits." Non-Destructive Testing, 8 (1975), 185-190.

60. F. C. Cuazzo, E. L. Cambiaggio, J. P. Damians and E. Rivier. "Influence of Elastic Properties on Rayleigh Wave Scattering by Normal Discontinuities." IEEE Trans. on Sonics and Ultrasonics, SU-24, No. 4 (1977), 280-289.

61. T. J. Jessop and M. Weld. "Current Research to Improve the Characterization and Sizing of Weld Defects by Ultrasonic Testing." British J. of NDT, 19, No. 6 (1977), 287-292.

62. E. Kittinger. "Correction for Transducer Influence on Sound Velocity Measurements by the Pulse Echo Method." Ultrasonics, 15 (1977), 28-31.

63. S. Golan. "Optimization of the Crack Tip Ultrasonic Diffraction Technique for Sizing Cracks." Mat. Eval., 39 (1981), 166-169.

64. E. Oran Brigham. The Fast Fourier Transform. 10th Edition. Englewood Cliffs, NJ: Prentice-Hall, Inc., 1974.

65. R. Bracewell. The Fourier Transform and Its Applications. 1st Edition. New York: McGraw-Hill Book Company, 1965.

66. C. R. Nylie. Advanced Engineering Mathematics. 4th Edition. New York: McGraw-Hill Book Co., 1975.

67. O. R. Gericke. Research Techniques in NDT. Ed. R. S. Sharpe. New York: Academic Press, 1970, 31-61.

68. H. A. Crostack. "Basic Aspects of the Application of Frequency Analysis." Ultrasonics, 15 (1977), 253-262.

69. J. L. Rose and P. A. Meyer. "Signal Processing Concepts for Flaw Characterization." British J. of NDT, 16, No. 4 (1974), 97-106.

70. E. E. Hundt and E. A. Frautenberg. "Digital Processing of Ultrasonic Data by Deconvolution." IEEE Trans. on Sonics and Ultrasonics, SV-27, No. 5 (1980), 249-252.

71. N. F. Haines. "Ultrasonic Spectroscopy." Physics in Technology, 7, No. 3 (1976), 108-115.

72. L. L. Morgan. "The Spectroscopic Determination of Surface Topography Using Acoustic Surface Waves." Acoustica, 30 (1974), 222-228.

73. F. B. Bifulco and W. Sachse. "Ultrasonic Pulse Spectroscopy of a Solid Inclusion in an Elastic Solid." Ultrasonics, 13 (1975), 113-116.

74. A. Kh. Vopilkin, I. N. Ermolov and V. G. Staseer. "Experimental Investigation of an Ultrasonic Spectral Method of Determining the Nature of Defects." TsNIITMASh, Translated from Defektoskopiya, 1 (1978), 34-43.

75. L. W. Zachary, C. P. Burger, L. W. Schmerr and A. Singh. "Surface Crack Characterization by Use of Dynamic Photoelastic Spectroscopy." Proc. SESA Spring Meeting Brookfield Center, CT: Soc. Exp. Stress Anal., 1979.

76. A. Singh, C. P. Burger, L. W. Schmerr and L. W. Zachary. "Dynamic Photoelasticity as an Aid to Sizing Surface Cracks by Frequency Analysis." Mech. of Non-Destructive Testing, New York: Plenum Pub. Co., 1980, 277-292.

77. A. Singh. "Crack Depth Determination by Ultrasonic Frequency Analysis Aided by Dynamic Photoelasticity." Master of Science Thesis, Iowa State University, 1980.

78. C. P. Burger, A. J. Testa and A. Singh. "Photoelastic Visualization in the Development of Quantitative Ultrasonics." Paper presented at the XVII Midwestern Mechanics Conference, Ann Arbor, Michigan, May 6-8, 1981. To be published in conference proceedings.

79. J. R. Birchak and C. G. Gordner. "Comparative Ultrasonic Response of Machined Slots and Fatigue Cracks in 7075 Aluminum." Mat. Eval., 34 (1976), 275-280.

80. C. P. Burger and A. J. Testa. "Rayleigh Wave Spectroscopy to Measure the Depth of Surface Cracks." Paper presented at the 13th Symp. on NDE, San Antonio, Texas, April 21-23, 1981. To be published in conference proceedings.

81. C. P. Burger and A. J. Testa. "On-Line FFT of Rayleigh Waves Determines the Depth of Surface Cracks." Paper presented at Ultrasonics International 81, Brighton, England, June 30-July 2, 1981. To be published in the conference proceedings.

82. A. J. Testa and C. P. Burger. "Rayleigh Spectroscopy for Characterizing Surface Cracks." Paper presented at the DARPA/AF--Review of Progress in Quant. NDE, Boulder, Colorado, August 3-7, 1981. To be published in conference proceedings.

ACKNOWLEDGMENTS

First of all, I would like to thank my wife, Dayra, and my children for their support and patience during my graduate years.

Behind every piece of work there is always someone that in many ways has done, supported and encouraged more work than the one that takes the credit for it. I thank very specially Dr. Christian P. Burger for having been this person. Furthermore, I thank him for being a good guide, professor, friend and family to all of the graduate students, especially myself.

Special thanks to Professor W. F. Riley for encouraging me a long time ago to become an engineer and eventually a doctor in the field. Also to Dr. H. J. Weiss for offering and maintaining a most valuable economic support during all my graduate career.

A note of appreciation to my committee members Dr. L. F. Greimann, Dr. W. W. Sanders, Dr. F. M. Graham, Dr. L. W. Schmerr and Dr. L. W. Zachary for their support and to all other professors with whom I was involved, either as student or as friend.

Thanks to Miss Brenda Nielsen for typing the manuscript and what seemed at times endless papers and for her support. Also thanks to Tom Elliott for all his help in the lab and coffee supply.

A very special note of appreciation and thanks to Mr. Andy Wonderlich at the ERI Shop and to the ERI in general for their outstanding work, either with our specimens or papers.

APPENDIX A.
APPLICATION OF BOUNDARY CONDITIONS TO THE RAYLEIGH WAVE PROBLEM

The displacement equation for a Rayleigh wave, (3.1), moving along the positive x-axis, Fig. 3.1, and extending into an elastic half space between $0 \leq y \leq \infty$ can be rewritten as

$$u = \frac{\partial \phi}{\partial x} - \frac{\partial \psi}{\partial y} \tag{A.1a}$$

$$v = \frac{\partial \phi}{\partial y} + \frac{\partial \psi}{\partial x} \tag{A.1b}$$

where u: displacements in the x-direction

v: displacements in the y-direction.

The governing normal and shear stress equation can be written as

$$\sigma_{xx} = \lambda\left(\frac{\partial^2 \phi}{\partial x^2} + \frac{\partial^2 \phi}{\partial y^2}\right) + 2\mu\left(\frac{\partial^2 \phi}{\partial x^2} - \frac{\partial^2 \psi}{\partial x \partial y}\right) \tag{A.2a}$$

$$\sigma_{yy} = \lambda\left(\frac{\partial^2 \phi}{\partial x^2} + \frac{\partial^2 \phi}{\partial y^2}\right) + 2\mu\left(\frac{\partial^2 \phi}{\partial y^2} + \frac{\partial^2 \psi}{\partial x \partial y}\right) \tag{A.2b}$$

$$\sigma_{xy} = \mu\, 2\left(\frac{\partial^2 \phi}{\partial x \partial y} + \frac{\partial^2 \psi}{\partial x^2} - \frac{\partial^2 \psi}{\partial y^2}\right) \tag{A.2c}$$

where λ and μ are Lamé constants.

By knowing the values of the potentials ϕ and ψ from Eq. (3.5), oen can now substitute the known boundary conditions into Eq. (A.2).

B.C.1: $\sigma_{yy} = 0$ at $y = 0$

then from Eq. (A.2a) one obtains

$$\lambda\left(\frac{\partial^2 \phi}{\partial x^2} + \frac{\partial^2 \phi}{\partial y^2}\right) = -2\mu\left(\frac{\partial^2 \phi}{\partial y^2} + \frac{\partial^2 \psi}{\partial x \partial y}\right) \tag{A.3}$$

but from Eq. (3.5)

$$\phi = A \exp[-y\sqrt{k^2 - k_\ell^2}] \exp[i(kx - \omega t)] \qquad (3.5a)$$

and

$$\psi = B \exp[-y\sqrt{k^2 - k_S^2}] \exp[i(kx - \omega t)] \ . \qquad (3.5b)$$

Upon substitution and differentiation one obtains

$$A[2\mu k^2 - (\lambda + 2\mu)k_\ell^2] + i2\mu Bk\sqrt{k^2 - k_S^2} = 0 \ . \qquad (A.4)$$

B.C.2: $\sigma_{xy} = 0$ at $y = 0$
then from Eq. (A.2c) one obtains

$$2\frac{\partial^2\phi}{\partial x \partial y} + \frac{\partial^2\psi}{\partial x^2} - \frac{\partial^2\psi}{\partial y^2} = 0 \ . \qquad (A.5)$$

Upon substitution of Eq. (3.5) and differentiation one obtains

$$-i\,A2k\sqrt{k^2 - k_\ell^2} - B(2k^2 - k_S^2) = 0 \ . \qquad (A.6)$$

Equations (A.4) and (A.6) will yield a non-trivial solution only if the determinant of the coefficient is zero.

$$\begin{bmatrix} [2\mu k^2 - (\lambda + 2)k_\ell^2] & i[2\mu k\sqrt{k^2 - k_S^2}] \\ -i[2k\sqrt{k^2 - k_\ell^2}] & -[2k^2 - k_S^2] \end{bmatrix} \begin{bmatrix} A \\ B \end{bmatrix} = \begin{bmatrix} 0 \\ 0 \end{bmatrix} \qquad (A.7)$$

from which one obtains

$$-2\mu k^2[2k^2 - k_S^2] + (\lambda + 2\mu)k_\ell^2[2k^2 - k_S^2] - 4\mu k^2\sqrt{k - k_\ell^2}$$
$$\sqrt{k^2 - k_S^2} = 0 \qquad (A.8)$$

dividing by k^4 and μ yields

$$-2\left[2 - \left(\frac{k_s}{k}\right)^2\right] + \frac{(\lambda + 2\mu)}{\mu}\left(\frac{k_\ell}{k}\right)^2\left[2 - \left(\frac{k_s}{k}\right)^2\right] - 4\sqrt{1 - \frac{k_\ell{}^2}{k}}\sqrt{1 - \frac{k_s{}^2}{k}} = 0 , \qquad (A.9)$$

but the term $\lambda + 2\mu/\mu$ in Eq. (A.9) is the ratio of the square of the shear and longitudinal wave numbers [5].

$$\frac{\lambda + 2\mu}{\mu} = \left(\frac{k_s}{k_\ell}\right)^2 \qquad (A.10)$$

Upon substitution of Eq. (A.10) into Eq. (A.9), one can arrive at Eq. (A.11)

$$\left(\frac{k_s}{k}\right)^6 - 8\left(\frac{k_s}{k}\right)^4 + 8\left[3 + 2\left(\frac{k_\ell}{K_s}\right)^2\right]\left(\frac{k_s}{k}\right)^2 - 16\left[1 - \left(\frac{k_\ell}{k_s}\right)^2\right] = 0 \qquad (A.11)$$

which upon solving yields the wave number k for the eigenvalue problem. There is only one real root for this equation, and it yields an approximate value of

$$\frac{k_s}{k} = \frac{0.862 + 1.14\nu}{1 + \nu} \qquad (3.7)$$

where k_s, k: shear and Rayleigh wave numbers

ν: Poisson's ratio.

It is obvious that the solution in Eq. (A.11) is independent of frequency; therefore, it is concluded that the phase velocity of the Rayleigh wave is non-dispersive.

Now, by substituting either of Eqs. (A.4) or (A.6) in terms of A or B, one can find one constant in terms of the other. This process yields

$$B = -iA \frac{k\sqrt{k^2 - k_\ell^2}}{2k^2 - k_S^2} . \qquad (A.12)$$

Therefore, one can finally write the potential functions as given in Eq. (3.6).

$$\phi = -A \exp\left[i(kx - \omega t) - y\sqrt{k^2 - k_\ell^2}\right] \qquad (3.6a)$$

$$\psi = iA \frac{2k\sqrt{k^2 - k_\ell^2}}{2k^2 - k_S^2} \exp\left[i(kx - \omega t) - y\sqrt{k^2 - k_S^2}\right] \qquad (3.6b)$$

APPENDIX B.
LSI-11 CONFIGURATION

Due to the many internal configurations to which a computer can be exposed to meet various needs, it is found necessary to describe the configuration used in the microprocessor for the ultrasonic tests presented in this paper.

Table B.1 presented below shows the order and position in which the various circuits must be located within the microprocessing unit to enable the full capabilities in Fig. B.1 through B.10.

Table B.1. Configuration of the LSI-11 microprocessor

	CONTENT	
Slot	Left	Right
1	Central Processing Unit	
2	32k Memory Bank	Floppy Disk Interface
3	Hard Disk Interface	
4	Continuity Card	Digital I/O
5	16 Channel A/D, 2 Channel D/A Converter	
6	Real Time Clock	
7	Serial Interface	D/A Converter
8	Free	
9	Free	
10	Free	

The final configuration within the ADAC-1000 (LSI-11 Microprocessor) and connections should look as presented in Figs. 11a and 11b.

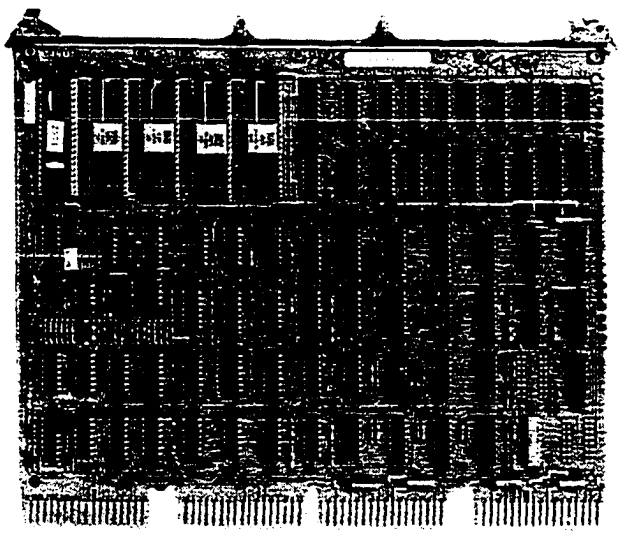

Figure B.1. LSI-11 central processing unit

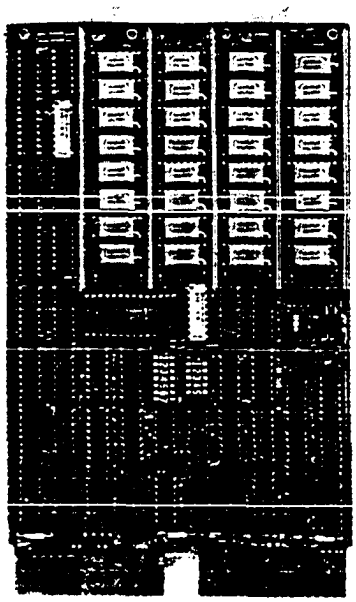

Figure B.2. 32k memory bank

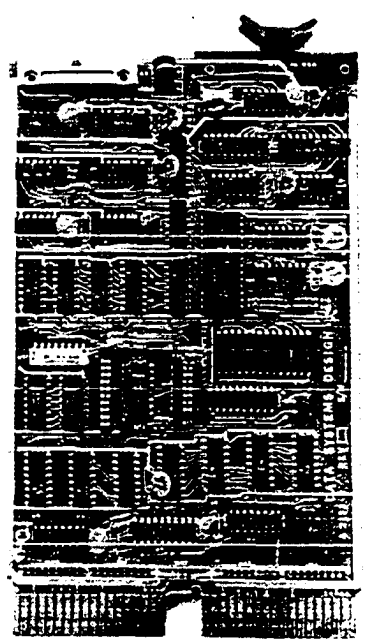

Figure B.3. Data system design floppy disk interface

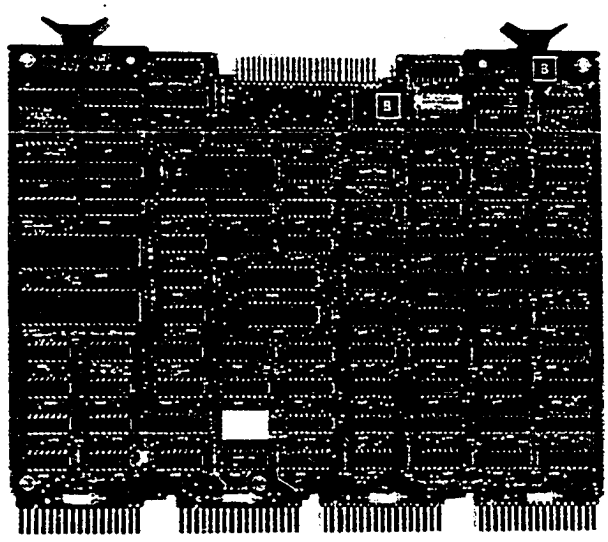

Figure B.4. Plessey hard disc interfacing card

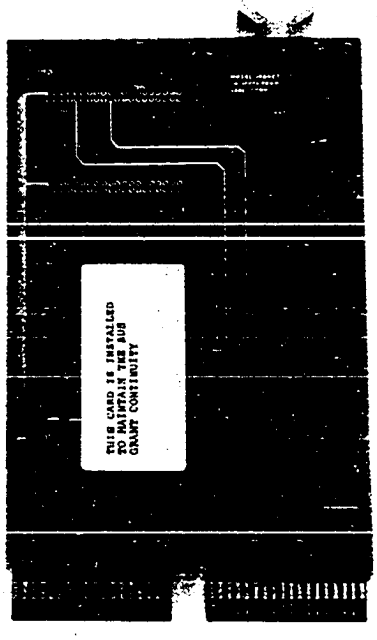

Figure B.5. Continuity card

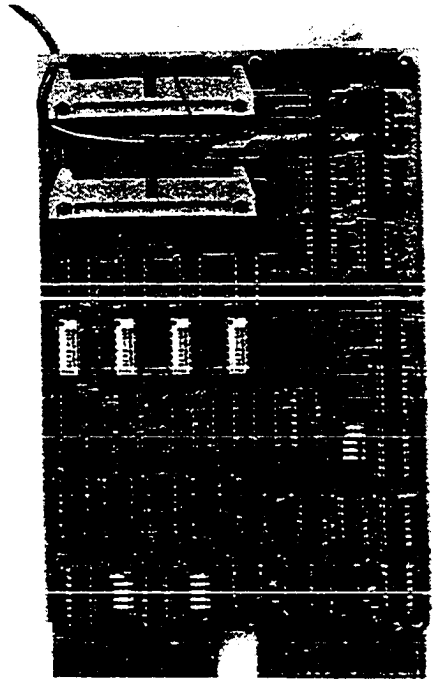

Figure B.6. ADAC 1632 digital I/O card

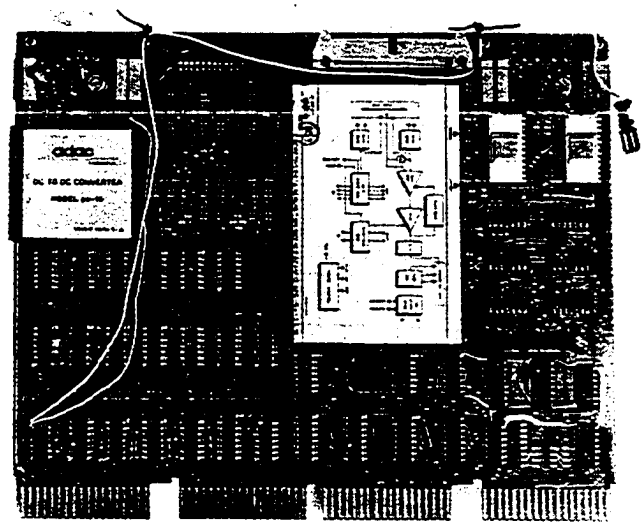

Figure B.7. ADAC 16 channel A/D converter, 2 channel D/A (model 1016)

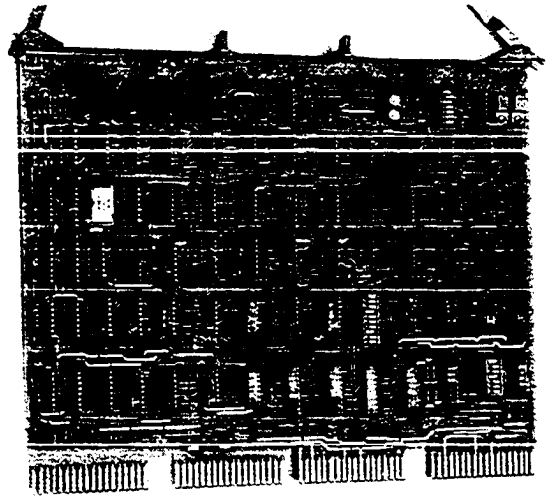

Figure B.8. Programmable clock

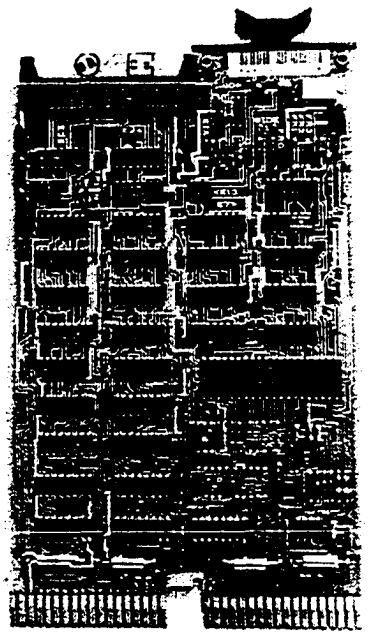

Figure B.9. Serial interface

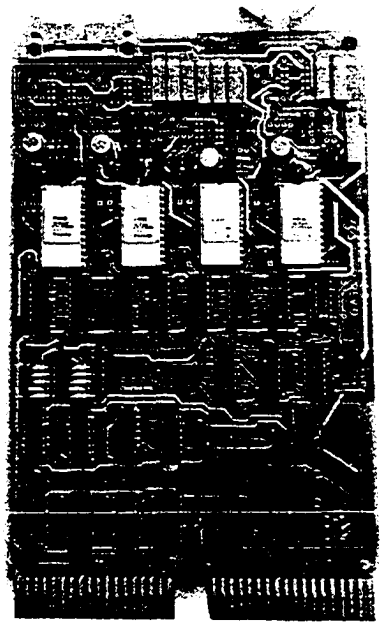

Figure B.10. ADAC 4 channel D/A converter

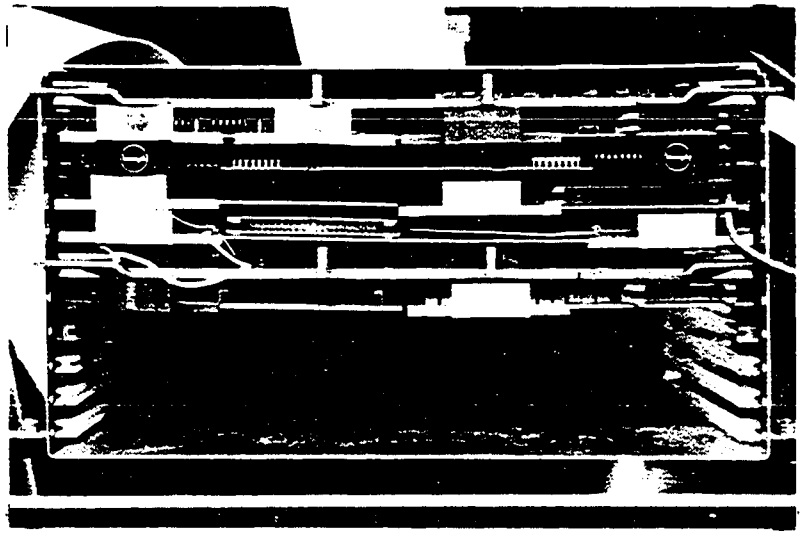

Figure B.11a. Typical LSI-11 card layout

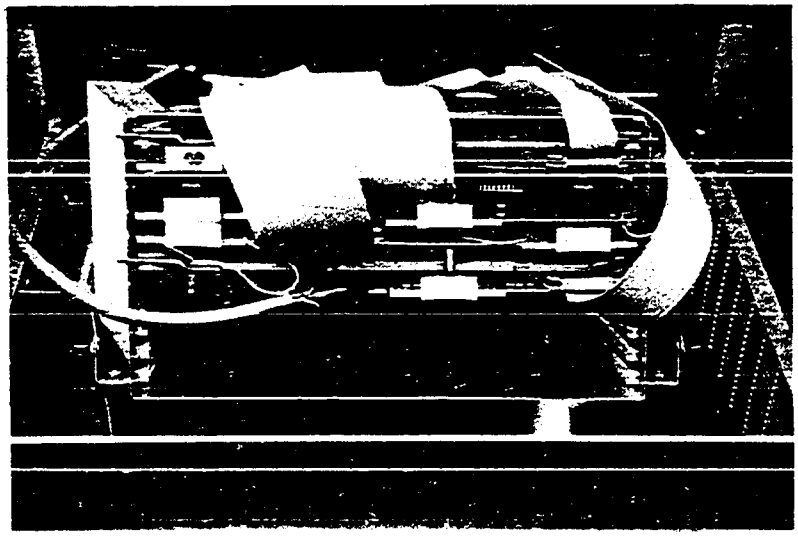

Figure B.11b. Typical LSI-11 cable connections

Figure B.12 is a schematic representation of the monitoring and control system of the ADAC-1000. It shows the details of the way in which the system handles itself internally.

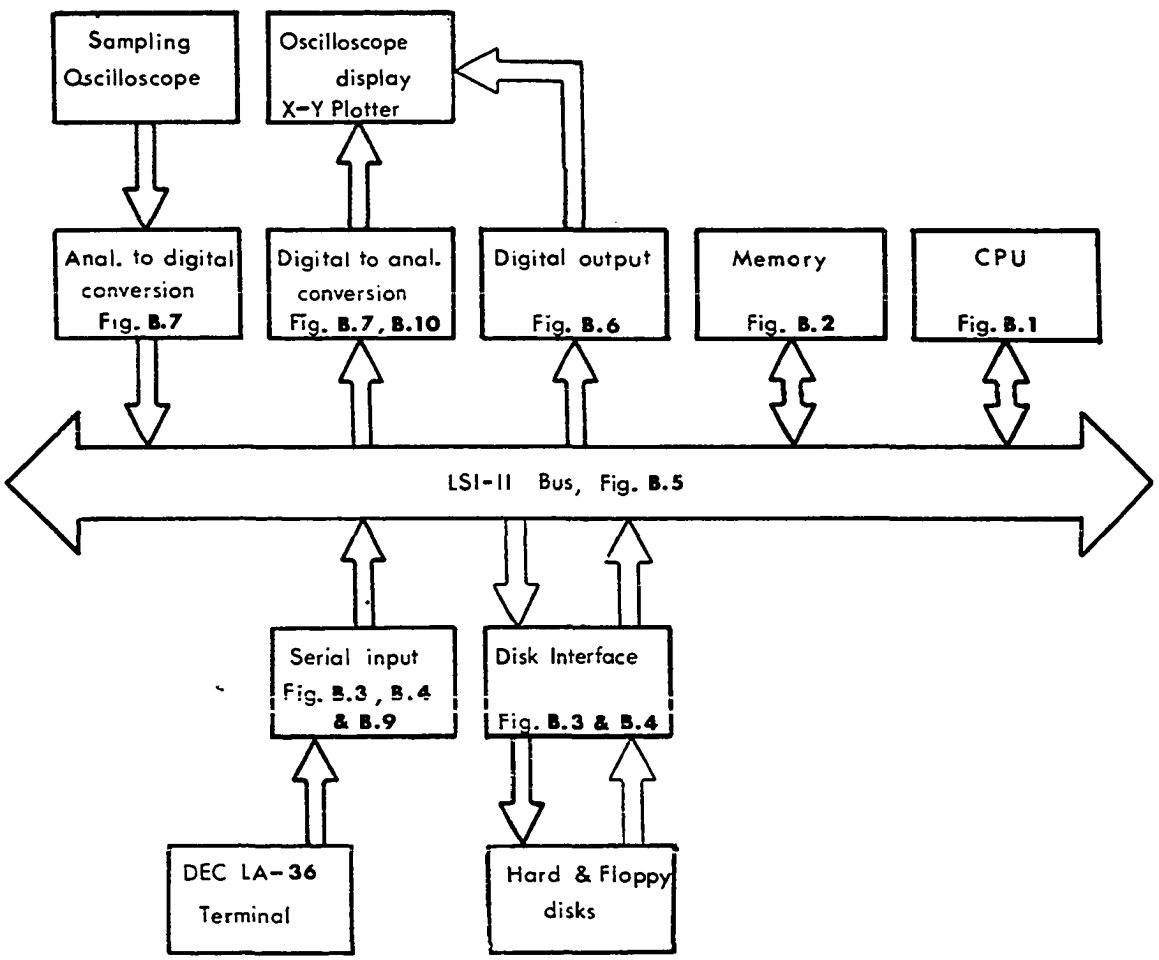

Figure B.12. Monitoring and control system of the ADAC-1000 microprocessor

APPENDIX C.
USER'S PROGRAMS FOR ULTRASONIC TESTING

The programs USPO and DATA were developed at Iowa State University by Charlie Sieck[1] and Doyle Heyveld[2] as part of an NSF grant (ENG 76-06970) and with partial support of the Department of Energy through Ames Laboratory under contract number W7405-ENG82, Office of Basic Energy Sciences.

[1,2]Currently with Caterpillar, Corporation.

USPO Program Documentation

REPRESENTS THE LEVEL (MUST BY BETWEEN 0 AND 10)

% REPRESENTS THE LEVEL (MUST BE BETWEEN 0 AND 11)

$ REPRESENTS THE LEVEL (IF LESS THAN 12) OR THE NUMBER OF POINTS SAMPLED (IF 12 OR GREATER)

CHANGE

A. C_@ WHERE @ IS THE POSITION IN PLIST TO BE CHANGED

1. PRINTS OUT THE CURRENT VALUE OF PLIST(@) AND PROMPTS FOR A NEW VALUE.
2. ACCEPTS THE NEW VALUE OF PLIST(@)

DISPLAY

A. DS--DISPLAY SAMPLE

1. SAMPLE.DAT IS READ INTO OBUF
2. THE MAXIMUM VALUE OF OBUF IS PRINTED TO TERMINAL
3. OBUF IS NORMALIZED TO 2047
4. OBUF IS DISPLAYED ON OSCILLOSCOPE UNTIL <RETURN> IS PRESSED

B. DR$-DISPLAY REAL

1. MAXIMUM ABSOLUTE VALUE OF REAL PART OF CBUF IS PRINTED.
2. THE REAL PART OF CBUF IS DISPLAYED ON OSCILLOSCOPE UNTIL <RETURN> IS PRESSED.

C. DI$-DISPLAY IMAGINARY

1. MAXIMUM ABSOLUTE VALUE OF IMAGINARY PART OF CBUF IS PRINTED TO TERMINAL.
2. THE IMAGINARY PART OF CBUF IS DISPLAYED ON OSCILLOSCOPE UNTIL <RETURN> IS PRESSED.

D. DM$-DISPLAY MAGNITUDE

1. MAXIMUM ABSOLUTE VALUE OF MAGNITUDE OF CBUF IS PRINTED TO TERMINAL

2. THE MAGNITUDE OF CBUF IS DISPLAYED ON OSCILLOSCOPE UNTIL <RETURN> IS PRESSED.

E. DP$-DISPLAY PHASE

1. THE MAXIMUM ABSOLUTE VALUE OF PHASE OF CBUF IS PRINTED TO TERMINAL
2. THE PHASE OF CBUF IS DISPLAYED ON OSCILLOSCOPE UNTIL <RETURN> IS PRESSED.

F. D -DISPLAY

1. DISPLAYS CURRENT CONTENTS OF OBUF (LOADED BY A PREVIOUS DISPLAY COMMAND

DECONVOLUTION

A. DV--DECONVOLUTION (DIVIDE)

1. PROMPTS WITH:

DIVISOR (REFERENCE) FILE NAME = ?

2. DIVIDES CONTENTS OF CBUF WITH SPECIFIED FILE

NOTE: BOTH THE CONTENTS OF CBUF AND THE FILE USED MUST BE OF DATA IN THE FREQUENCY DOMAIN, I.E: AN FFT MUST HAVE BEEN PERFORMED TO OBTAIN CONTENTS OF CBUF AND CONTENTS OF THE FILE

FFT

A. FF%-FORWARD FOURIER TRANSFORM

1. IF %>0, PLIST(16) IS SET TO %
2. APPLIES A HANNING WINDOW TO THE FIRST AND LAST 10 PERCENT OF THE SAMPLE IN THE REAL PART OF CBUF. THE SIZE OF THE SAMPLE IS DETERMINED FROM PLIST (7), THE SAMPLE LEVEL.
3. ZEROES OUT THE REAL PART OF CBUF ABOVE THE SAMPLE AND ALL THE IMAGINARY PART OF CBUF.

B. FN%-FORWARD FOURIER TRANSFORM WITH NO WINDOW

1. IDENTICAL TO PART A., BUT WITH NO HANNING WINDOW APPLIED.

C. FR%

1. IF %<>0, PLIST(16) IS SET TO T.
2. PERFORMS A REVERSE FFT AT A LEVEL SPECIFIED IN PLIST(16)

LIST

A. LR--LIST REAL

1. PROMPTS WITH:
   STARTING POINT = ?
   # OF POINTS = ?
2. LISTS ON TERMINAL REAL CONTENTS OF PORTION OF OBUF SPECIFIED.

B. LI--LIST IMAGINARY
1. SAME PROMPTS AS A.
2. LISTS ON TERMINAL THE IMAGINARY CONTENTS OF PORTION OF OBUF SPECIFIED.

C. LM--LIST MAGNITUDE
1. SAME PROMPTS AS A.
2. LISTS ON TERMINAL THE MAGNITUDE OF PORTION OF OBUF SPECIFIED.

D. LS--LIST SAMPLE
1. SAMPE PROMPTS AS A.
2. LISTS ON TERMINAL PORTION OF SAMPLE FROM SAMPLE.DAT AS SPECIFIED

E. L---LIST PLIST
1. LISTS THE CONTENTS OF THE 30 PLIST ADDRESSES

PLOT

A. PS--PLOT SAMPLE
1. SAMPLE.DAT IS READ INTO OBUF
2. THE ABSOLUTE MAXIMUM OF THE SAMPLE IS LISTED AND A PROMPT IS ISSUED FOR THE PLOT MAXIMUM. IF <RETURN> IS PRESSED, THE PLOT MAXIMUM IS TAKEN TO BE THE SAMPLE MAXIMUM, OTHERWISE THE VALUE ENTERED IS TAKEN AS THE PLOT MAXIMUM.
3. THE SAMPLE DATA IN OBUF IS PLOTTED WITHOUT A BORDER.

B. PR$-PLOT REAL
1. THE REAL PART OF CBUF IS LOADED INTO OBUF. (FOR THE NUMBER OF POINTS SPECIFIED)
2. THE SAME PROMPT AND PROCEDURE AS A.

C. PI$-PLOT IMAGINARY
1. THE IMAGINARY PART OF CBUF IS LOADED INTO OBUF. (FOR

THE NUMBER OF POINTS SPECIFIED)

2. SAME PROMPT AND PROCEDURE AS A.

D. PM$-PLOT MAGNITUDE

1. THE MAGNITUDE OF CBUF IS LOADED INTO OBUF (FOR THE NUMBER OF POINTS SPECIFIED)

2. SAME PROMPT AND PROCEDURE AS A.

E. PP$-PLOT PHASE

1. THE PHASE OF CBUF IS LOADED INTO OBUF (FOR THE NUMBER OF POINTS SPECIFIED)

2. SAME PROMPT AND PROCEDURE AS A.

F. PD--PLOT DISPLAY

1. PLOTS THE CURRENT CONTENTS OF OBUF, PLOTTED WITH A BORDER.

G. P---PLOT

1. A BORDER IS PLOTTED.

2. THE CURRENT CONTENTS OF OBUF ARE PLOTTED.

H. PB--PLOT BORDER

1. A BORDER IS PLOTTED WITH 10 DIVISIONS, HORIZONTALLY AND VERTICALLY

READ

A. R---READ (COMPLEX FILES)

1. PROMPTS WITH:

FILE NAME = ?

2. READS FILE (OF COMPLEX NUMBERS) INTO CBUF

NOTE: THE FILE READ IN MUST HAVE BEEN WRITTEN WITH A W COMMAND (SEE WRITE).

B. RS--READ SAMPLE

1. PROMPTS WITH:

FILE NAME = ?

2. READS FILE (SAMPLE FILE) INTO SAMPLE.DAT

NOTE: THE FILE READ IN MUST HAVE BEEN WRITTEN WITH A WS COMMAND (SEE WRITE).

SAMPLE

A. S_#-SAMPLE

1. IF #>0, PLIST(7) IS SET TO #
2. DATA IS SAMPLED INTO OBUF AT THE PLIST(7) LEVEL BY SAMPLING PLIST(5) TIMES AT EACH POINT FOR PLIST(4) SCANS, THEN THE DATA IS DIVIDED BY PLIST(4) TIMES PLIST(5).
3. THE AVERAGE, DETERMINED FROM THE FIRST PLIST(14) PERCENT OF THE SAMPLE, IS SUBTRACTED FROM ALL POINTS.
4. THE SAMPLE DATA IS COPIED TO SAMPLE.DAT ON DK:(=RK1:)
5. THE SAMPLE DATA IS COPIED INTO THE BEGINNING REAL PART OF CBUF.
6. THE SAMPLE IS DISPLAYED ON OSCILLOSCOPE.

B. SS#-SAMPLE SLOWER
   1. THE SAMPLING DELAY, PLIST(6) IS DOUBLED
   2. REMAINING PROCEDURE SAME AS PART A.

C. SF#-SAMPLE FASTER
   1. THE SAMPLING DELAY, PLIST(6), IS DIVIDED BY 2.
   2. REMAINING PROCEDURE SAME AS PART A.

D. SR--SAMPLE REAL
   1. MOVES THE DATA FROM SAMPLE.DAT TO REAL PART OF CBUF AT A LEVEL OF PLIST(7)

WRITE

A. WS--WRITE SAMPLE
   1. PROMPTS WITH:
      FILE NAME = ?
   2. WRITES OBUF TO SPECIFIED FILE

B. WR--WRITE REAL
   1. PROMPTS WITH:
      FILE NAME = ?
   2. WRITES REAL PORTION OF OBUF TO SPECIFIED FILE

C. WP--WRITE PHASE
   1. PROMPTS WITH:
      FILE NAME = ?
      SCOPE TIME BASE IN NSEC/DIV = ?
   2. WRITES PHASE FROM REAL AND IMAGINARY PORTION OF OBUF TO SPECIFIED FILE

D. WI--WRITE IMAGINARY

1. PROMPTS WITH:

FILE NAME = ?

2. WRITES IMAGINARY PORTION OF OBUF TO SPECIFIED FILE

E. W---WRITE REAL AND IMAGINARY

1. PROMPTS WITH:

FILE NAME

2. WRITES THE REAL AND IMAGINARY PORTIONS OF OBUF TO THE SPECIFIED FILE.

ZERO

A. Z---ZERO

1. PROMPTS WITH:

START OF TAPER DOWN, WIDTH OF TAPER, END ?

2. PLACES A 1-COS(X) TAPER BEGINNING AT THE SPECIFIED POINT, AND THEN PROCEEDS TO ZERO THE REST OF THE SPECIFIED PORTION OF CBUF.

DATA Program Documentation

AD - ADD TWO COLUMNS (ALL ROWS)

PROMPTS:

ADD COLUMN = ?

TO COLUMN = ?

PUT RESULTS IN COLUMN = ?

CC - COPY ONE COLUMN TO ANOTHER COLUMN (ALL ROWS)

PROMPTS:

COPY FROM COLUMN = ?

TO COLUMN = ?

CO - CORRELATION BETWEEN TWO COLUMNS (STARTING AT ROW 1)

PROMPTS:

OBSERVED DATA COLUMN = ?

MODELED DATA COLUMN = ?

ENDING ROW = ?

CR - COPY BY ROWS FROM ONE COLUMN TO ANOTHER

PROMPTS:

COPY FROM COLUMN = ?

TO COLUMN = ?

FROM ROW = ?

THROUGH ROW = ?

INTO ROW = ?

CS - CUBIC SPLINE INTERPOLATION (STARTING AT ROW 1, REQUIRES TWO WORK COLUMNS PAST FINAL Y-COLUMN)

PROMPTS:

INITIAL X-COLUMN = ?

INITIAL Y-COLUMN = ?

FINAL X-COLUMN = ?

FINAL Y-COLUMN = ?

OF INITIAL POINTS = ?

OF FINAL POINTS = ?

DC - DISPLAY COLUMN ON SCOPE

PROMPTS:

```
        DISPLAY COLUMN = ?
        THROUGH ROW = ?
DI - DIVIDE ONE COLUMN BY ANOTHER (ALL ROWS, SKIPS ROWS WITH A 0 ,
     DEMONIMATOR)
       PROMPTS:
         DIVIDE COLUMN = ?
         BY COLUMN = ?
         PUT RESULT IN COLUMN = ?
EP - EVALUATE A POLYNOMIAL (STARTING AT ROW 1, ORDER COEFFICIENTS FROM
     SMALLEST TO LARGEST POWER OF X)
       PROMPTS:
         X-COLUMN = ?
         Y-COLUMN = ?
         COEFFICIENT COLUMN = ?
         ORDER OF POLYNOMIAL = ?
         # OF POINTS = ?
ET - EXAMINE TITLE (PUT THE COLUMN NUMBER AFTER THE ET)
GE - GENERATE A COLUMN (ALL ROWS)
       PROMPTS:
         GENERATE COLUMN = ?
         X(_,_) = ?
         INCREMENT (PER ROW) = ?
IN - INPUT DATA (STOPS IF THE FIRST CHARACTER IN A LINE IS E)
       PROMPTS:
         INPUT COLUMNS = ?
         BEGINNING ROW = ?
LI - LIST COLUMNS
       PROMPTS:
         LIST COLUMNS = ?
         BEGINNING ROW = ?
         ENDING ROW = ?
LO - LOG (BASE 10) OF A COLUMN (SKIPS ROW IF ARGUMENT <=0.)
       PROMPTS:
```

```
        COLUMN TO TAKE THE LOG OF = ?
        COLUMN TO PUT THE LOG IN = ?
LS - LEAST SQUARES REGRESSION
     REQUIRES THAT THE OBSERVATIONS MATRIX BE SET UP STARTING IN THE
     STARTING COLUMN, THE COEFFICIENTS WILL BE PLACED IN THE COLUMN
     FOLLOWING THE MATRIX.  THE OBSERVED DATA COLUMN SHOULD FOLLOW THE
     COEFFICIENT COLUMN AND A GENERATED DATA COLUMN IS PLACED AFTER THE
     OBSERVED DATA COLUMN.  THUS AN N-TERM MODEL REQUIRES N+3 COLUMNS.
     THIS COMMAND CAN ALSO BE USED AS A MATRIX EQUATION SOLVER USING
     GAUSS-ELIMINATION BY SPECIFYING AS MANY POINTS AS TERMS IN THE
     MODEL.  THE ORIGINAL MATRIX AND VECTOR ARE NOT DESTROYED.
       PROMPTS:
         # OF POINTS = ?
         # OF TERMS IN MODEL = ?
         STARTING COLUMN = ?
MM - MINIMUM,MAXIMUM (STARTING AT ROW 1)
       PROMPTS:
         COLUMNS = ?
         ENDING ROW = ?
MU - MULTIPLY TWO COLUMNS (ALL ROWS)
       PROMPTS:
         MULTIPLY COLUMN = ?
         BY COLUMN = ?
         PUT RESULT IN COLUMN = ?
PB - PLOT BORDER
       PROMPTS:
         # OF X-TICKS = ?
         # OF Y-TICKS = ?
PE - PERCENT ERROR BETWEEN TWO COLUMNS (IF THEORETICAL=0,ERROR=EXPERI-
     MENTAL)
       PROMPTS:
         THEORETICAL COLUMN = ?
         EXPERIMENTAL COLUMN = ?
         PERCENT ERROR COLUMN = ?
```

PF - POLYNOMIAL FIT (SETS UP OBSERVATIONS MATRIX FOR THE LEAST SQUARES ROUTINE ABOVE. THUS FOR AN N-TH ORDER POLYNOMIAL THE WORKSPACE SHOULD CONTAIN N+4 CONTIGUOUS COLUMNS.)

PROMPTS:

OF POINTS = ?

ORDER OF POLYNOMIAL = ?

BEGINNING WORKSPACE COLUMN = ?

X-COLUMN = ?

Y-COLUMN = ?

PL - PLOT ONE COLUMN VS ANOTHER

PROMPTS:

X-COLUMN = ?

Y-COLUMN = ?

BEGINNING ROW = ?

ENDING ROW = ?

DESIRED XMIN = ?

DESIRED XMAX = ?

DESIRED YMIN = ?

DESIRED YMAX = ?

SHOULD A BORDER BE PLOTTED ?

X-INCREMENT = ?

Y-INCREMENT = ?

CONNECT THE POINTS ?

PRINT SYMBOL AND SIZE = ?

PM - PLOT ACCORDING TO THE MAXIMUMS AND MINIMUMS SET IN CORE

PROMPTS:

X-COLUMN = ?

Y-COLUMN = ?

SHOULD A BORDER BE PLOTTED ?

X-INCREMENT = ?

Y-INCREMENT = ?

CONNECT THE POINTS ?

PRINT SYMBOL AND SIZE = ?

```
PR - POLAR TO RECTANGULAR CONVERSION (X&Y ARE ADJACENT, MAG&THETA ARE
     ADJACENT)
       PROMPTS:
         X-COLUMN = ?
         MAG-COLUMN = ?
RE - READ DATA FROM DISK
       PROMPTS:
         INPUT FILE NAME = ?
         BEGINNING COLUMN = ?
RP - RECTANGULAR TO POLAR CONVERSION (SAME AS PR)
       PROMPTS:
         X-COLUMN = ?
         MAG-COLUMN = ?
SM - SET MAXIMUMS AND MINIMUMS IN CORE
       PROMPTS:
         XMIN = ?
         XMAX = ?
         YMIN = ?
         YMAX = ?
SU - SUBTRACT COLUMNS (ALL ROWS)
       PROMPTS:
         SUBTRACT COLUMN = ?
         FROM COLUMN = ?
         PUT RESULT IN COLUMN = ?
TI - TITLE INPUT (PUT COLUMN NUMBER AFTER THE TI)
       PROMPTS:
         TITLE FOR COLUMN _ = ?
WR - WRITE COLUMNS TO DISK
       PROMPTS:
         OUTPUT FILE NAME = ?
         BEGINNING COLUMN = ?
         ENDING COLUMN = ?
```

APPENDIX D.

FREQUENCY SCALE COMPUTATIONS

After performing a Fast Fourier Transformation (FFT) on a signal sampled by means of the USPO program, it is necessary to find the frequency scale of the transform or the frequency spectrum. The following computations demonstrate how these scales are found.

Let's define the various levels, powers of 2[1], of the sampling, transforming and displaying operations, as follows:

N: Sampling Level (0 to 10)

M: FFT Level (0 to 11)

K: Display Level (0 to 12).

Assume the scope setting to be x units/div when sampling, then the total time across the screen is

$$T = 10x \quad ; \tag{D.1}$$

then one can say that the resolution in the time domain is

$$\Delta t = T/2^N$$

or

$$\Delta t = 10x/2^N \tag{D.2}$$

upon substitution of Eq. (D.1). If one now selects the FFT level, M, to be equal or larger than the sampling level, N, the expanded time window, T′, will become

$$T' = 2^M \Delta t$$

which upon substitution of Eq. (D.2) becomes

---

[1]These levels or powers of 2 are discussed under the Programming--USPO section of this dissertation.

$$T' = 2^{(M-N)}(10x). \tag{D.3}$$

By definition, the frequency resolution will be the inverse of the period, or

$$\Delta f = \frac{1}{T'} = \frac{1}{2^{(M-N)}(10x)}; \tag{D.4}$$

and the maximum frequency will be

$$f_{max} = 2^M \Delta f = \frac{2^M}{2^{(M-N)}(10x)}$$

or

$$f_{max} = \frac{2^N}{10x}. \tag{D.5}$$

Now, not always does one want to display the full frequency spectrum; therefore, if the display level is smaller than the FFT level, it is necessary to scale the maximum displayed window frequency as follows:

$$f_{max/disp.} = \frac{2^K}{2^M} f_{max} = \frac{2^{(K+N-M)}}{10x}. \tag{D.6}$$

Table D.1 has been developed for various choices of scope setting, sampling, transformation and displaying levels.

Table D.1. Table for the selection of scales for FFT and frequency spectrums, in MHz

	Diff Between FFT Level And Sample Level	Display Level			
		6	7	8	9
100 ns/div	0	64			
	1	32	64		
	2	16	32	64	
	3	8	16	32	64
200 ns/div	0	32	64		
	1	16	32	64	
	2	8	16	32	64
	3	4	8	16	32
500 ns/div	0	12.8	25.6	51.2	
	1	6.4	12.8	25.6	51.2
	2	3.2	6.2	12.8	25.6
	3	1.6	3.2	6.4	12.8
1 µs/div	0	6.4	12.8	25.6	51.2
	1	3.2	6.4	12.8	25.6
	2	1.6	3.2	6.4	12.8
	3	0.8	1.6	3.2	6.4
2 µs/div	0	3.2	6.4	12.8	25.6
	1	1.6	3.2	6.4	12.8
	2	0.8	1.6	3.2	6.4
	3	0.4	0.8	1.6	3.2

APPENDIX E.

RAYLEIGH WAVE SPECTROSCOPY TO MEASURE THE DEPTH OF SURFACE CRACKS[1]

A. J. Testa and C. P. Burger
Department of Engineering Science and Mechanics
and Engineering Research Institute
Iowa State University
Ames, IA 50011 USA

---

[1]This paper was presented by the author at the 13th Symposium on NDE, San Antonio, Texas, April 21-23, 1981. To be published in the symposium proceedings.

ABSTRACT

Rayleigh waves are eminently suited for the detection and characterization of surface breaking and near surface defects. The paper describes how the property of an R-wave, according to which its frequency content varies with depth below a surface, may be used to measure the depth of surface breaking cracks. The method involves the signal analysis of a selected portion of the transmitted surface waves after interaction with a crack. The paper describes how the relevant portion of the total transmitted signal can be automatically selected by an on-line minicomputer. An FFT of this signal is then performed and pattern recognition procedures are used to identify that specific characteristic of the frequency spectrum that indicates the depth of the crack. Since the method does not rely on time of flight or amplitude measurements, it is insensitive to the path of the crack, to roughness of the crack surface, to residual stresses at the crack tip, to weld splatter or oil between the transmitter and receiver transducers, and to other operational variables such as circuit damping and separation between transducers.

INTRODUCTION

Shallow surface breaking cracks form an important category of defects. They represent the origin and early growth stages of the majority of fatigue failures. It is, therefore, important for quantitative life predictions to know their initial depths and to monitor their early growth. Yet a reliable ultrasonic inspection procedure for characterizing such defects is not available. Various amplitude and time of flight methods have been proposed for measuring relatively deep open cracks and slots [1-3]. Although these methods are accurate for artificial flaws, they generally overestimate the depth of such cracks in real structures, probably because they are affected to unknown extents by residual stresses at the surface and at crack tips and by internal changes in material properties [4-6]. There is a need for an ultrasonic measurement of crack depth that is independent of the usual operational, material and stress variables that affect the older methods.

Rayleigh surface waves are attractive for interrogating surface and near surface defects. Their energy is contained in a shallow region less than two wavelengths below the surface so that they are not affected by far-surface reflections and by deep structural changes. They are not as dispersive as bulk waves and will follow gently curved surfaces for long distances without much attenuation. There is, therefore, much contemporary interest in the scattering of R-waves from shallow defects [7-13].

One feature of a broadband Rayleigh wave has not hitherto been considered for ultrasonic inspection. Since the effective energy of a specific frequency component of a R-wave is confined to a distance from the surface of less than 1 to 1-1/2 wavelengths, a broadband wave will have a frequency spectrum which varies with depth. On the surface the wave will possess the full frequency spectrum of the surface pulse. At some depth below the surface, however, the spectrum will be devoid of the higher frequencies; i.e., the shorter wavelengths. The significance of this property for quantitative NDE was first recognized by Singh and Burger from dynamic photoelastic visualizations of the

interactions between slots and surface waves [14-18]. They postulated that an open surface breaking defect with a depth less than the longest effective wavelength in a broadband Rayleigh pulse will act as a low pass filter with cut-off close to the frequency that has a wavelength equal to the depth of the defect. The transmitted Low Frequency Rayleigh (LFR) should be separable from the other transmitted waves and will contain, in its more limited frequency spectrum, the necessary information about the depth of slots and open surface breaking cracks. This behavior is illustrated in Fig. E.1a.

Stage I in the figure depicts an incident Rayleigh wave. It contains all the frequencies of the broadband incident pulse; hence, the name "All Frequencies Rayleigh (AFR)". The shape of the diagram indicates not only that the energy decays exponentially with depth below the surface, but also the frequency distribution with depth. All frequencies are present at the surface, but only the lower frequencies exist deeper into the material.

Stage II shows the Rayleigh waves that are generated when the incident pulse interacts with a slot. First there is the back reflected Rayleigh from the front face of the slot. It has a large amount of energy and contains all the frequency components of the incident wave. It is, therefore, an All Frequencies Rayleigh (AFR). In reality, the frequency spectrum of this wave is severely modified by induced resonances of various planes of the slot [13]. Then there is the All Frequencies Rayleigh wave which rounds the upper left-hand corner and proceeds down the face of the slot. It has a much lower amplitude than the back reflected wave. Lastly, there is the Low Frequencies Rayleigh wave (LFR) which represents the deeper portions of the incident wave that cuts under the slot. The precise mechanism by which that wave ultimately manifests itself as a forward scattered LFR on the surface is not understood; but it is clear, from photoelastic and ultrasonic data, that it eventually forms into a distinct wave, here called LFR.

The AFR which propagated down the front face of the slot ultimately rounds the tip and after shedding a large amount of its energy as a shear wave at the tip [14,18], proceeded up the back face and onto the far surface. It is still an AFR even though of greatly reduced amplitude. Stage III shows the two fundamental Rayleigh waves, the leading LFR and the transmitted AFR. They appear as a wave packet which need to be separated if Singh's postulate is to be used for the quantitative NDE of cracks.

There are, obviously, other secondary transmitted waves present in the total forward scattered signal. They arise from various mode conversions from bulk and surface waves at the slot. They are not shown in Fig. E.1.

Singh confirmed his postulate with ultrasonic tests on wide slots in steel [14,16,17]. This paper is concerned with refinements in the ultrasonic test procedures that are necessary if Singh's insight into the behavior of the transmitted surface wave is to be used for the quantitative NDE of cracks.

TEST PROCEDURES

The ultrasonic tests were performed on narrow slots of 0.56 ± 0.5 mm and on electric discharge machined (EDM) slits with widths that varied from 0.28 mm to 0.08 mm in various sized specimens of 1018 plain carbon steel. The technique for testing and signal analysis that was developed on these specimens was then applied to open fatigue cracks in A387 steel. Slots, slits and cracks that varied in depth from 1.03 mm to 4.87 mm were tested. The transducers were regular 5 MHz wideband Rayleigh wave units consisting of P-wave crystals mounted on 90° Lucite wedges. They were placed on opposite sides of a slit in a pitch-catch mode. The signal from the receiver was sampled and displayed on a digital sampling oscilloscope from where it was transferred to a LSI-11 minicomputer. Here the signal was processed in the complex frequency domain with a Fast Fourier Transform procedure. The final real and imaginary components

were added vectorially, and the resultant frequency spectrum was displayed as a "relative amplitude" vs "frequency" plot.

Figure E.2a is an amplitude vs time plot of the reference (incident) wave as sensed by the receiving transducer when there was no slot between the two wedges. Figure E.2b is the frequency spectrum of this wave.

After the wave has interacted with a defect, it is modified and appears on the oscilloscope screen in the form shown in Fig. E.3a. This is the relative amplitude vs time plot of the composite wave packet shown as AFR + LFR in Stage III of Fig. E.1. It includes some secondary mode converted waves in addition to the two basic Rayleigh waves. Figure E.3b presents the results of the FFT of the complete signal as shown in Fig. E.3a. The slot was 1.03 mm deep.

The dotted line near the bottom of Fig. E.3b was drawn in by hand to represent the shape of the frequency spectrum of the reference wave with greatly reduced amplitude to match the relative amplitude of the high frequency portion of the main spectrum. If all the frequency components of the reference wave were reduced in the same ratio, this would have been the shape of FFT of the total transmitted wave. Clearly, the low frequency components were not as severely attenuated as their high frequency counterparts.

The acoustic wave velocities for the steel were

- C_P = Dilatational Wave Velocity - 5.85 mm/μs,
- C_S = Shear Wave Velocity = 3.23 mm/μs,
- C_R = Surface Wave Velocity = 2.96 mm/μs.

If the path length around the slot between transmitter and receiver is calculated, the transmitted AFR wave in Stage III of Fig. E.1 can be identified on Fig. E.3a from its arrival time. It is the double pulse which is centered at about 4μs. The overall signal in Fig. E.3a was split at the beginning of the AFR into "Leading Waves," which should include the LFR and the Transmitted Rayleigh waves which includes the AFR.

In order to analyze either portion of the signal in Fig. E.3a, the other part had to be zeroed digitally and the transition point smoothed with a cosine function. The actual procedure is to select a window of points, then the computer is commanded to apply a function 1-cosx starting at one end of the window to the other making the last point a zero and every point outside the window, thereafter, also zero.

Smoothing was necessary to avoid the artificial introduction of high frequency components into the spectrum. Some spurious frequencies are inevitable with this procedure; but with care, they can be kept small in number and in magnitude.

Figure E.4a shows the results of the FFT on the "Transmitted Rayleigh" portion in Fig. E.3a. As before, the attenuated shape of the reference wave is shown dotted.

The low frequency peak at about 0.55 MHz coincides with the narrow peak at the same frequency on Fig. E.3b. The second peak (1.15 MHz) of Fig. E.3b is completely absent. In fact, it almost coincides with the valley at 1.25 MHz on Fig. E.4a.

Figure E.4b is the frequency spectrum of the "Leading Waves"; i.e., of the left-hand portion of Fig. E.3a. It is almost completely devoid of high frequencies. The peak is not well defined but rather stretches from 1.15 MHz to 1.25 MHz. These two values coincide respectively with the second peak on Fig. E.3b and the bottom of the valley on Fig. E.4a. The frequency where the curve first levels out after the low frequency peak (3 MHz) coincides with a wavelength of 2.96/3 = 0.89 mm. This is considered to be the cut-off point below which the deeper portion of the incident R-wave passes underneath the slot while most of the energy in the shallower portion, including all the higher frequency components, is reflected by the front fact of the slot. From this single result, a gross approach could state that the effective depth of a R-wave is $1.03/0.89 = 1.16\lambda$. Beyond this depth the energy in a surface wave is of little value for NDE. Here λ = wavelength.

Figure E.5 shows the frequency spectra of the leading waves from four different slots. The progressively lower frequencies at cut-off

for the deeper slots is clear. A similar shift towards lower frequencies occurs in the low frequency peaks. This confirms the postulate according to which the bottom of a slot acts as a cut-off point for the deeper portions of a R-wave. The LFR wave which results may consist of more than just a single simple R-wave, but it still retains only the low frequency components of the incident wave.

In Fig. E.3b the cut-off wavelengths and peak wavelengths, equivalent to the frequencies C_1 to C_4 and the peaks of the curves in Fig. E.5, is plotted versus slot depth for nine different specimens. The equations for the two lines are:

$$\lambda_C = 0.02 + 0.82d \text{ with } r = 1.0$$

$$\lambda_P = 2.25d^{0.69} \text{ with } r^2 = 0.96$$

where

λ_C = Cut-off Wavelength

λ_P = Peak Wavelength

d = Slot Depth

r and r^2 are the correlation values for the line and curve fits.

Since both curves should go through zero, the intercept 0.02 could be ignored so that $\lambda_C = 0.82d$ as indicated on Fig. E.6.

EFFECTS OF VARIABLES

To demonstrate the flexibility of the proposed method and its possible use in the evaluation of open fatigue cracks, a series of tests was performed on narrow EDM slots and on an irregularly shaped open fatigue crack. Broadband Rayleigh wave transducers with center frequencies at 5 MHz and 2.25 MHz were used to demonstrate that the results are insensitive to transducer frequency as long as the pulse contains significantly strong components at frequencies with wavelengths larger than the crack depth.

Transducer Separation and Wave Groups

Figure E.7 shows the whole group of transmitted R-waves after a 2.25 MHz broadband pulse had interacted with a 2.2 mm deep by 0.076 mm wide EDM slot in 1018 steel. A_1 and A are the undercut LFR^{2t} and AFR^t (Fig. E.1 and E.3a) respectively. When the incident portion of AFR that runs down the front face of the slot reaches the tip, most of its energy mode converts to a shear wave [18] which propagates through the specimen to the opposite surface. It reflects back from this surface and impinges on the tip of the slit where it reconverts to a Rayleigh wave that travels up the back face and along the top surface at a specific distance behind the AFR^t determined by the specimen depth. Wave pocket B derives from this wave. The last group, C, is possibly shear waves from secondary reflections.

In Fig. E.7a the transducers were spaced 40 mm apart, 20 mm on either side of the slit. The time difference between A and B is 29.8 μs which coincides with the path described before. When the receiving transducer is moved further away from the slot, to 50 mm, Fig. E.7b is recorded. The spacings between A_1, A and B are unchanged confirming that they are all Rayleigh waves. Wave C gained on B and is, therefore, a faster wave, correctly identified as a S-wave.

Behavior of EDM Slits

The experiments presented in Figs. E.2 through E.6 were performed on relatively wide slots (0.5 to 0.6 mm). The same procedure was applied also to waves A1 and A of Fig. E.6, which was obtained from an Electric Discharge Machined slit which was only 0.076 mm wide. The aim of this test was to see if the double corners of a machined slot has significance in the interpretation of the test results. The results of a series of tests on this slit are given in Fig. E.8.

Figure E.8a presents the shape in the time domain of the wave received when the separation between the transducers was 40 mm with no slot between them. The frequency spectrum is shown by the dashed line.

It is narrower than for the transducer used in Figs. E.2 through E.6 and has an actual center frequency of 2.1 MHz.

In Fig. E.8b the combined group of waves A_1 and A of Fig. E.7a has been expanded and divided, as in Fig. E.3, into AFR and LFR. The dashed lines show the spectrum for the whole group. There is a clear change from Fig. E.8a with multiple modulations.

Figure E.8c is the representation of the AFR after the low frequency Rayleigh wave had been zeroed digitally. The spectrum has a remarkable resemblance to that of the reference wave in Fig. E.8a. Clearly, most of the frequencies in the incident wave are still present though much attenuated.

Figure E.8d shows only the LFR (A_1 in Fig. E.7a). It contains the same characteristic peak and cut-off features noticed in Fig. E.5. The wavelengths for the peak and cut-off points respectively come to λ_p = 3.66 mm and λ_c = 1.78 mm when the two frequencies are divided by the R-wave velocity in steel 1018. If these values are read into Fig. E.3b, the predicted slit depth is 2.05 mm and 2.2 mm, respectively. The prediction from λ_p is off by 7%; that from λ_c is spot-on!

Yield Zones at the Slit Tips

With such encouraging results, a new series of tests was run to evaluate the effect of residual stresses at the tips of slits. This time the EDM slit was 2.3 mm deep and 0.508 mm wide in steel 1018. The transducers were the 5 MHz wide-band pair that was used on the slots.

Figure E.9 is a superposition of the results from three tests on the same specimen with progressively larger yield zones at the tip of the slit. In the most extreme case, the originally straight specimen was bent to a deformation angle of 1° at the slit. Whilst there are small changes in the overall spectra for the three conditions, the cut-off and low frequency peaks remained unchanged. The prediction depths from Fig. E.3b are 2.35 mm for λ_p and 2.3 mm from λ_c!

Rayleigh Wave Interaction with a Real Crack

If the initial postulate is to be of real value, then it should also hold for an irregularly-shaped open fatigue crack. Such a crack was grown in a specimen of A-387 steel. The average depth of the crack was 4.2 mm, and it was interrogated with the 5 MHz transducers spaced 20 mm before and after the crack.

Figure E.10a shows the complete transmitted wave R^t consisting of parts A_1 (LFR) and A (AFR). The spectrum has many modulations because of the rough surfaces of the crack. The crack depth is near the lower limit of the frequency spectrum of the reference wave so that it is small in amplitude and broad in shape. If the dividing line between AFR and LFR is chosen as shown, Figs. E.10b and E.10c are obtained.

The frequency spectrum of the leading waves (AFR) (Fig. E.10b) again shows the distinctive low frequency peak and the cut-off point. The equivalent wavelengths for these points are shown on the figure. When read into Fig. E.6, the predicted crack depths are:

- From λ_p, d_p = 3.9 mm for an error of 6%;
- From λ_c, d_c = 4.25 mm for an error of only 1%.

Figure E.10c once again shows that the frequency spectrum of the LFR has a shape that is very similar to that of reference wave (Fig. E.2b).

Other Tests

Additional tests confirmed that the essential characteristics used to size cracks by the method described above is unaffected by the extent of damping in the test electrical circuit and by oil or weld splatter between the transducers.

CONCLUSIONS

Much work still remains to be done to refine this method sufficiently for it to be used reliably in the day to day characterization of shallow cracks. Under investigation at the moment are the effects of corrosion products in a crack and of partial or complete closure of a fatigue crack. However, the evidence presented here confirms the original postulate that a crack will act as a low pass filter for the deeper portions of Rayleigh surface waves and that the cut-off point for the "filter" can be related to the crack depth.

ACKNOWLEDGMENTS

This research was performed on equipment purchased with a grant from the National Science Foundation (No. ENG77-06970). The work was supported in part by the Ames Laboratory under contract No. W7405-ENG82, Director of Energy Research, Office of Basic Energy Sciences, WPAS-KC-02-01 and by the Department of Engineering Science and Mechanics and the Engineering Research Institute at Iowa State University.

REFERENCES

1. P. A. Doyle and C. M. Scab. "Crack Depth Measurement by Ultrasonics: A Review." Ultrasonics, Vol. 6, No. 4 (July 1978), 164-170.

2. M. G. Silk. "Defect Sizing Using Ultrasonic Diffraction." British J. of NDT, Vol. 21, No. 1 (January 1979), 12-15.

3. M. G. Silk. "Sizing Crack-Like Defects by Ultrasonic Means." Research Techniques in Non-Dest. Testing, Vol. 3, Ed. R. S. Sharpe, London: Academic Press, 1977.

4. B. G. Yee, J. C. Couchman, J. W. Hagemayer and F. H. Chay. "Stress and the Ultrasonic Detection of Fatigue Cracks in Engineering Metals." Non-Dest. Testing, Vol. 7 (1974), 245.

5. D. M. Corbly, P. F. Packman and H. S. Pearson. "Accuracy Precision of Ultrasonic Shear Wave Flaw Measurements on a Function of Stress on the Flaw." Mat. Eval., Vol. 30 (1970), 103-110.

6. B. H. Lidington, D. H. Saunderson and M. G. Silk. "Interference Effects in the Reflection of Ultrasound from Shallow Slits." Non-Dest. Testing, Vol. 6 (1973), 185-190.

7. J. Achenbach. "Detection of Interior and Surface-Breaking Cracks." Proc. DARPA/AF, Review of Progress in Quantitative NDE, San Diego, California, July 1980.

8. D. A. Mendelsohn, J. Achenbach and L. M. Keer. "Scattering of Elastic Waves by a Surface-Breaking Crack." Wave Motion, Vol. 2 (1980).

9. R. J. Hudgell, L. L. Morgan and R. F. Lumb. "Non-Destructive Measurement of the Depth of Surface Breaking Cracks Using Ultrasonic Rayleigh Waves." British J. of NDT, Vol. 16, No. 15 (September 1974), 144-149.

10. L. L. Morgan. "The Spectroscopic Determination of Surface Topography Using Acoustic Surface Waves." Acoustica, Vol. 30 (1974), 222-228.

11. K. G. Hall. "Crack Depth Measurements in Rail Steel by Rayleigh Waves Aided by Photoelastic Visualization." Non-Dest. Testing, (London), Vol. 9, No. 3 (June 1976), 121-126.

12. L. J. Bond. "A Computer Model of the Interaction of Acoustic Surface Waves with Discontinuities." Ultrasonics, Vol. 17 (1979), 71-77.

13. G. P. Singh and A. Singh. "Deconvolution Procedure for Crack Depth Measurement Using Rayleigh Waves." Proc. DARPA/AF, Review of Progress in Quantitative NDE, San Diego, California, July 1980.

14. A. Singh. "Crack Depth Determination by Ultrasonic Frequency Analysis Aided by Dynamic Photoelasticity." M. S. Thesis, Iowa State University, 1980.

15. A. Singh, C. P. Burger, L. W. Schmerr and L. W. Zachary. "Dynamic Photoelasticity as an Aid to Sizing Surface Cracks by Frequency Analysis." Mech. of Non-Dest. Testing, Ed. W. W. Stinchcomb, New York: Plenum Press, 1980, 277-292.

16. C. P. Burger and A. Singh. "An Ultrasonic Technique for Sizing Surface Cracks." Proc. DARPA/AF, Review of Progress in Quantitative NDE, San Diego, California, July 1980.

17. A. Singh and C. P. Burger. "A New Technique for Determining the Depth of Surface Cracks by Rayleigh Waves." ASNT, Fall Conference, Houston, Texas, October 1980.

18. C. P. Burger, A. J. Testa and A. Singh. "Dynamic Photoelasticity as an Aid in Developing New Ultrasonic Test Methods." Proceedings of the 1981 Fall Meeting of the Society for Experimental Stress Analysis, Dearborn, Michigan, May 1981.

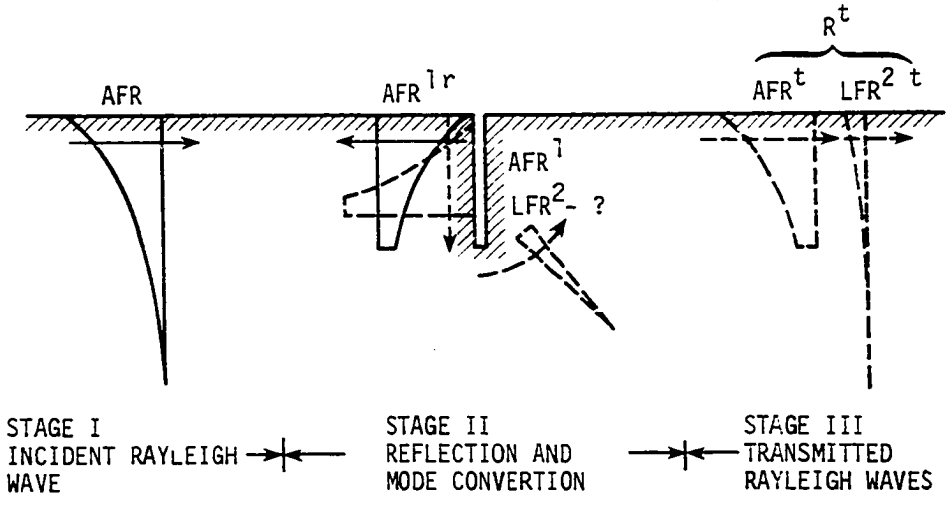

Figure E.1. Rayleigh wave interaction with a slot

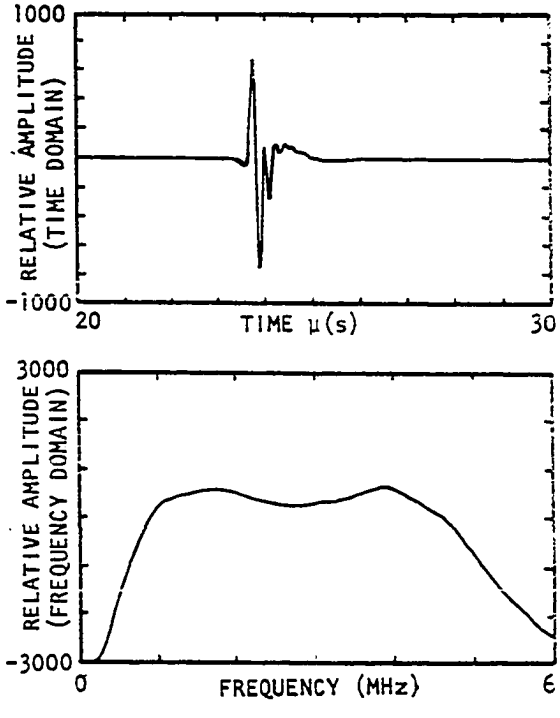

Figure E.2. a. Time scan;
b. Frequency spectrum

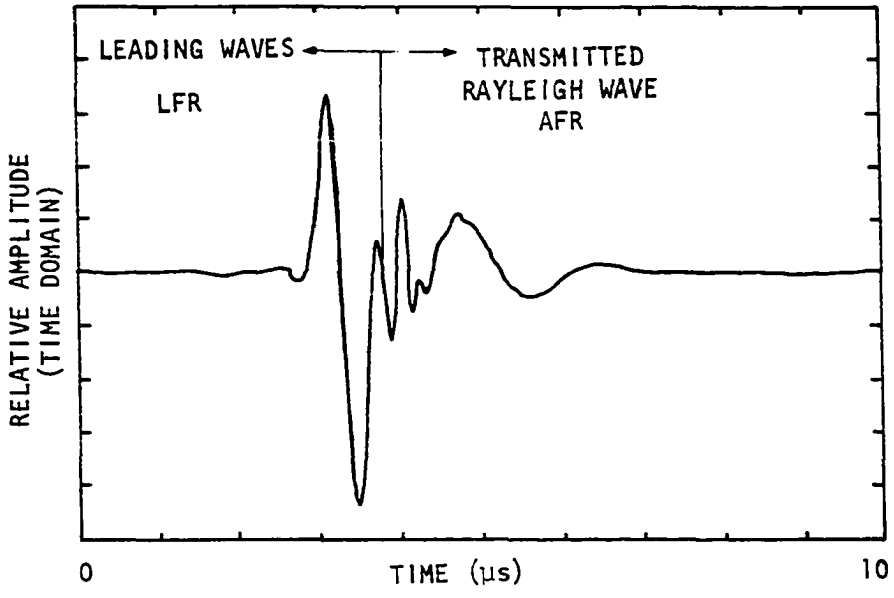

a. Time scan of all waves

a

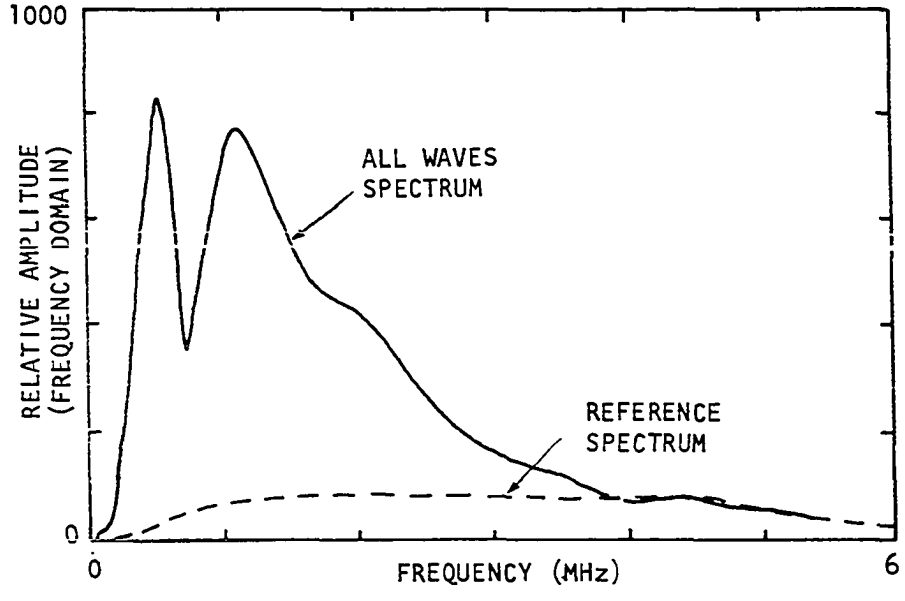

b. Frequency spectrum of all waves

b

Figure E.3. Study of the interaction of a Rayleigh wave and a 1.03 mm deep slot in steel

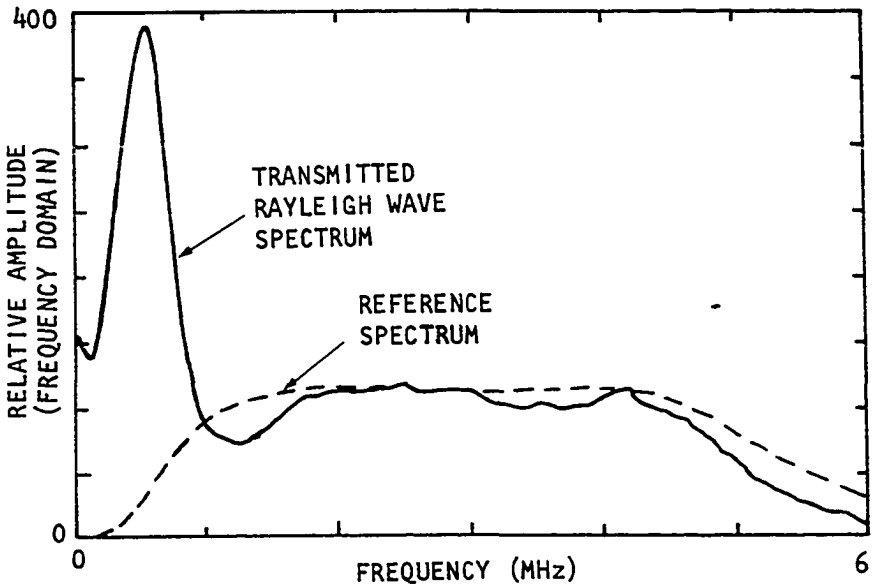

a

a. Frequency spectrum for the right hand portion (AFR) of Fig. E.3a

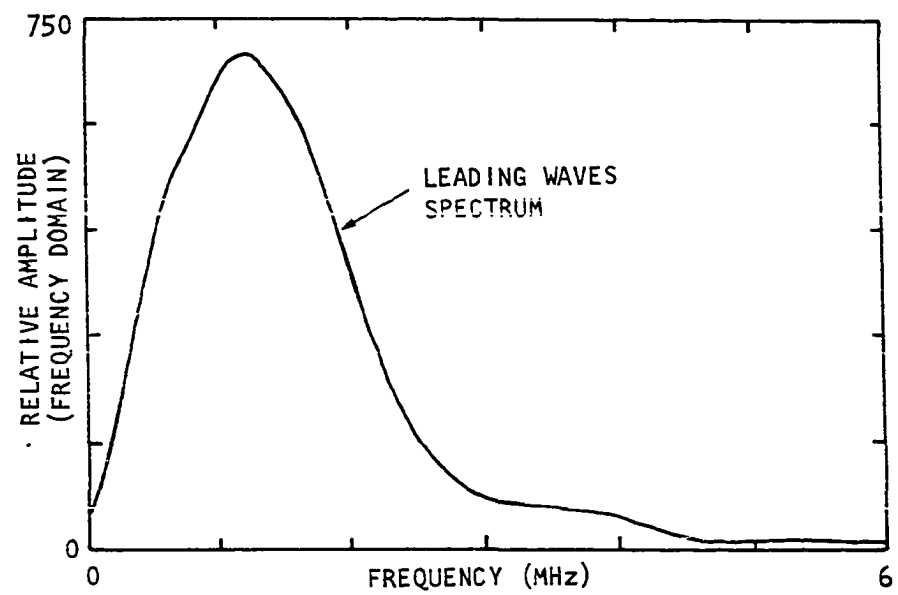

b

b. Frequency spectrum for the loading waves in Fig. E.3a

Figure E.4. Study of the interaction of a Rayleigh wave and a 1.03 mm deep slot in steel

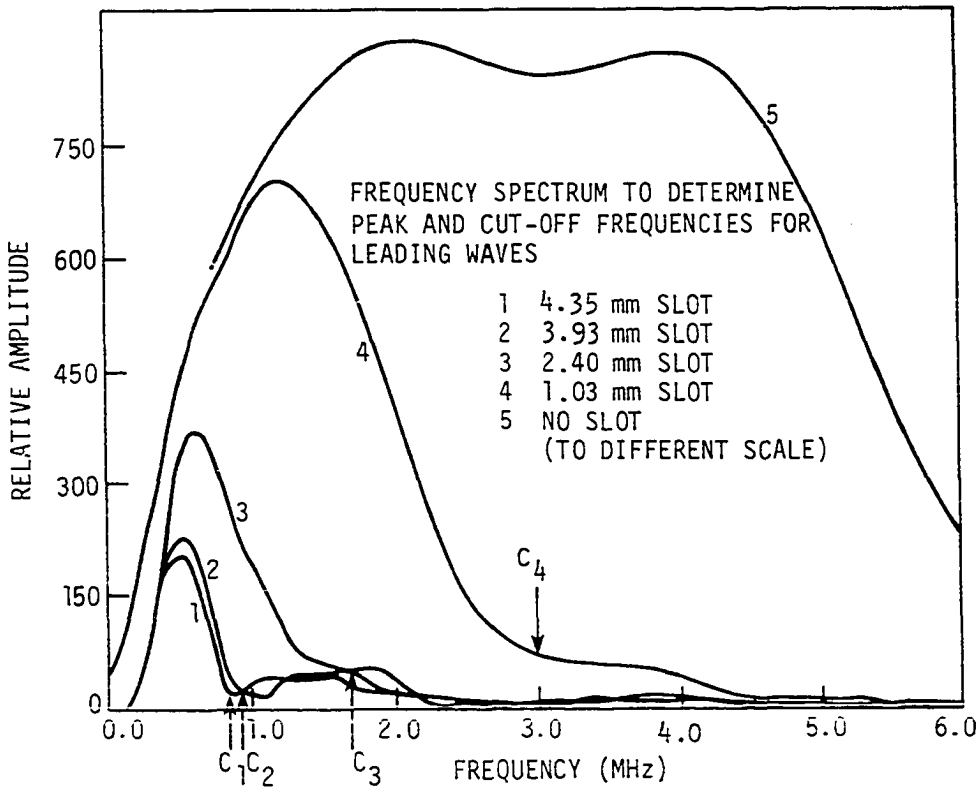

Figure E.5. Frequency spectra for four different slot depths and their respective cut-off (C_1 - C_4) frequencies

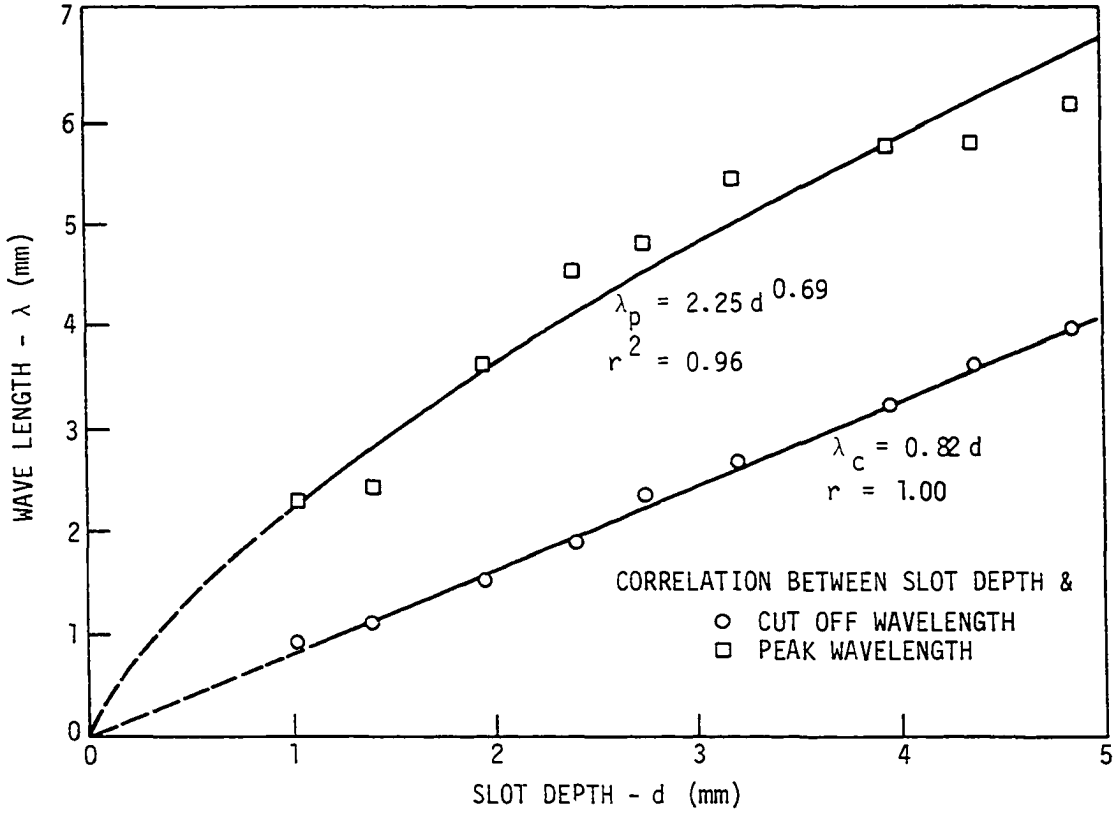

Figure E.6. Correlation between depth of slots and cut-off or peak wavelengths
λ_c = cut-off wavelength
λ_p = peak wavelength

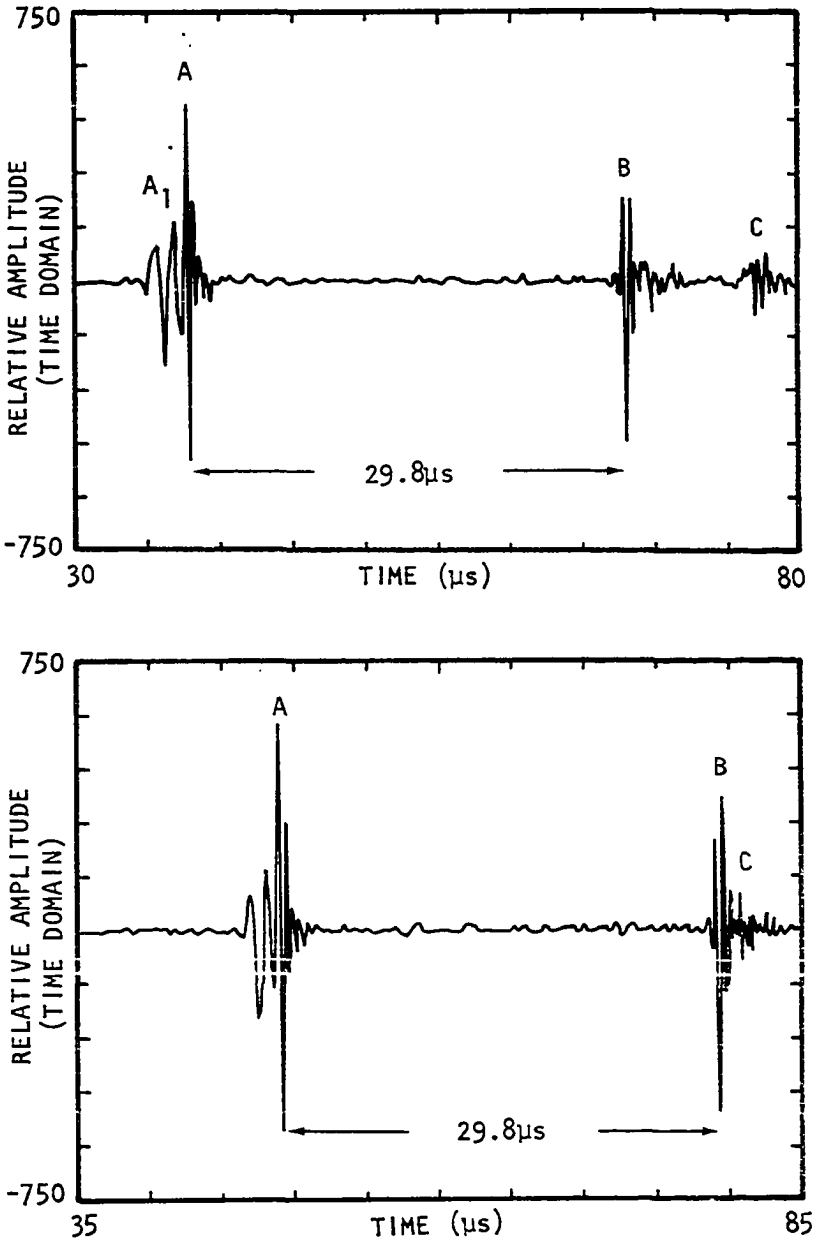

Figure E.7. Effect of separation between transducers
a. 20 mm on either side of slit
b. 20 mm in front and 50 mm behind slit

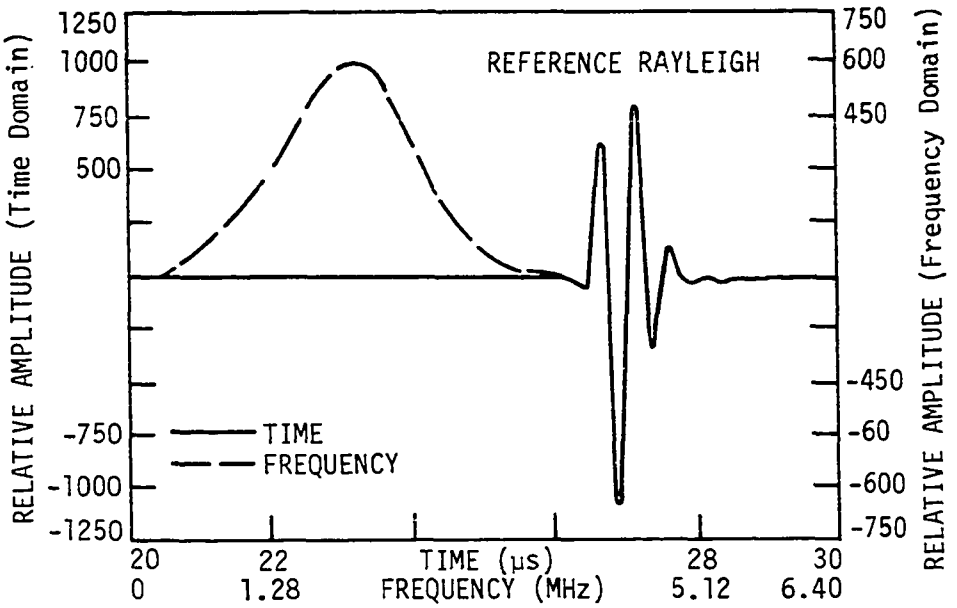

a. No slot - reference wave

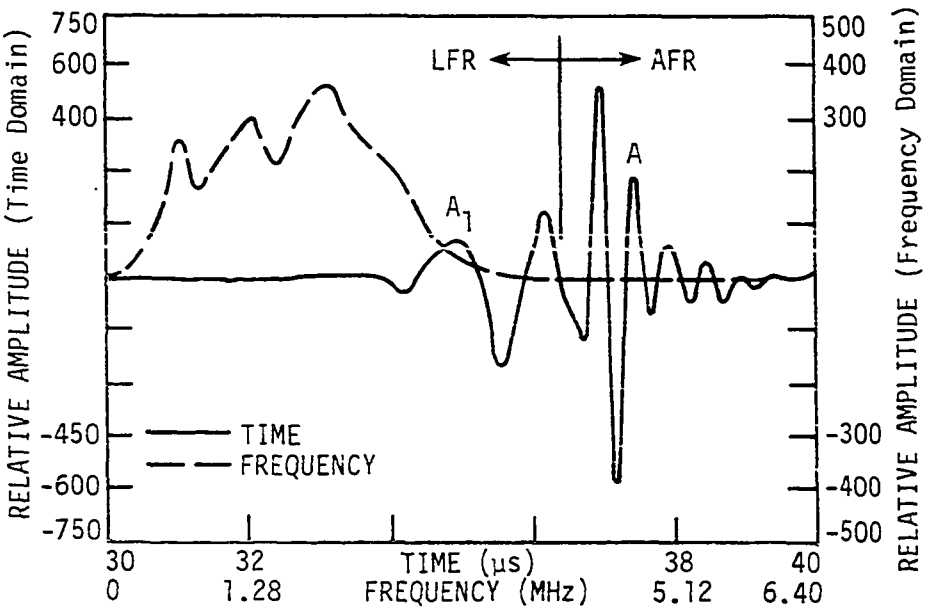

b. Total transmitted wave after slot (AFR + LFR)

Figure E.8. Combined time and frequency plots of the transmitted Rayleigh waves from a 2.2 mm deep slot using 2.25 MHz transducers

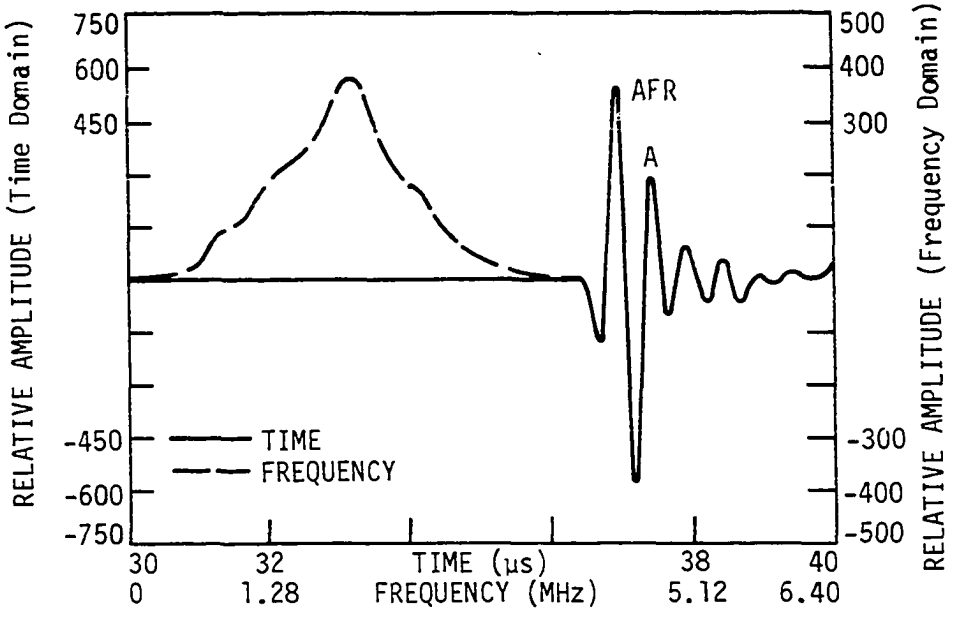

c. AFR^t

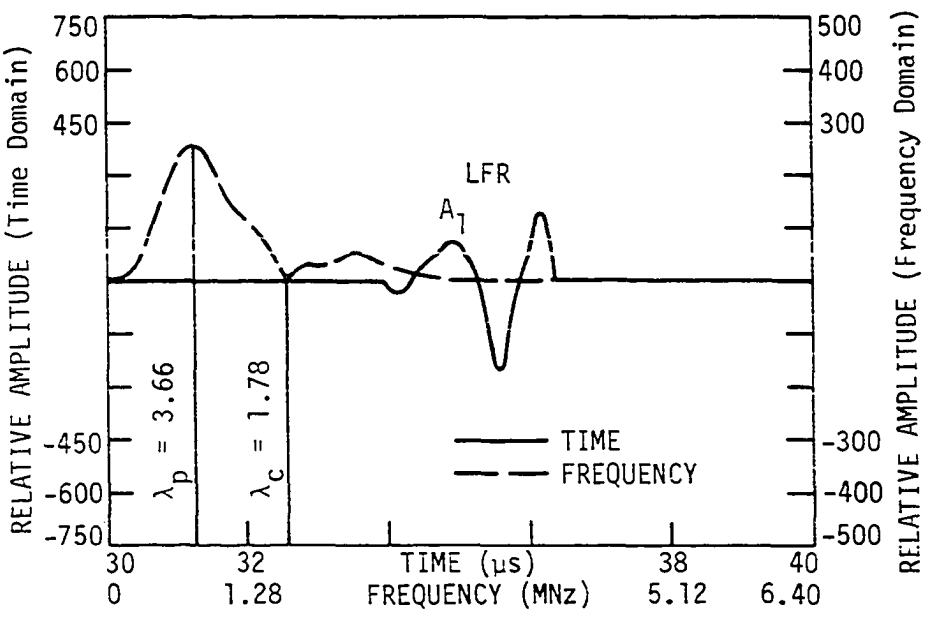

d. LFR

Figure E.8. (cont.)

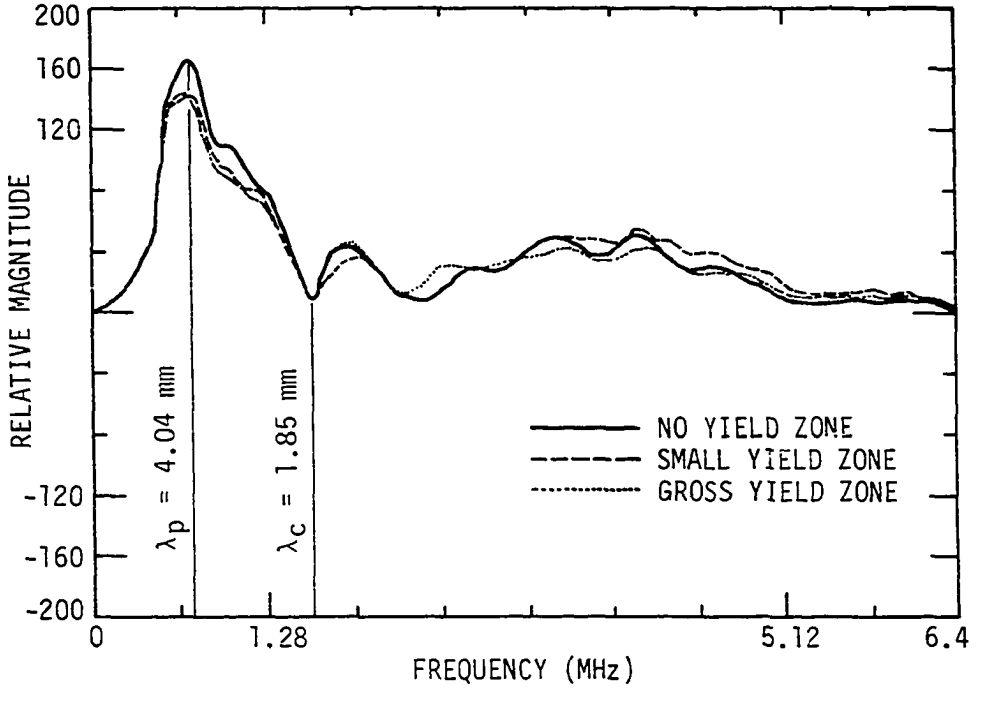

Figure E.9. The effect of crack tip residual stresses on the frequency spectra of the LFR wave

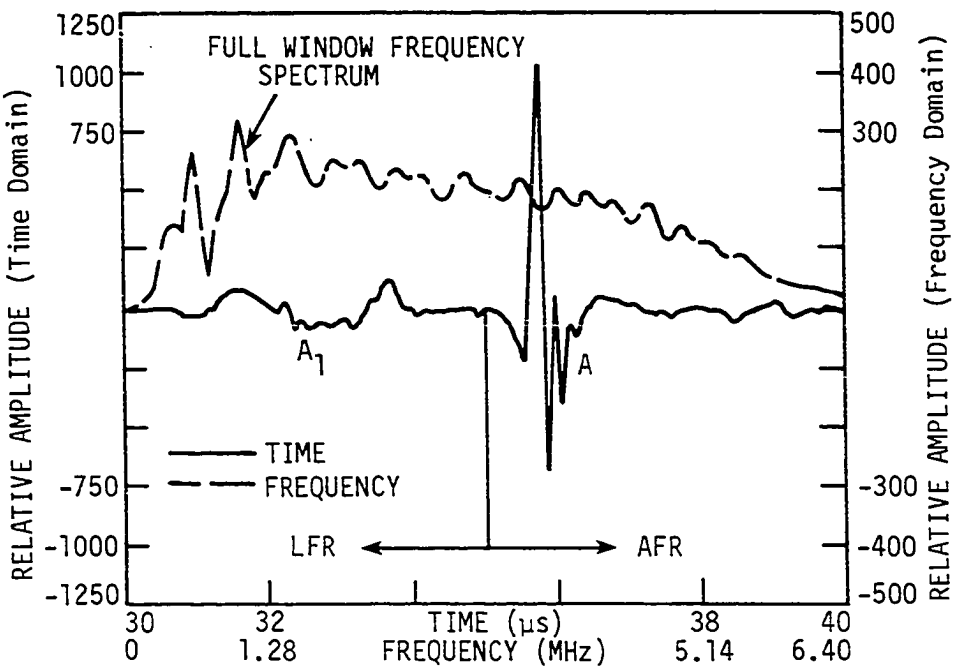

a. AFR + LFR

Figure E.10. The results from a 6.2 mm deep, irregularly shaped fatigue crack

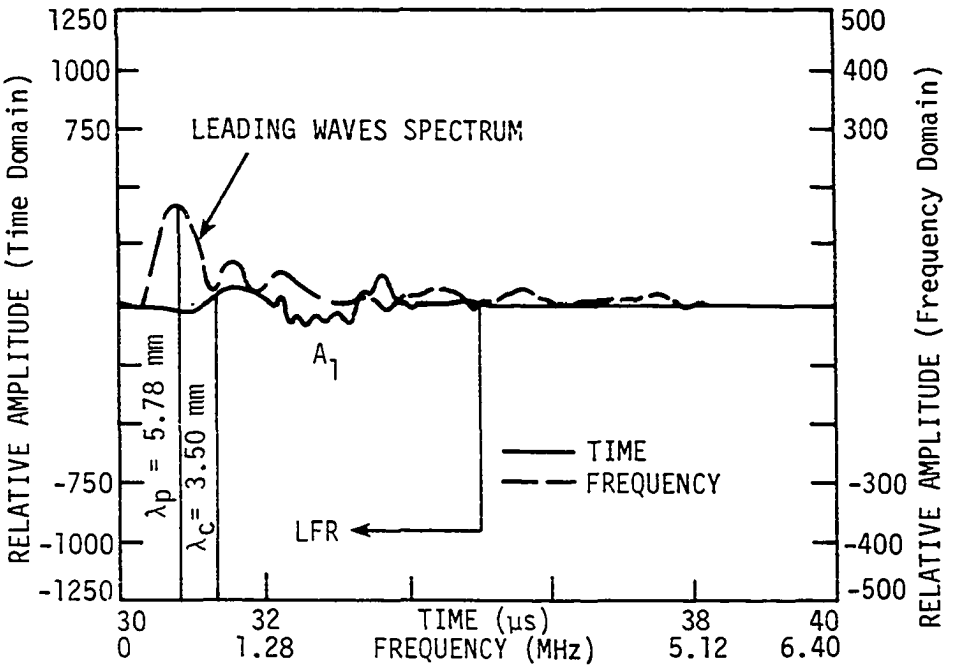

b. LFR only

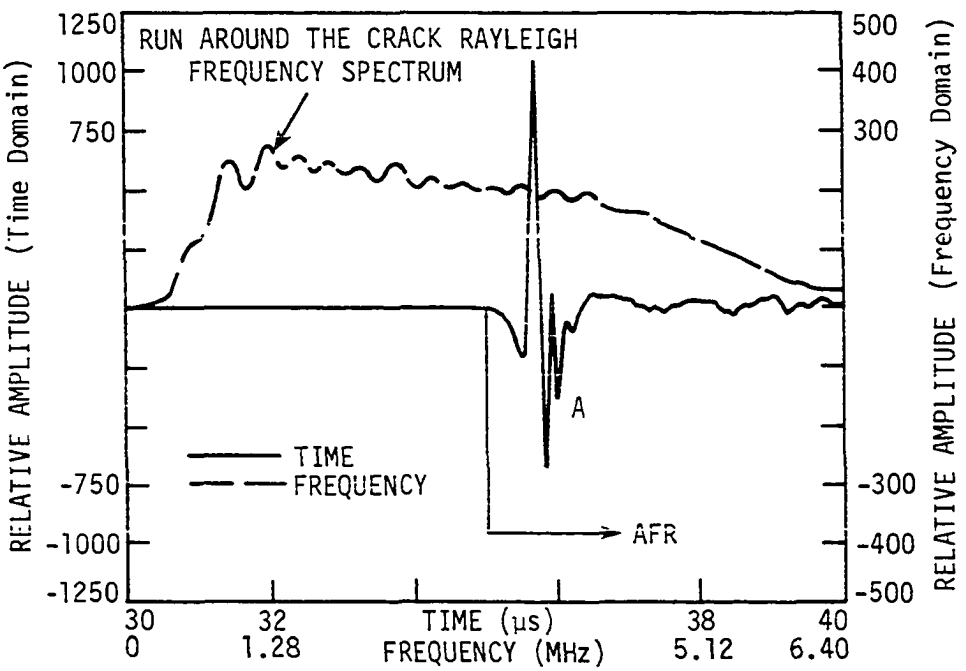

c. AFR only

Figure E.10. (cont.)

APPENDIX F.

RAYLEIGH SPECTROSCOPY FOR CHARACTERIZING SURFACE CRACKS[1]

A. J. Testa and C. P. Burger
Department of Engineering Science and Mechanics
and Engineering Research Institute
Iowa State University
Ames, IA 50011 USA

[1]This paper was presented by the author at the AF/DARPA Review of Progress in Quantitative NDE, at the University of Colorado, Boulder, Colorado, August 2-7, 1981. To be published in the AF/DARPA Proceedings.

ABSTRACT

The property of a broadband Rayleigh wave, whereby its frequency spectrum varies with depth below the surface, is used to measure the depth of irregularly shaped open fatigue cracks in steel. Spectroscopic procedures are applied to the forward scattered, or transmitted, wave after the Rayleigh wave has interacted with a surface crack. Results are presented for measurements on slots, EDM slits and fatigue cracks. It is shown that the same procedures can be applied equally well to any of the three types of defects and that the effectiveness of the method is unaffected by residual stresses and by the shape or path of the defect. Preliminary results are presented for tests on partially closed surface defects.

INTRODUCTION

Previous studies to determine the depth of open shallow slots and slits considered the affect that such "defects" have on the frequency spectra of the transmitted or "forward scattered waves" [1-4]. It was shown that when the slots are shallower than the depth of the lower frequency components in an incident surface wave, the wave is divided into two parts. The deeper portion of the incident wave diffracts at the tip of the slot or slit and appears, ultimately, as a low frequency Rayleigh leading the shallower portion of the incident Rayleigh that does travel around the defect.

Since surface breaking fatigue cracks represent a large body, if not the largest body, of structurally dangerous defects, it was decided to investigate how well the earlier procedures, as described above, could work in determining the depth of such cracks. The work reported here is specifically concerned with measuring the depth of "open" cracks with depths less than the depth of the incident Rayleigh wave.

Many techniques for interrogating surface cracks have been developed through the years. Most of them are based on time of flight measurement of acoustic waves with some others using amplitude measurements and very few using frequency information [5-12]. These techniques have used various wave forms for their purposes; however, it is believed by the writers that surface waves are better suited for defects close to the surface; therefore, they have been selected for the research herein presented.

The principal aim of this investigation is to establish an inspection method which can reliably size surface cracks and, in addition, remain relatively insensitive to most operational variables that affect the existing methods [13-18]. Some supporting work has been done in the past which opened the doors to the method described in this text [1,19-22]. More recent work has been presented at various conferences [2-4]. This paper presents recent progress in the characterization of open cracks.

THE RAYLEIGH WAVE

These highly energetic waves have been selected to do all of the continuing research because they have some outstanding properties. Surface waves contain most of their energy confined to a layer about 1 to 1-1/2 wavelengths in depth from the free surface. In addition, they exhibit, in the case of a broadband Rayleigh wave, a range of frequencies at the surface. Figure F.1a represents a typical time scan of a Rayleigh wave and Fig. F.1b is the corresponding frequency spectrum at the surface. This spectrum will lose its higher frequencies as the wave goes deeper into the material because the higher frequencies cannot penetrate as deeply as the lower frequencies.

Another good characteristic of these waves is their capability to travel long distances with relatively small attenuation. Their nature is also non-dispersive as long as they travel on a flat surface.

RAYLEIGH WAVE INTERACTION WITH A SLOT

The displacements of a Rayleigh wave, as predicted by theory [23-25], decay exponentially with depth. Because of the proportionality that exists between displacement and energy in elastic systems, it is considered a good assumption to represent the energy decay of such a wave in an exponential form. Figure F.2 depicts the interaction process of a Rayleigh wave with a slot using the suggested configuration for its energy distribution with depth. Stage I is representative of the energy distribution of a typical incident Rayleigh wave. This wave is called for short the incident AFR, which stands for All Frequency Rayleigh. Stage II shows very specifically the generated Rayleigh waves upon interaction of the incident AFR. Much energy is lost to mode conversions to P- and S-waves, but this is not depicted in the figure. The AFR energy that impinges on the slot generates a reflected All Frequency Rayleigh wave, called AFR_r, and a transmitted All Frequency Rayleigh, AFR_t. The latter travels along the slot face and, eventually, around the slot and back up to the surface. However, the

lower energy of the original AFR, which did not directly impinge on the slot, mode converts to some other wave which eventually reaches the surface and reconverts back into a Rayleigh wave. This wave which generates from the lower frequency deep energy in the incident AFR is called LFR_t, or Low Frequency Rayleigh, because its spectrum, as will be shown later, does not contain the higher frequencies present in the original wave at the surface. Hence, the total time scan of the transmitted package of signals, Stage III, should contain two distinct waves, the LFR_t and the AFR_t. These two waves are usually separable, and experiments have been conducted to check the validity of the interaction scheme described for Fig. F.2 with very encouraging results [26].

TESTING EQUIPMENT AND MATERIALS

The results to be presented herein were obtained from an actual fatigue crack grown in A387-74A-Gr.22 steel with 2-1/4% Chromium and 1% Molibdenum. The testing probes were nominal 5.0 MHz P-wave transducers broadbanded between 0.5 - 5.5 MHz as shown in Fig. F.1b. The spectrum of the waves generated can be modified by means of electronic damping provided in the signal generator. For this reason a central frequency is not obvious in Fig. F.1b. Rayleigh waves are generated by mounting the transducers on a 90° Lucite wedge.

All the tests are run by placing the transmitter and the receiver in line at equal distances on either side of the crack (in this case, 15 mm on each side). The signal processing is accomplished by means of an LSI-11 microprocessor with built in programs to handle the analysis of the data.

EXPERIMENTATION

It is important to observe whether or not the behavior of an open crack is the same as that of a slot (previously discussed). In addition, it is necessary to seek information on the closed portion of a partially open fatigue crack.

Figures F.3a and F.3b depict the fatigue crack that was tested. After it was grown down to point b Fig. F.3b, the crack was opened by applying an external load that caused sufficient permanent yielding at the crack tip to keep the crack fully open after removal of the load. After this, the specimen was further fatigued to extend the crack from point b to point a in Fig. F.3b. Upon removal of the cyclic load, the portion from a to b was tightly closed (invisible to the eye). The gap in the closed portion of the crack was estimated to be less than 5μm.

This partially closed crack was first tested without cleaning the specimen; i.e., the crack was polluted with cutting oil and steel particles. The sequence signals shown in Fig. F.4 were obtained. Figure F.4a is a sampling of all the transmitted waves. It includes the Rayleigh wave which derives from the shear that is reflected from the far surface below the crack as described in reference 3. The group of waves that has been studied for the slot and slit cases is shown on the Transmitted Wave Group. An expansion of these waves is shown as the solid line in Fig. F.4b. Two new waves can be identified that were not present with slots or slits. These are the Thru Transmitted Rayleigh (TTR) and the All Frequency Rayleigh generated at the tip of the closed portion of the crack; i.e., point a, called the (AFR_a). The TTR represents the portion of the energy from the incident Rayleigh wave that passed through the crack using as coupling medium the impurities contained in the crack. Wave AFR_a is that portion of the run around the crack Rayleigh wave that does not turn at the tip of the open crack (point b), but rather turns at the tip of the closed crack (point a). Wave AFR_b is the Rayleigh wave that turns around at the tip of the open portion of the crack. A preliminary check on these statements can be performed by using the time of travel technique to measure paths followed by the waves.

The time difference between the TTR and the AFR_b (Fig. F.4a) should be twice the depth of the open portion of the crack. Knowing that the Rayleigh wave velocity in this material is approximately $v_R = 3.0$ mm/μs,

one can readily establish that the path traveled was d_{open} = 1/2(17.66 - 15.4)(3.0) = 3.4 mm. This value should agree with the measured external open portion of the crack which is shown as 3.0 mm on Fig. F.3b. Since the internal depth of the open portion of the crack is likely to be more than 3 mm, the time domain data confirms that the AFR_b and TTR waves, indeed, are Rayleigh waves following the described paths.

Next, the time between the AFR_b and AFR_a should represent the time needed by the AFR_a to travel twice the additional path a - b. From time measurements this path can be calculated to be d_{closed} = 1/2(15.4 - 13.27)(3.0) = 3.2 mm. This additional crack length checks well with the externally measured closed increment of 3.2 mm shown in Fig. F.3b.

Among the waves observed in Fig. F.4b, one can still distinguish the strong LFR, but it is now polluted by the TTR. It leads both the AFR_a and the AFR_b so presumably the LFR is derived from the "cut-off" at the open tip b. As was mentioned earlier, the LFR diffracts at the crack tip and manifests itself as a Rayleigh wave on the surface upon reconvertion. Since it actually leads the TTR, which, as a through-transmitted wave, travels the shortest of all the possible paths, it could not have propagated as a Rayleigh wave all the way. A mode conversion must have occurred at the tip which then reconverted to a Rayleigh wave at the top surface, some distance away from the crack itself. The question whether it is, indeed, a Rayleigh wave is answered later in this paper.

The solid line in Fig. F.4c represents the LFR combined with the TTR. The dashed line is the frequency spectrum of these waves only. From this type of spectrum, the peak frequencies (f_p) and the cut-off frequencies (f_c) are selected. If the frequency spectrums of the waves in Fig. F.4c and F.4b are compared, one finds that the spectrum of the LFR is very dominant.

The next step was to load the specimen in bending and check the variations in the signals to establish with more certainty their origin. All the figures from here on are arranged in the same manner as Figs. F.4.

Upon the application of a 1000 lb load at the center span of the specimen (opposite to the crack), the scans in Fig. F.5 were obtained. There is no obvious shift of signals in Fig. F.5a when compared with Fig. F.4a. Figure F.5b does indicate a slight reduction in the amplitude of the TTR; and Fig. F.5c indicates a shift of the cut-off, f_c, frequency toward a lower value which indicates a deepening of the diffraction point.

In references 3 and 4, curves were developed for predicting the depth of slits and slots from a knowledge of the cut-off frequency (f_c), or more precisely, the cut-off wavelength ($\lambda_c = v_R/f_c$). Later, this sequence of tests will be used in the same manner, and the two curves will be compared. If the values obtained so far for the cut-off wavelengths are used with the slot prediction curves, Fig. F.11, one will find that the curves yield values in the order of 3.0 to 3.2 mm. This indicates that the LFR was generated at the open tip and not at the closed tip of the crack. Therefore, this shows that the method may be insensitive to closed cracks, which is not the most desirable fact. However, one must recognize two things at this stage: first, the time of travel between the two tips can still be used; and second, the method is being tested at its limits (a +6.0 mm deep crack).

The signals depicted in Fig. F.6 were obtained upon increasing the load to 2000 lbs. From Fig. F.6a it is observed that the AFR_a has become the dominant run-around-the-crack Rayleigh, while the AFR_b has almost disappeared. In addition, the LFR has broadened more which is an indication of it being generated at deeper levels. The TTR is very weak which indicates that the coupling bond between the crack walls is not so good any more. Figure F.6c shows what is believed to be the LFR and its frequency spectrum. Obviously, it is very difficult to choose any particular frequency due to the many modulations which are present. This may be caused by the fact that at this moment there may be a mixed diffraction created by the polluting material and the actual crack tip at those lower levels of the crack, therefore creating additional phase cancellation problems.

Figure F.7 represents the time scan of the signals when the specimen is loaded to 4000 lb. It is observed that the TTR has disappeared completely, and the portion containing the LFR has spread over a longer time interval (Fig. F.7b). At this point, the crack was open to about 1 mm wide at the top, and its length to the tip "a" could easily be tracked visually. Permanent yielding at the tip, however, was small if any at all. The frequency spectrum of the LFR shown in Fig. F.7c yields a cut-off wavelength λ_c = 4.34 mm which if used in conjunction with the equations for slot data in Fig. F.11, yields a crack depth of only 5.3 mm rather than the measured external value of 6.2 mm. This difference will be explained later as the rest of the data is analyzed.

The crack was then cleaned while holding the specimen under load to remove as much pollutants as possible, then the next series of tests were performed.

First the load was removed and the crack allowed to close to its original configuration (same as used for Fig. F.4). Figure F.8 shows the results. One's first observation is that though transmission is now small, the TTR has about vanished, as should be expected.

The specimen was then loaded, as before, to double the former load. With a load of 8000 lbs, the results in Fig. F.9 were obtained. They should be compared to Fig. F.7, especially Fig. F.9b to F.7b. When the depth is estimated from the line for slots (Fig. F.11) at λ_c = 4.26 mm, the depth again comes out to be 5.2 mm. It, therefore, seems as if the slot curves may not be good in predicting the crack depths. To settle this argument the specimen was loaded until the crack stayed fully open and with enough permanent strain to remain open after unloading (refer to Fig. F.3). The top surface of the specimen was then machined incrementally to leave even shorter cracks as depicted in Fig. F.10. After the final machining and testing, the specimen was fractured so that the actual crack profile could be obtained (Fig. F.10). This figure also depicts the various levels at which samples were taken.

The total amounts of cut material totals 3.79 mm, and the computed average depth of the failure line with respect to the final machined surface is 2.61 mm. This yields a total initial average depth of about 6.4 mm.

Predicted values for the depth of the crack were calculated by using the slot data equations given in Fig. F.11. The resulting values are tabulated in Table F.1. The terms "cut-off" and "peak" refer to the points f_c, λ_c and f_p, λ_p, respectively, as in Figs. F.4 through F.9. The terms are according to the nomenclature used in references 1 through 4, 19 through 22 and 26.

The error presented in Table F.1 for the cut-off data is linear with depth. When plotted separately on Fig. F.11, the data for the open (yielded) fatigue crack can be compared with the data for slots and slits in that they all yield reasonably straight correlation lines for the cut-off values. A best fit line through the cut-off data yields $\lambda_c = 1.2 + 0.48d$ or $d = -2.5 + 2.08\ \lambda_c$ with a correlation coefficient of almost 1.0. Peak values of wavelength (λ_p) have not been emphasized here, although they are plotted in Fig. F.11, because it has been found that they are very sensitive to testing conditions. That is not the case for the cut-off values. The cut-off line is relatively insensitive to typical variations in test conditions.

CONCLUSIONS

Actual cracks do not have flat profiles so that testing with a large diameter transducer provides an unknown average depth. Despite this built-in uncertainty, the data obtained for the crack remains slightly different from that for slots and slits.

Current testing is repeating the data for slots but at higher sampling levels, thus providing more accurate values upon performing the Fast Fourier Transformation. There are indications already that the slope of the slot data is shallower than previously established but still not the same as that for the crack data.

Preliminary statistical studies of the data indicate that within the standard deviation of the data, it is still possible to consider the crack data similar to the slot data within an 85% confidence limit. However, more tests are being performed with several different cracks ranging from 0.5 to 8 mm in depth. More reliable statistical analysis should then be possible.

ACKNOWLEDGMENTS

This research was performed on equipment purchased with a grant from the National Science Foundation (No. ENG77-06970). The work was supported by the Engineering Research Institute and the Department of Engineering Science and Mechanics at Iowa State University.

REFERENCES

1. A. Singh. "Crack Depth Determination by Ultrasonic Frequency Analysis Aided by Dynamic Photoelasticity." M. S. Thesis, Iowa State University, 1980.

2. C. P. Burger, A. J. Testa and A. Singh. "Dynamic Photoelasticity as an Aid in Developing New Ultrasonic Test Methods." Proc. of the 1981 Fall Meeting of the Society for Experimental Stress Analysis, Dearborn, Michigan, May 1981. To be published in conference proceedings.

3. C. P. Burger and A. J. Testa. "Rayleigh Wave Spectroscopy to Measure the Depth of Surface Cracks." Proc. of the 13th Symposium on NDE, San Antonio, Texas, April 1981. To be published in conference proceedings.

4. C. P. Burger and A. J. Testa. "On-Line FFT of Rayleigh Waves Determines the Depth of Surface Cracks." Proc. of Ultrasonics Int'l. '81, Brighton, England, July 1981. To be published in conference proceedings.

5. M. G. Silk. "The Determination of Crack Penetration Using Ultrasonic Surface Waves." NDT Int'l., Vol. 9, No. 6 (December 1976), 290-297.

6. M. G. Silk. "Defect Sizing Using Ultrasonic Diffraction." British J. of NDT, Vol. 21, No. 1 (January 1979), 12-15.

7. R. J. Hudgell, L. L. Morgan and R. F. Lumb. "Non-Destructive Measurement of the Depth of Surface Breaking Cracks Using Ultrasonic Rayleigh Waves." British J. of NDT, Vol. 16, No. 15 (September 1974), 144-149.

8. M. V. Grigorev, A. K. Gurvich, V. V. Grebennikov and S. V. Semerkhanov. "Ultrasonic Technique for the Determination of Crack Dimensions." Soviet J. of NDT, Vol. 15, No. 6 (June 1979), 495-500.

9. B. T. Khuri-Yakub and G. S. Kino. "Acoustic Surface Wave Measurements of Surface Cracks in Ceramics." J. Am. Ceram. Soc., Vol. 63, No. 1-2 (January-February 1980), 65-71.

10. L. L. Morgan. "The Spectroscopic Determination of Surface Topography Using Acoustic Surface Waves." Acoustica, Vol. 30 (1974), 222-228.

11. K. G. Hall. "Crack Depth Measurements in Rail Steel by Rayleigh Waves Aided by Photoelastic Visualization." Non-Dest. Testing (London), Vol. 9, No. 3 (June 1976), 121-126.

12. P. A. Doyle and C. M. Scab. "Crack Depth Measurement by Ultrasonics: A Review." Ultrasonics, Vol. 6, No. 4 (July 1978), 164-170.

13. B. G. Yee, J. C. Couchman, J. W. Hagemayer and F. H. Chay. "Stress and the Ultrasonic Detection of Fatigue Cracks in Engineering Metals." Non-Dest. Testing, Vol. 7 (1974), 245.

14. D. M. Corbly, P. F. Packman and H. S. Pearson. "Accuracy Precision of Ultrasonic Shear Wave Flaw Measurements on a Function of Stress on the Flaw." Mat. Eval., Vol. 30 (1970), 103-110.

15. B. H. Lidington, D. H. Saunderson and M. G. Silk. "Interference Effects in the Reflection of Ultrasound from Shallow Slits." Non-Dest. Testing, Vol. 6 (1973), 185-190.

16. F. C. Cuozzo, E. L. Cambiaggio, J. P. Damiano and E. Rivier. "Influence of Elastic Properties on Rayleigh Wave Scattering by Normal Discontinuities." IEEE Trans. on Sonics and Ultrasonics, Vol. SV-24, No. 4 (July 1977), 280-289.

17. S. Golan. "Optimization of the Crack Tip Ultrasonic Diffraction Technique for Sizing Cracks." Mat. Eval., Vol. 39 (February 1981), 166-169.

18. L. Kittineer. "Correction for Transducer Influence on Sound Velocity Measurements by the Pulse Echo Method." Ultrasonics, Vol. 15, (January 1977), 28-30.

19. A. Singh, C. P. Burger, L. W. Schmerr and L. W. Zachary. "Dynamic Photoelasticity as an Aid to Sizing Surface Cracks by Frequency Analysis." Mech. of Non-Dest. Testing, Ed. W. W. Stinchcomb, New York: Plenum Press (1980), 277-292.

20. L. W. Zachary, C. P. Burger, L. W. Schmerr and A. Singh. "Surface-Crack Characterization by Use of Dynamic Photoelasticity Spectroscopy." Paper presented at the SESA Spring Meeting, San Francisco, California, May 20-25, 1979.

21. A. Singh and C. P. Burger. "A New Technique for Determining the Depth of Surface Cracks by Rayleigh Waves." ASNT, Fall Conference, Houston, Texas, October 1980.

22. C. P. Burger and A. Singh. "An Ultrasonic Technique for Sizing Surface Cracks." Proc. DARPA/AF, Review of Progress in Quantitative NDE, San Diego, California, July 1980.

23. I. A. Viktorov. "Rayleigh and Lamb Waves." First ed. New York: Plenum Press, 1967.

24. J. D. Achenbach. "Wave Propagation in Elastic Solids." Vol. 16, London: North-Holland Publishing Co., 1973.

25. H. Kolsky. "Stress Waves in Solids." First ed. London: Clarendon Press, 1953.

26. A. J. Testa. "Non-Destructive Measurement of Surface Cracks Using Ultrasonic Rayleigh Waves." Ph.D. Dissertation, Iowa State University, 1981.

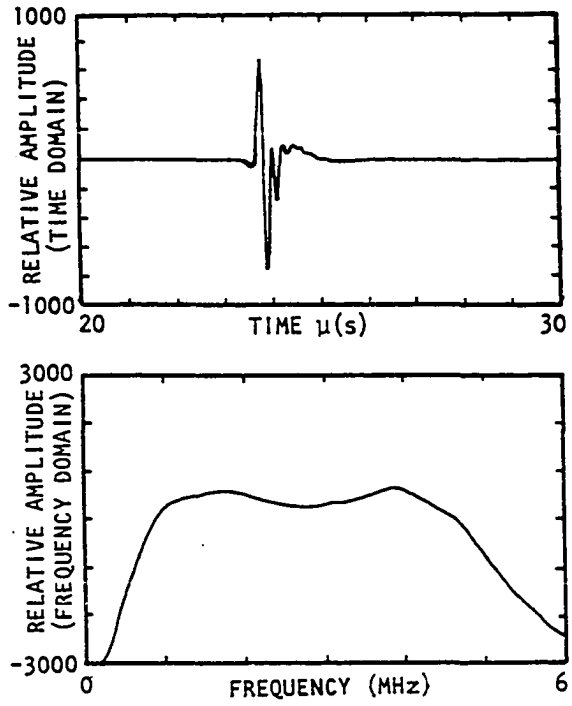

Figure F.1. a. Time scan; b. Frequency spectrum

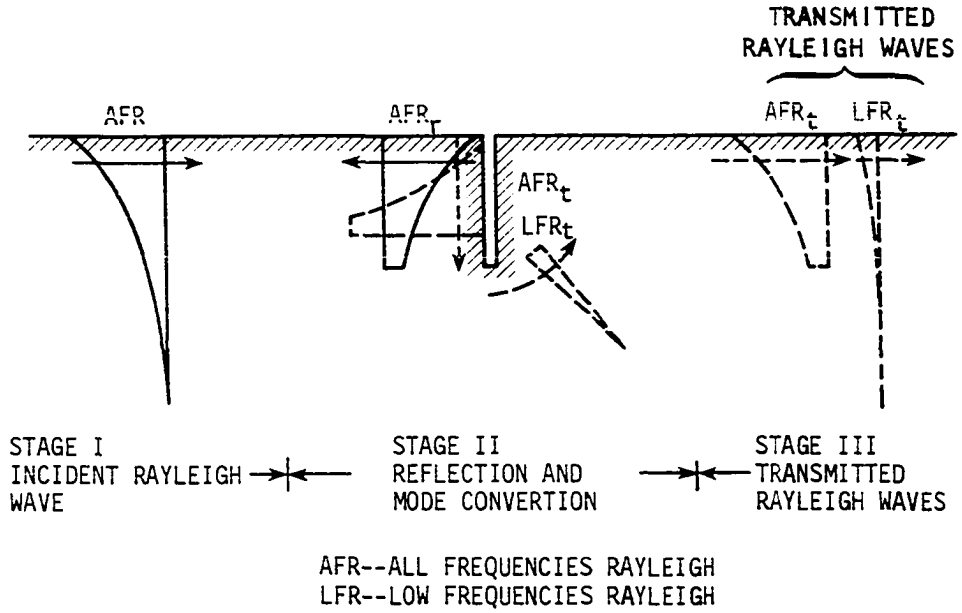

Figure F.2. Rayleigh wave interaction with a slot

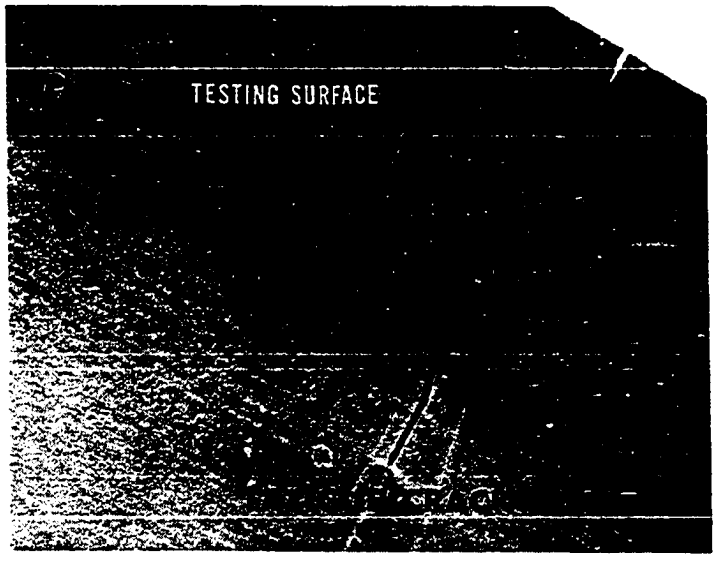

Figure F.3a. Fatigue crack in A387 steel

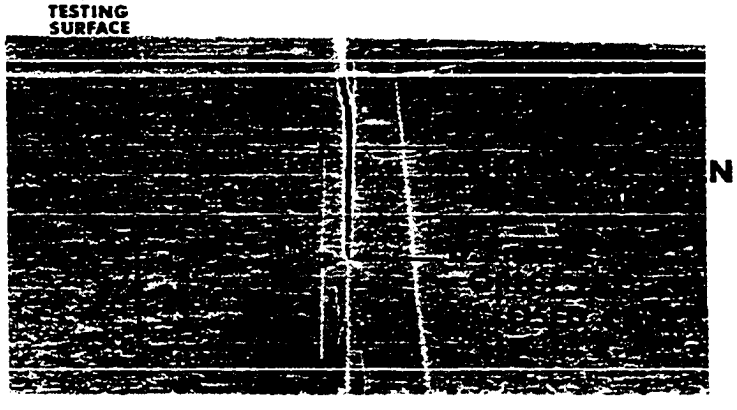

Figure F.3b. Side view of fatigue crack in A387 steel

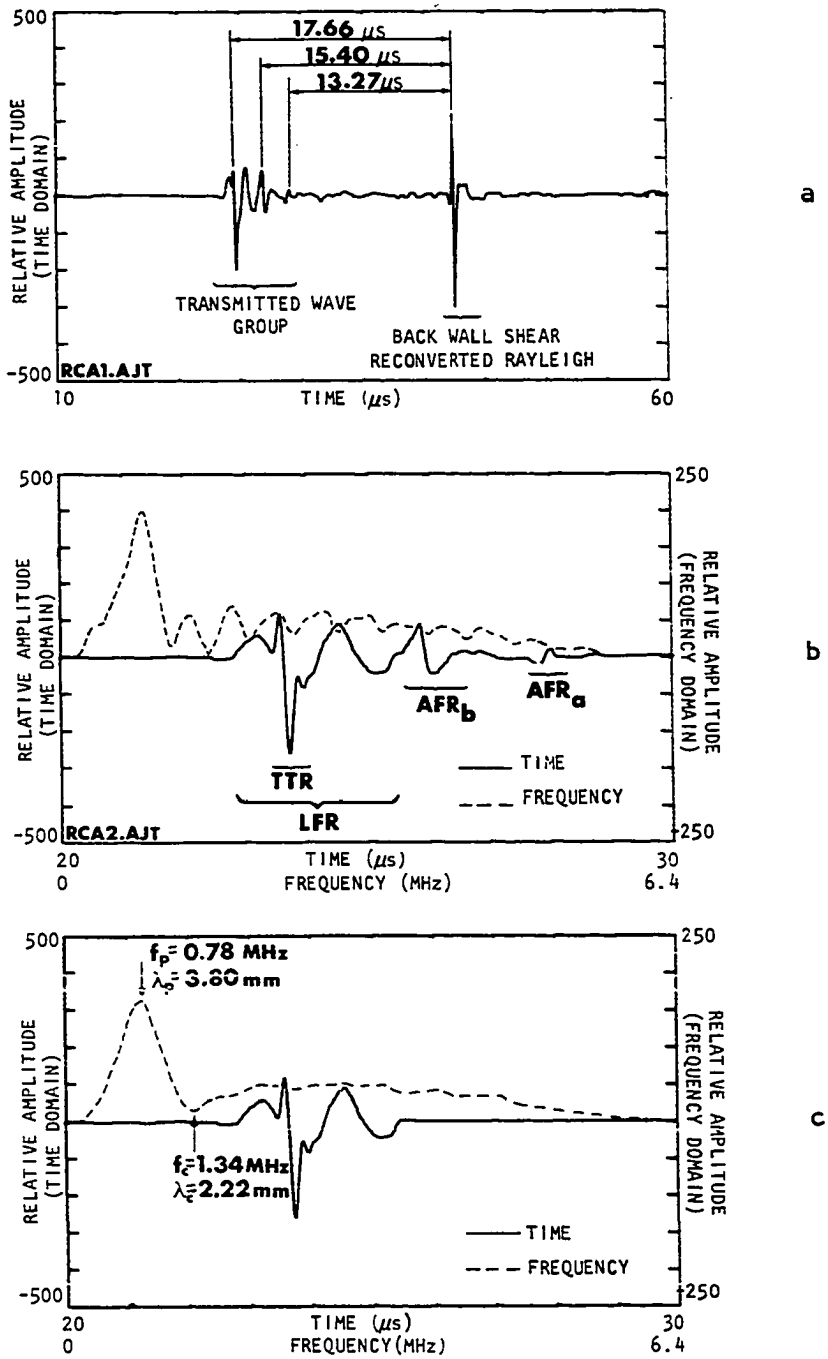

Figure F.4. Sequence of samples of polluted fatigue crack under no load
a. Full view of transmitted signals
b. Transmitted wave group and FFT
c. Leading wave group and FFT

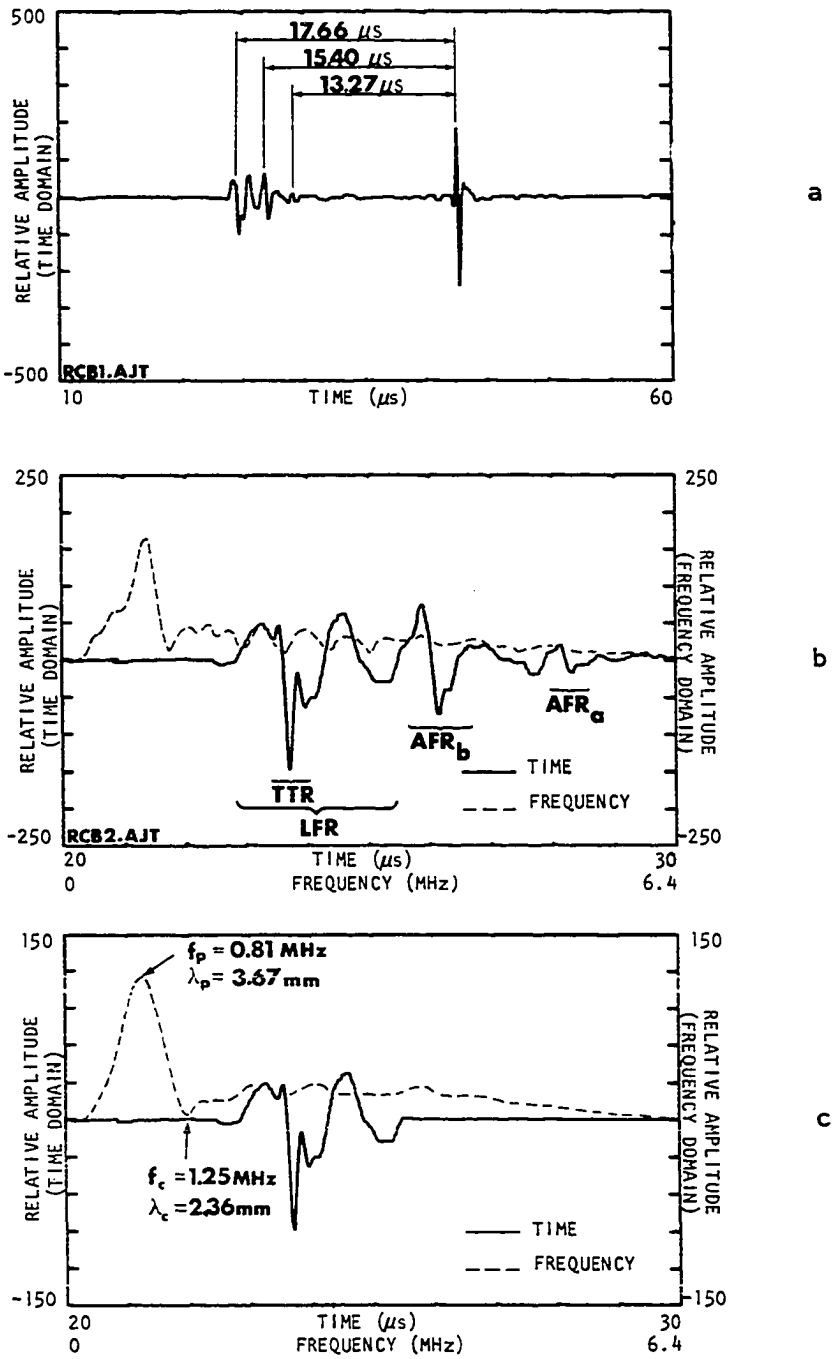

Figure F.5. Sequence of samples of polluted fatigue crack under a 1000 lb flexural load
a. Full view of transmitted signals
b. Transmitted wave group and FFT
c. Leading wave group and FFT

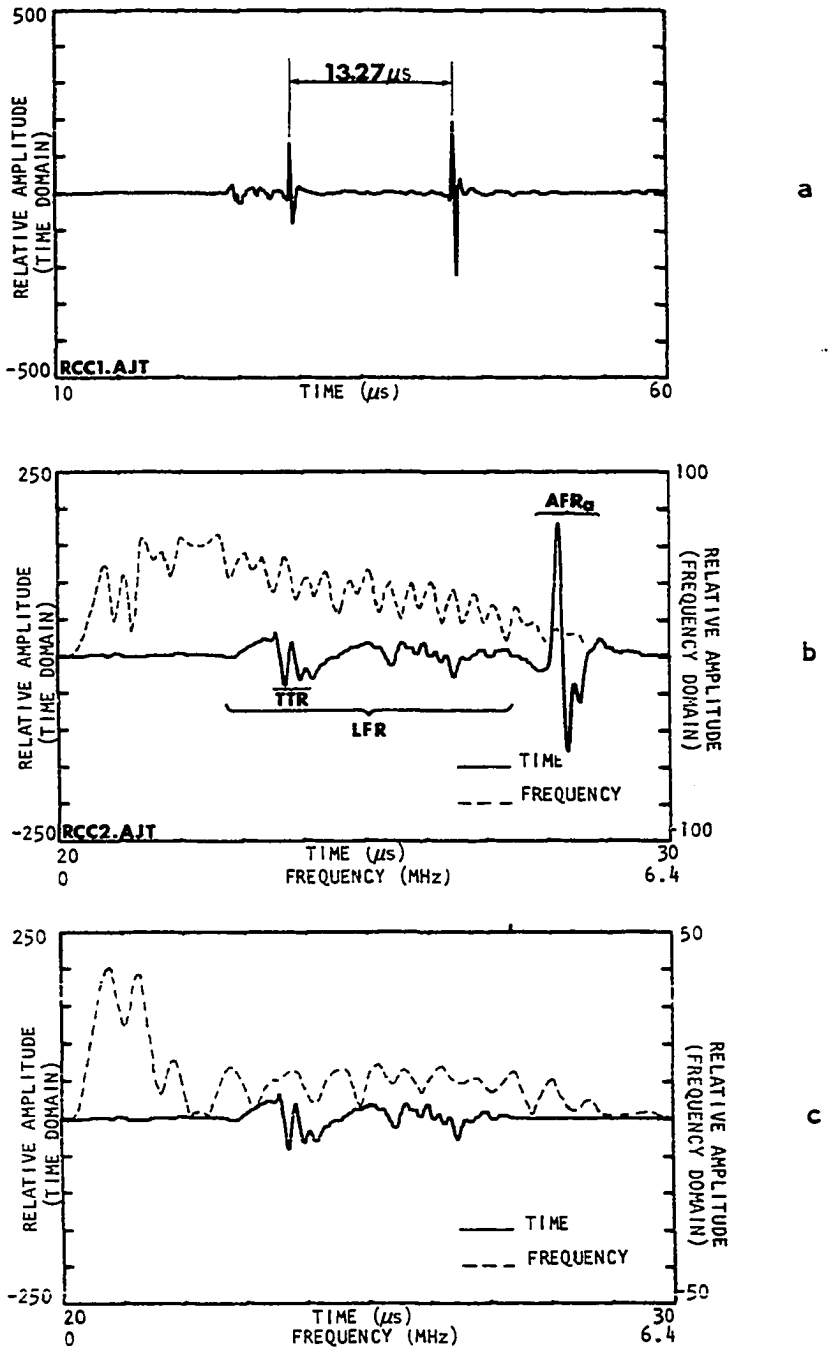

Figure F.6. Sequence of samples of polluted fatigue crack under a 2000 lb flexural load
a. Full view of transmitted signals
b. Transmitted wave group and FFT
c. Leading wave group and FFT

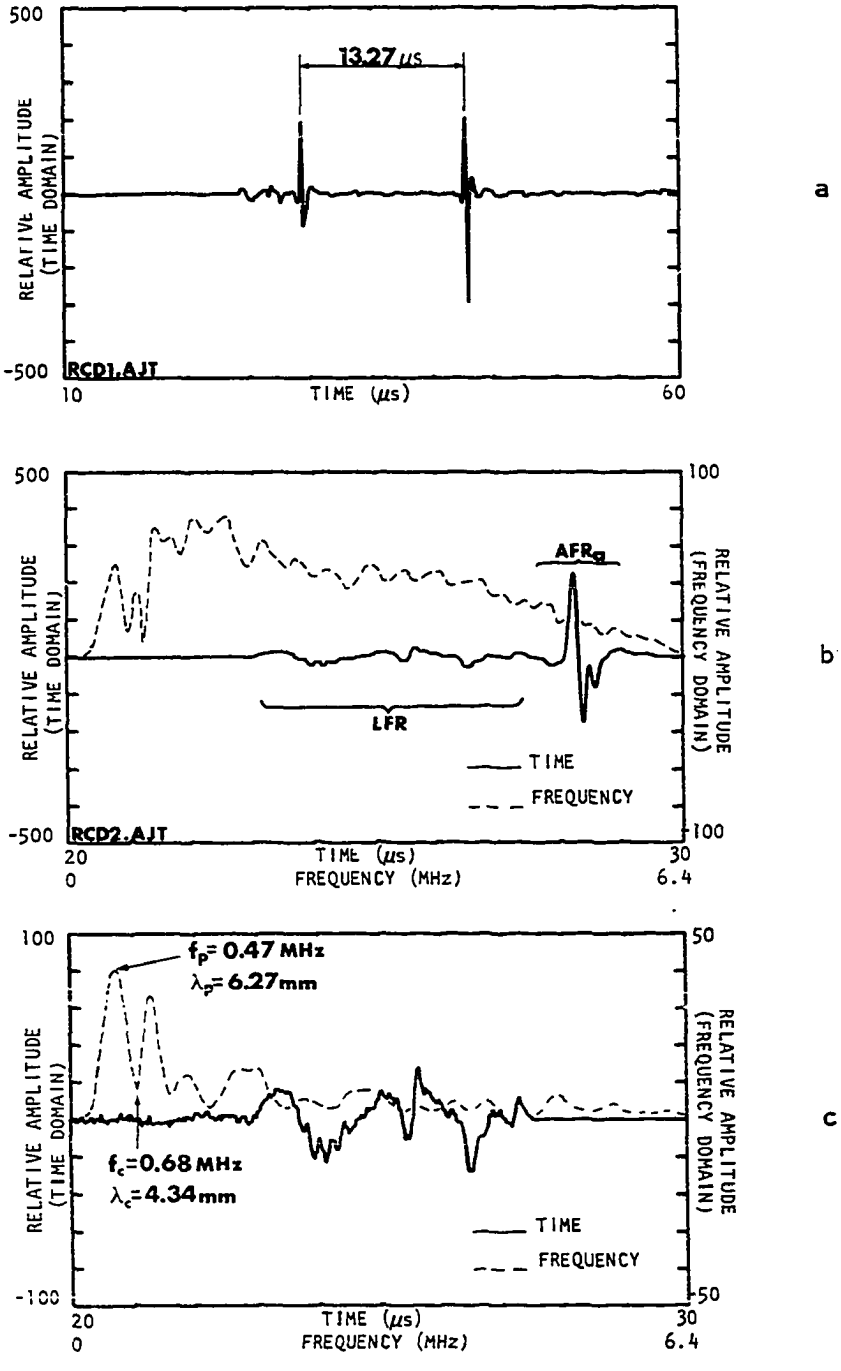

Figure F.7. Sequence of samples of polluted fatigue crack under a 4000 lb flexural load
a. Full view of transmitted signals
b. Transmitted wave group and FFT
c. Leading wave group and FFT

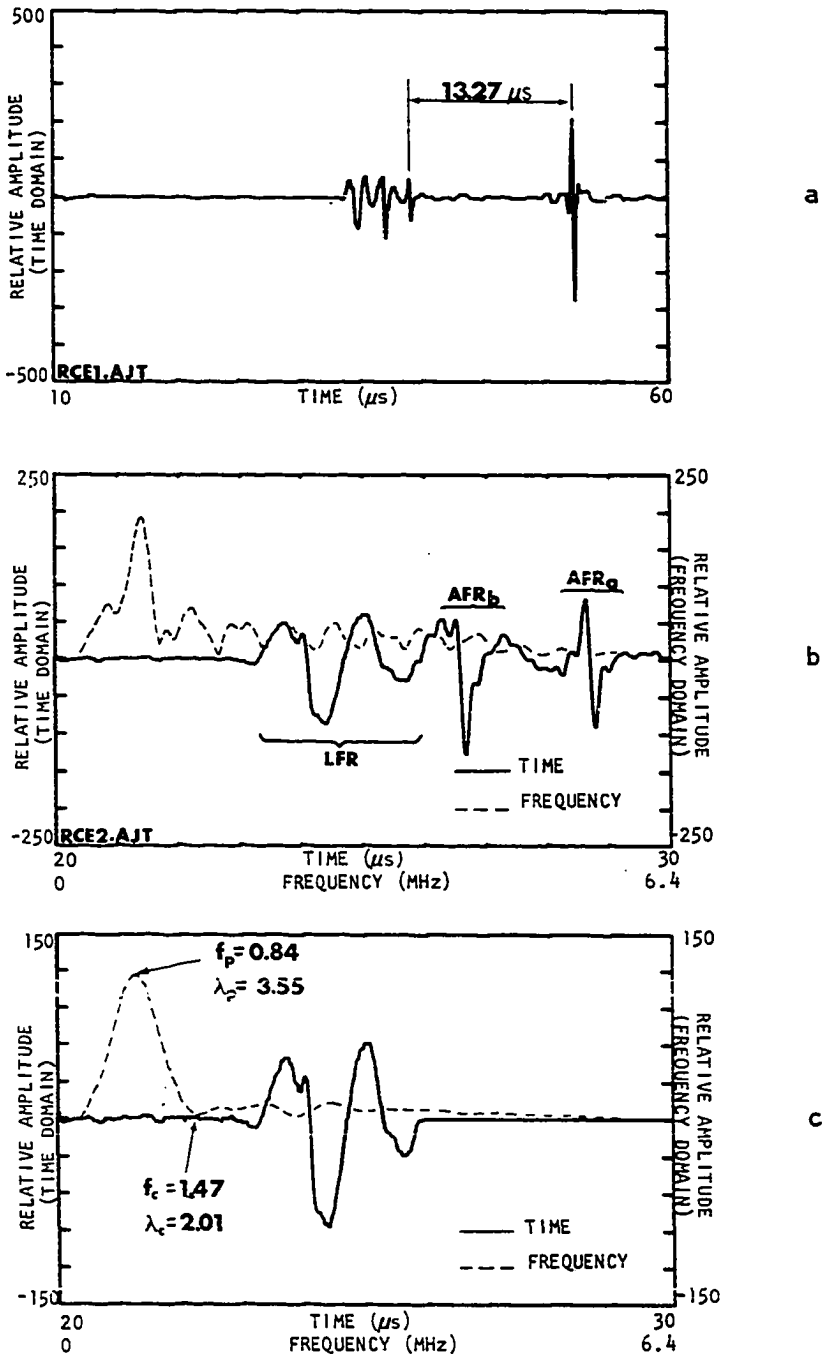

Figure F.8. Sequence of samples of clean fatigue crack under no load
a. Full view of transmitted signals
b. Transmitted wave group and FFT
c. Leading wave group and FFT

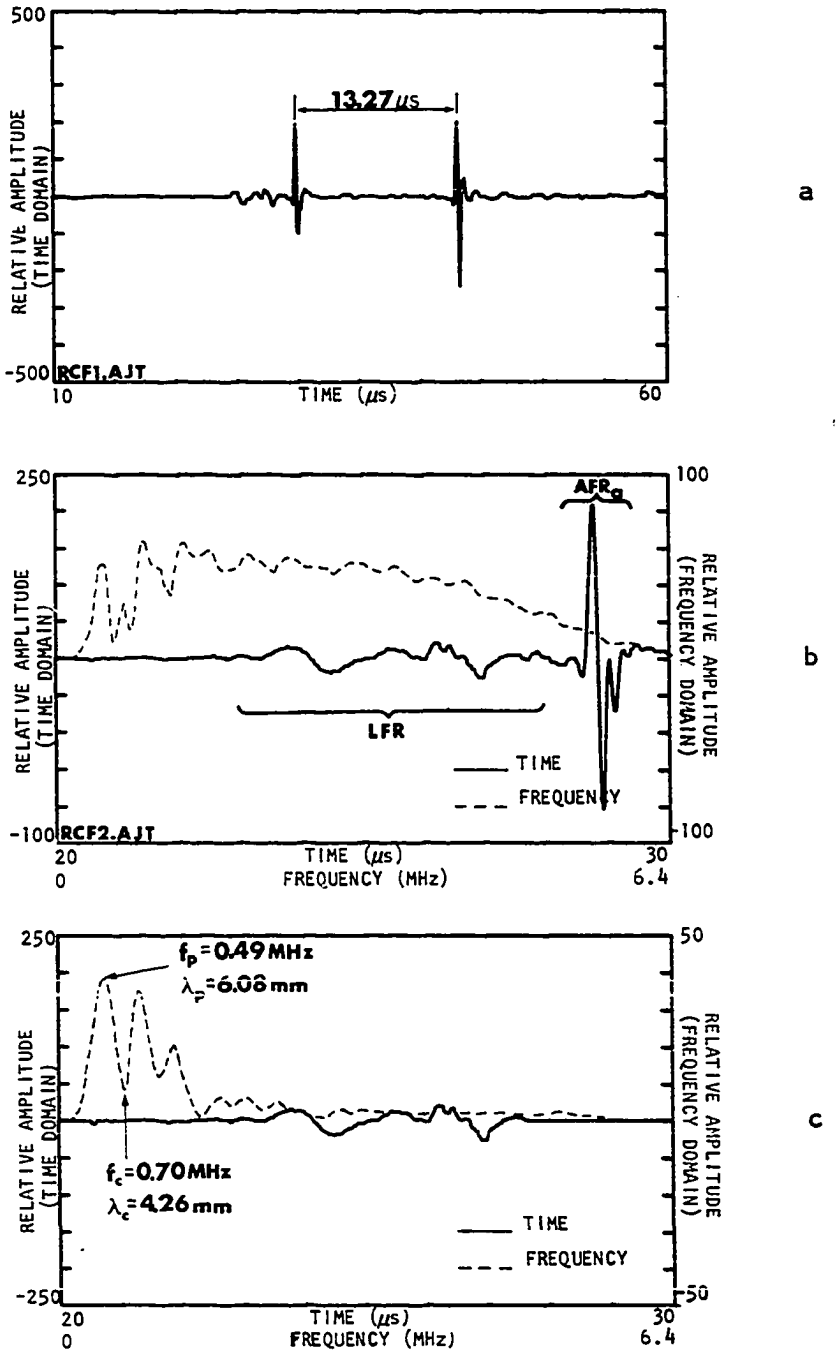

Figure F.9. Sequence of samples of clean fatigue crack under an 8000 lb flexural load
a. Full view of transmitted signals
b. Transmitted wave group and FFT
c. Leading wave group and FFT

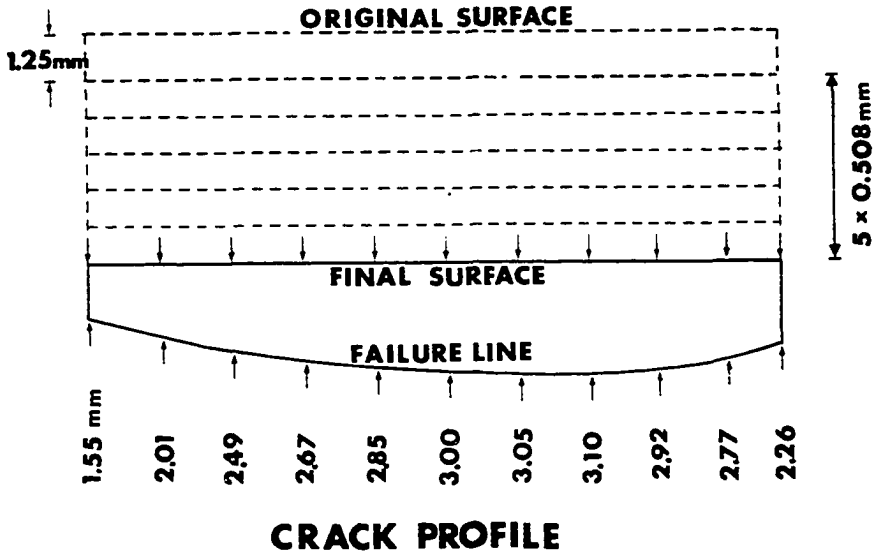

Figure F.10. Fatigue crack profile

Table F.1. Predicted crack depths from equations derived from slot data

AVERAGE DEPTH mm	PREDICTED DEPTHS mm			
	CUT OFF	% ERROR	PEAK	% ERROR
6.40	5.20	+ 19	4.22	34
5.15	4.47	+ 13	3.25	37
4.64	4.18	+ 10	3.36	28
4.13	3.99	+ 3	3.05	26
3.63	3.60	- 1	2.52	31
3.12	3.28	- 5	2.52	19
2.61	2.95	- 13	2.25	14

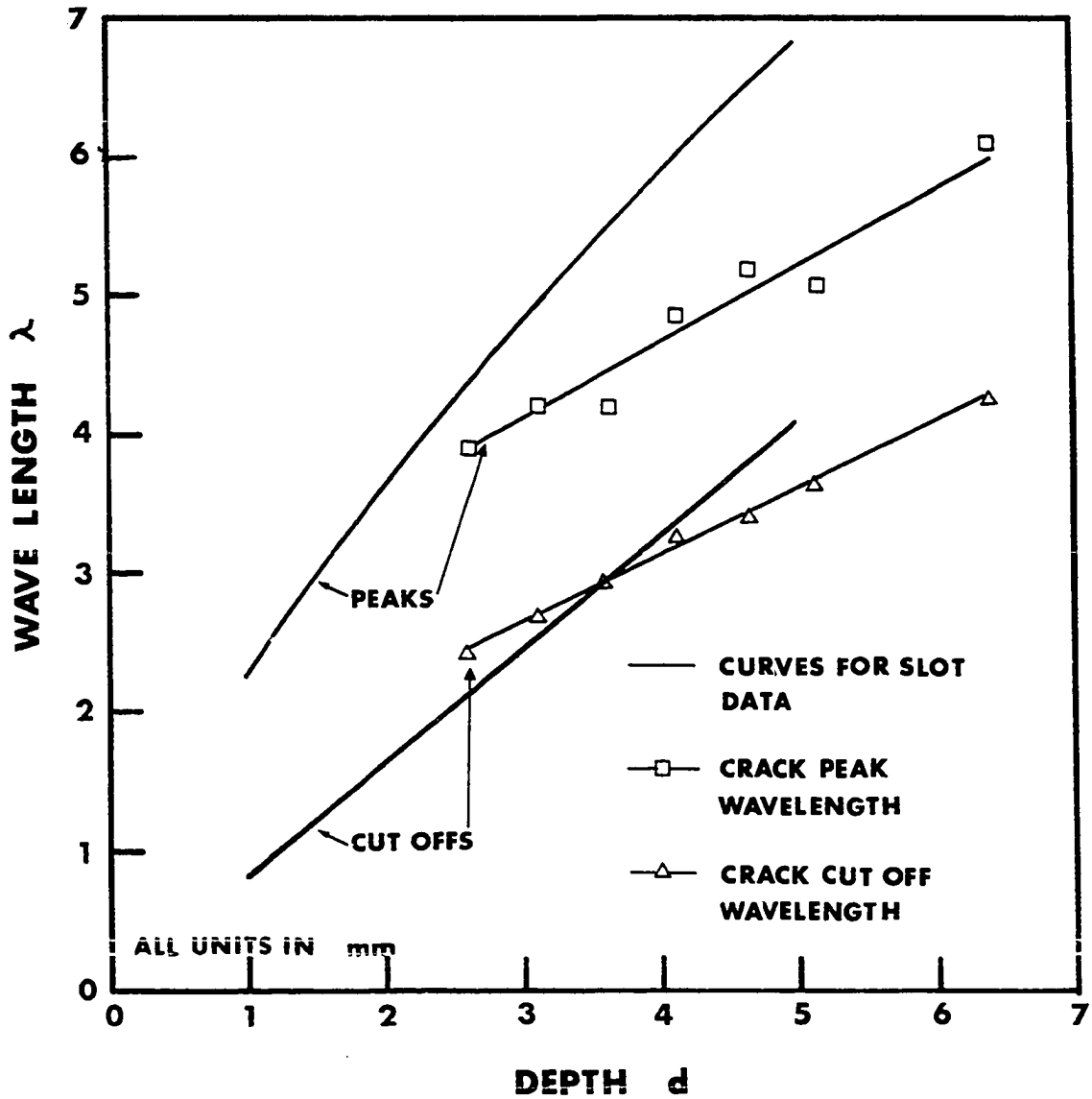

SLOT	CRACK
$\lambda_p = 2.25\,d^{0.69}$	$\lambda_p = 2.46 + 0.55\,d$
$\lambda_c = 0.82\,d$	$\lambda_c = 1.20 + 0.48\,d$

Figure F.11. Slot and crack data results and equations